Stimulus-induzierte Desynchronisation von gekoppelten Oszillatoren mit Zeitverzögerung: Theorie und Anwendung bei neurologischen Patienten

Inaugural Dissertation

zur

Erlangung des Doktorgrades

der Mathematisch-Naturwissenschaftlichen Fakultät

der Universität zu Köln

vorgelegt von

Valerii Krachkovskyi

aus Kiew

2006

Berichterstatter: Prof. Dr. Tassilo Küpper

Prof. Dr. Rüdiger Seydel

Tag der mündlichen Prüfung: 26 April 2006

Contents

Chapter 1

Introduction

The thesis is devoted to a mathematically challenging issue: stimulus-locked transient responses of oscillators coupled with delay. Apart from the purely mathematical aspects, this work is relevant from a medical point of view:
(i) for the development of novel brain stimulation techniques and
(ii) for the analysis of evoked brain responses, both for basic research and clinical diagnosis.

Brain stimulation: In several neurological diseases like Parkinson's disease (PD) or essential tremor the brain function is severely impaired by synchronization processes [10]. Parkinsonian resting tremor appears to be caused by a population of neurons located in the thalamus and the basal ganglia, where the pathologically strongly synchronized neurons fire in a synchronized and intrinsically periodical manner at a frequency similar to that of the tremor [32, 40, 30]. In contrast, under physiological conditions these neurons fire incoherently [39]. In patients with PD this neuronal cluster acts like a pacemaker and activates premotor areas and the motor cortex [71], where the latter synchronize their oscillatory activity [56].

In patients with advanced PD or essential tremor who do not respond to drug therapy any more, depth electrodes are permanently implanted in target areas like the thalamic ventralis intermedius nucleus or the subthalamic nucleus [3, 6]. Electrical deep brain stimulation (DBS) is performed by administering a permanent high-frequency (HF) (> 100 Hz) periodic pulse train via the depth electrodes [3]. However, HF DBS may lead to side effects like dysarthria, dysesthesia or cerebellar ataxia [72]. On the other hand, 11-15 % of PD patients have unsatisfactory outcomes in spite of proper electrode placement [31].

To improve deep brain stimulation novel stimulation protocols have been developed with methods based on statistical physics and nonlinear dynamics (see [57, 46, 21]). The goal of these techniques is to selectively counteract the pathological synchronization processes. On this way, uncovering the mechanisms of the pathological neuronal synchrony represents a challenging task in the development

of novel deep brain stimulation techniques for the therapy of such diseases.

<u>Evoked brain responses</u>: Transient responses of coupled oscillators to pulsatile stimuli are relevant in several other fields of the natural sciences. Such responses are typically studied by experimentalists to obtain information on dynamical systems and to characterize the system's inventory of reactions. For example, in neurology stimulus evoked electroencephalography responses are a standard tool for clinical diagnosis, where transient short-term brain responses evoked by sensory stimuli play a key role in the study of cerebral information processing and diagnosis. A stimulus-locked response of a neuronal population is typically analyzed with a cross-trial averaging (CTA), where an ensemble of post-stimulus responses is averaged across trials [9, 18]. However, as has been shown in the recent studies [58] based on a stochastic phase resetting approach [57], the CTA techniques may lead to misinterpretations or even artifacts, and a detailed study of stimulus-locked system responses is required. In particular, this concerns complex systems and systems with delay which are inevitably present in nature.

In the thesis two systems of two phase oscillators coupled with delayed self-feedback (see chapters 2,3) and coupled with delay (see chapter 4) are considered. Both systems are subject to an external stimulation. Different phenomena in the dynamics of coupled oscillators are studied intensively. Phase oscillators belong to one of the simplest classes of oscillators, but nevertheless, as we shall see, they demonstrate a rich variety of dynamic regimes and thus can help to model different aspects of reality.

The first part of the thesis (chapters 2,3) explains the formation of complex transient responses of two phase oscillators coupled with delayed feedback in the presence of stimulation and noise. We study the influence of the strong external stimulation on the system. We show that, depending on the dynamical regime, responses of the system on the stimuli can follow different scenarios. They can vary from two-cluster responses for stimulated phase-locked regime, as has been found for coupled phase oscillators without delay [58], to multicluster responses for the case of periodically modulated phase synchronization. The stimulation can induce switching between different stable synchronized states for multistable regime. Stimulation can even completely change the type of long-term dynamics of the system, e.g., from synchronized to desynchronized one, if the corresponding multistable regime is stimulated. We also investigate how the in- and post-stimulus system transients depend on system and stimulation parameters. We explore the mechanism of the maximal post-stimulus transient and clustering and determine optimal values of stimulation parameters.

In the second part of the thesis (chapter 4) we study the transmission of a stimulus effect from the first, directly stimulated oscillator to the second non-stimulated oscillator. This type of transmission is fundamental for communication of networks of oscillators, e.g., in networks of neuronal populations with

rhythmic activity. In that case a single oscillator serves as a macroscopic model for a neuronal population. The estimation of transmission times is of great importance in neuroscience and neurology:

(i) Transmission times provide the functional roles of different brain areas and constitute the so-called mental chronometry (see [51], chapter four), according to which sensory information is subsequently processed in different brain areas and is transmitted from an active area to next areas.

(ii) The estimation of transmission times is a routine procedure in clinical diagnosis, used to detect delays in neuronal pathways, which are increased due to diseases like multiple sclerosis (see [64]) etc.

(iii) There is an elaborated standard procedure for the estimation of transmission times. Identical stimuli are administered repetitively, and the neuronal responses are registered, e.g., with electroencephalography (EEG) or magnetoencephalography (MEG). To extract what is supposed to be the actual stimulus evolved response, one averages over an ensemble of single responses [7, 9]. The assumption behind this procedure is that a single response is of the form $x(t) = r(t) + \xi(t)$, where r is a stereotypical response, and ξ is noise (e.g., Gaussian white noise). With increasing number of single responses the noise cancels out, and the averaged response $\langle x \rangle$ converges to $r(t)$. The transmission time between two neuronal populations (1 and 2) is then determined as time elapsing between the extrema of the corresponding averaged responses $\langle x_1 \rangle$ and $\langle x_2 \rangle$.

The results presented here clearly demonstrate that the timing sequence obtained with cross-trial averaging may not correlate at all with the actual transmission of a stimulus' effect within a pathway. In contrast, the phase resetting approach, exploited in the thesis, enables a reliable detection of transmission times.

1.1 Mathematical modeling of neuronal dynamics

Mathematical modeling is playing an increasingly important role in the brain sciences. Since J. Hopfield introduced his new type of neurons combined in a neural networks [22], neuronal network have occupied one of the leading places in neuronal modeling. Up to now, a tremendous number of different investigations has been undertaken in neuronal networks. Different types of models of neurons were considered, different network architectures were proposed and tested. A huge variety of tasks confronts the researcher, ranging from pure dynamical and phenomenological tasks up to the understanding of processes of learning and cognition in the brain. Different levels of modeling are by convention split into macro- and microscopic levels.

On the microscopic level, the object of the investigations is a neuron. Several models serve as a simple approximation of its dynamics. One of the most popular models of this type is the famous Hodgkin-Huxley model[23]. In it ion channels

and currents are represented by appropriate variables and their interaction is described by four differential equations. This system of equations describes one hypothetical neuron: an input signal influences the neuron (synaptic activation), which may cause firing of the neuron (spike generation, bursting). Using these neurons, the researcher can also build networks.

On the macroscopic level of modeling many neurons are considered together. Some common features of neurons are studied (for examples the number of synapses), but other characteristics of neurons are neglected. This type of modeling helps in situations when one needs to describe the behavior of a large amount of neurons, i.e., neuronal populations. In this case a neuronal population is often considered as a whole. There are two main approaches to modeling neuronal populations: either primarily to describe an element of the population (neuron) by some dynamical model and secondarily to fix the number of these elements close to a thermodynamical limit or directly to describe a population by some system of equations. In our work we prefer the latter approach.

We are interested in the rhythmic activity of the brain. Moreover, we study the interaction between two hypothetical neuronal populations. Any rhythmic activity could be correspondingly modeled by oscillatory systems. Many important classes of oscillators are well known. Of these we will just mention limit-cycle oscillators, relaxation oscillators, Lorenz and Rössler oscillators, phase oscillators etc. Each such oscillator could serve as a model of rhythmic activity of a neuronal population. The interaction between populations could be modeled by a specific coupling in a system. Lorenz and Rössler oscillators are of a special type and we will not discuss them here. Limit-cycle and phase oscillators can model a wider class of objects in nature.

For example, recently extensive studies have been made of coupled limit-cycle oscillators by Reddy V. Dodla *et al.* (see [47, 48]). In [48] periodic forced response of a system of two limit-cycle oscillators was investigated. These oscillators interacted via a delayed coupling. The authors aimed to find the conditions of the appearance of synchronization in the system. Coupling in the system is linear through the complex variable $Z(t)$. Many bifurcation diagrams and a deep analysis provide an description of the dynamics in the system.

In general, the presence of coupling in a system incites a researcher towards the analysis of the appearence of synchronization in a system. The remarkable book by Kuramoto "Chemical Oscillations, Waves and Turbulence" [28] deals with oscillating fields of different types. It gives numerous asymptotic methods for analyzing the dynamics in such systems. Among the systems considered, Kuramoto derived a system of phase oscillators globally coupled via a mean field:

$$\dot{\psi}_\alpha(t) = \omega_\alpha + \frac{K}{N} \sum_{\alpha'=1}^{N} \sin(\psi_\alpha - \psi_{\alpha'}) \tag{1.1}$$

where N is a number of oscillators, $\psi_i, \ i = 1, N$ are phase variables of each

oscillator, ω_i, $i = 1, N$ are natural frequencies of oscillators, K is a coupling parameter. In this book it was analytically shown that there is a critical value of coupling K_c such that for $K > K_c$ full synchronization of all N oscillators takes place in the system.

Extensive studies of dynamics in the Kuramoto model for a finite number of phase oscillators is found in [45]. The authors showed that already for $N = 4$ for some parameter sets chaos enters the system. Many other dynamical regimes were investigated, also for some symmetric cases.

Synchronization plays an important role in the transmission of information in the brain. It is well known that in the brain a certain rhythmic activity is always present (for example α rhythm) where millions of neurons interact with each other and as result of their interaction a common rhythmic signal evolves. The transmission of a signal from one neuron to another occurs according to a certain time sequence.

In our work we try to model a phenomenon which seems to take place in Parkinson disease, where two neuronal populations interact and one of them (driving) generates a pathological rhythm at which the other (driven) oscillates. Our main goal is to determine the parameter values at which synchronization occurs and how to break this synchronization.

One of the examples of how the theory of synchronization works in practice is given by the experiments done on the paddlefish (see [37]). The paddlefish has a long rostrum (i.e. "nose") with a spot of nervous receptors on it. This makes the fish an ideal object for experiments. The fish is stimulated through some spots by an external periodic force and the synchronization of different nervous receptors is studied. As a result a good agreement of n to m frequency entrainment between theory and practice was observed.

Wider classes of problems are also considered. The authors of [24] propose a method of detection for mutual phase synchronization in multivariate signals. Moreover, they test their method on ensembles of phase oscillators and on weakly coupled Lorenz systems. The novelty of their method is that synchronization indices take into account the spatio-temporal structure of data and thus are bivariate, which facilitates the detection of phase synchronization.

However, in ensembles of interacting oscillators in nature, communication between the individual elements inevitably takes place with some delay in time. This can be caused by a finite transmission speed of a signal, by a finite distance between oscillators, etc.. There are two pioneering articles in which systems of phase oscillators with a time-delayed coupling were considered.

One of them [52] was written in 1989 by Schuster and Wagner. Therein two phase oscillators interact with delay in such a way that the signal from the one oscillator influences the dynamics of the other oscillator after τ delay time and vice versa. The authors analyzed the appearance of synchronized states in the system as a function of the coupling strength K and delay τ parameters. They

reported the coexistence of many stable synchronous states as K grows. We use their model in chapter 4 adding a stimulation term to it. There we study the stimulus transmission between two oscillators.

The other article [73] written by Yeung and Strogatz in 1999 deals with a population of N phase oscillators with a time delayed coupling. Their model reads

$$\dot{\theta}_i(t) = \omega_i + \frac{K}{N} \sum_{j=1}^{N} \sin(\theta_j(t - \tau) - \theta_i(t) - \alpha) \tag{1.2}$$

where θ_i, $i = 1, N$ are phase variables of each oscillators, ω_i, $i = 1, N$ are natural frequencies of oscillators, K is a coupling parameter, τ is a delay parameter, α is a "phase frustration" parameter. The authors determine stability regions (analytically and numerically) of incoherent (desynchronous) states in the system for certain distributions of natural frequencies at limit where $N \to \infty$. The stability regions of the incoherent states become smaller and smaller as the coupling and the delay parameters grow. Some other examples of systems of phase oscillators coupled with a time delay can be found in [8, 38].

Wiener postulated in [65] that every cybernetic system should have some feedback loop in it. This is especially pertinent in the neuronal sciences, where not only a whole brain but even small neuronal systems demonstrate the ability to learn. That is why many neuronal models have feedback signals. We mention a few interesting articles.

In [54] scientists consider a model of two neurons which interact with each other with delays τ_1 and τ_2. Additionally, self-feedback loops with delay τ_s are present. The authors studied the stability of a trivial solution of their model in a parameter space of time delays and coupling. They showed that the trivial fixed point can lose stability in five different ways: either through a pitchfork bifurcation or a Hopf bifurcation or three other types of codimension-two bifurcations. In our model (see chapter 2) we construct a similar model with a different dynamical description of a single newron and negligibly small τ_1, τ_2.

In another important paper [1], possible architectures which dominate in the nervous system and are suitable for a neuronal computing are discussed on theoretical and experimental levels. The authors first consider two known cases, feed forward and recurrent network architectures. After that they come to the surprising conclusion that studies of sensorimotor networks reveal a third important class of architecture - architecture where computations depend on long-scale feedback loops. A comprehensive scheme of interaction was given between thalamico-cortical brain areas and muscles nerves. Using the language of automatic control theory, the scientists built closed-loop contours representing a nervous signal propagation. **In our model in chapter 2, we model a brain-**

muscle contour of a similar kind.

The last important aspect of our models concerns a stimulation of the system. In practice, functioning of the brain is mostly studied in two ways either by a lesioning or by an application of external stimuli (visual, audio, electrical etc.) with further registration of a brain activity. We used the second approach. This area is extremely rich in scientific publications, we mention just a few of them relevant for us.

The chapter by Lopes da Silva "Event-related Potentials: Methodology and Quantification" in [33] deals with the problem of the relation of a measured brain signal to a real brain response (reaction) on a stimulus. It is postulated that the measured signal could be considered as the sum of a real signal and noise. Then by a simple averaging of many trials one can reconstruct the real signal since the noisy part is diminished due to averaging. The authors also speculate about the possibility of extracting of the real signal from a frequency domain of the transformed measured signal. Such a simplicity of the method, however, does not necessary leads to a true result. In contrast, Tass shows in [59] models of possible interaction between neuronal populations and demonstrates that averaging is not always a clue to the problem. Among the models used, Tass employs a model of coupled phase oscillators. As we also have similar models, **we used his type of stimulation in both our models.**

Under direction of Tass and in collaboration with him many other different models in different areas of science were developed and a large variety of effective stimulations were applied. Thus, for example in [75] the authors apply a pulse stimulation to the system of chemical oscillators arranged over grid nodes of an 8 x 8 squared array. It is possible by means of the stimulation to suppress the synchrony level in the system. Different initial phases and protocols of the stimulation were tested. Another intelligent technique of a desynchronization of phase oscillators is proposed in [58]. Here the author demonstrates the benefits of using double-pulse stimulation, where the first pulse brings the system to some predefined state and the second impulse hits the system at the most appropriate moment. The concept of how to stimulate "intelligently" biological systems is to be found in [60]. Therein some algorithms of a stimulus application are discussed and illustrated.

Two other good examples of a stimulus application in oscillatory systems are described in [46] and [21]. The first article is devoted to a consideration of an ensemble of limit-cycle oscillators. Global coupling in the ensemble is introduced. Two different nonlinear stimulations using delayed feedback are considered: the individual case, where every oscillator is stimulated by its own stimulus; and the global case, where all oscillators are stimulated by a common stimulus. It is shown that the application of the proposed stimulations not only desynchronizes the ensemble, but forces every oscillator to return to its natural frequency (or close to it). The second article deals with two models: a system of phase oscillators

and a system of Morris-Lecar equations, modeling neurons from the subthalamic nucleus. The authors base their stimulation technique on the so-called slaving principle (see [19]). They stimulate the whole oscillator population through four stimulation sources (four electrodes) and by means of this divide all N oscillators into four subpopulations. The scientists showed that after such a procedure resynchronization takes a considerable amount of time in comparison to a simple stimulation by one electrode. Other examples of systems with delayed feedback can be found in physics [69, 47, 73, 50], lasers [70, 26, 13], neural networks [35, 74], biology [12, 11], and medicine [5, 55].

In chapter 4, we study transmission of a stimulus from one stimulated oscillator to another coupled to it, but not stimulated. In the literature there are several main approaches how to estimate a transmission time. One of them is based on the assumption, that peaks in averaged signals of both oscillators correspond to moments of maximal effect of a stimulation. Such an estimate we will call the average transmission time. The other approach the reader can find in [68]. In this paper, the author proposed to calculate some quantity which characterizes a system and is obtained using some information from a gliding window of measurements. The time τ of the centre of that window which maximizes the quantity above determines a transmission delay in the system. We call such an approach the correlation like estimate. As the last approach we shall use intensively in our work is a resetting transmission time estimate, which is introduced by Tass in [61]. Here the maximal effect of a stimulation is associated with the maximal reset of trials of each oscillator. The maximal reset of trials in its turn is determined by phase resetting analysis indices (see Appendix). The latter approach is robust with respect to parameter changes and reveals some interesting properties of a dynamical system considered (for details see chapter 4).

1.2   Outline of the thesis

The main goals of the dissertation are:
- to understand the dynamics of the models of phase oscillators using both analytical and numerical methods;
- to find out the effects of an external stimulation on the oscillators dynamics;
- to determine the role of a time delay in a system quantitatively and qualitatively;
- to test different approaches of the cross trial analysis in application to stimulation trials.
To fulfill these goals the thesis is divided into the following parts.
After the introduction (chapter 1), there are three main chapters in which two different systems of phase oscillators are considered. In chapters 2, 3 the system of two phase oscillators is presented. The interaction between the oscillators is

assumed to be instantaneous. However, each oscillator is influenced by a delayed self-feedback, which is present in a coupling term. The coupling with delayed self-feedback causes different dynamical regimes in the dynamics of the system. We give a short description of them. The system is investigated under the impact of a stimulation. The clustering phenomena are observed and their formation is explained. Moreover, the question of a possible effective reset by the stimulation is answered.

In the next chapter (chapter 4) a complementary system of two phase oscillators is presented. Complementary in the sense that now an interaction between oscillators takes place with a time delay. In contrast to the previous case each oscillator "feels" itself instantaneously. This system without stimulation was considered by Schuster and Wagner in [52]. The system again is subject to an external stimulation. Now only the first oscillator is stimulated. The transmission time of a stimulus to the second oscillator is investigated. Different cross-trail analysis techniques were used to determine this time.

After the three main chapters, we give an overview of possible prospects for the work dealt in the dissertation.

Discussion and conclusions complete the thesis.

Chapter 2

System of two phase oscillators coupled with delayed feedback: The dynamics

In this chapter we introduce a system of two phase oscillators coupled with a delayed feedback. The proposed system models some aspects of brain dynamics, namely the interaction of two neuronal populations in a brain, sending and receiving electrochemical signals to each other and the periphery. We are interested in this interaction because in a brain of patients suffering from Parkinson's disease such a situation hypothetically exists where two neuronal populations express some pathologic rhythmic activity. Our goal is to try to model this phenomenon, to understand the possible mechanisms behind it and, by means of an external stimulation of the system to eliminate the undesired activity. Therefore two chapters (including this) deal with the same model. In the second chapter, the theoretical effect of a stimulation is discussed, and this chapter contains results of the stimulation of the system from the first chapter, obtained during computer simulations.

The structure of the first chapter is as follows: we formulate a problem in the first section and derive an appropriate model. In the second section the dynamics in the proposed model is extensively described. In the first subsection of the second section, we study a general bifurcation scenario in the system when the coupling strength K grows. There is a wide variety of different dynamical regimes depending on the coupling value. As one of our main goals is to investigate a rhythmic activity in the system we specify for each of the regimes whether it is synchronous or desynchronous. So for the small coupling K desynchronous dynamics is preserved. After some threshold for K the first pair of phase-locked states appears through a saddle-node bifurcation. These phase-locked states belong to a special kind of limit cycle. One of them is stable and loses its stability via a Hopf bifurcation as the coupling increases further and thus a stable limit cycle comes into the dynamics of the system. The following pairs of phase-locked

states appear at larger coupling and the stable pairs in their turn undergo Hopf bifurcation. Finally with the growth of K stable limit cycles develop through a cascade of bifurcations to a chaotic attractor and chaotic synchronization is observed. At last the chaotic attractor undergoes crisis bifurcation and becomes desynchronous. Therefore for sufficiently large K the dynamics in the system surprisingly returns to the desynchronous state.

After the subsection describing the bifurcation scenario in the system, we concentrate our attention to phase-locked states. We show diagrams in the τ-K plane (τ is a delay in the system) in which the curves of the appearance of phase-locked states are depicted. Moreover, stability regions corresponding to each stable phase-locked state are plotted. For some parameters it was possible to find analytic results about phase-locked states. These results are formulated as theorems. The section ends with a review of which bifurcation mechanism causes the appearance-disappearance of phase-locked states depending on smooth changes of parameters K and τ.

The last subsection in the second section gives a comparison of two systems: two coupled phase oscillators (described above) and a system of two coupled limit-cycle oscillators. We consider in parallel a bifurcation scenario in both systems as a function of the coupling parameter K. We only compare phase dynamics of systems, neglecting the amplitude dynamics of coupled limit-cycle oscillators. Similarities are evident concerning the origin of phase-locked states and their further evolution via a Hopf bifurcation. The ways of developing to chaotic attractors in the two systems are different. Thus the system of two limit-cycle oscillators coupled with delay could serve as a prototype for our system of two phase oscillators coupled with delay in some interval of coupling K, but outside this interval the dynamics could be essentially different.

2.1 Derivation of the model

The main idea behind the consideration of the proposed system is to model the interaction between two neuronal populations in the brain which interact with each other and the peripheral nervous system. Similar models have been considered in [1], where large-scale feedback loops in the brain of human and rat are extensively studied. For example, Fig. 2.1(a),(b) gives a schematic representation of possible loops in the nervous system, which solve a simple task of maintaining of the muscles tone in a human being's elbow.

The main control parameter of the system is θ, which represents the absolute position of the joint. The whole scheme is based on a comparison principle. A descending command θ_0 on each step is compared in the block Δ with the feedback signal of the control parameter θ. The parameter θ is proportional to a position of the joint. As result of the comparison, the control signal $\pm G(\theta - \theta_0)$ is generated which imposes changes in θ according to the law $d\theta/dt = G(\theta - \theta_0)$

Figure 2.1: Feedback control in the spinal innervation of the muscles in a human being's elbow joint.

(see Fig.2.1(b)). In this way, the brain accomplishes the motor control task of keeping the absolute angle of the elbow joint at a certain value by means of closed neuronal loops.

We see that the variable θ is used both for generating a control task (θ_0) and for checking whether the results of the control task are fulfilled satisfactorily ($G(\theta - \theta_0)$). The whole system can be represented by a chain: brain-hand-brain. In our model, we consider a similar system where two loops brain-hand-brain (left and right ones) interact with each other and are supposed to fulfill their tasks of maintaining the muscle tone. We first denote $\psi_1 = \theta_1$ and $\psi_2 = \theta_2$ which

are control parameters of the left and right loops, respectively. If we assume that in an external loop signals ψ_1 and ψ_2 are not changed, but just return to the brain with a time delay then analogously to Fig.2.1(b) $\psi_1(t) = \theta_1^0(t), \psi_2(t) = \theta_2^0(t)$ and $\psi_1(t - \tau) = \theta_1(t), \psi_2(t - \tau) = \theta_2(t)$, where τ is the time delay.

Thus signals from both populations in the brain $\psi_1(t)$ and $\psi_2(t)$ are sent to a periphery (elbows), and afterwards return to the brain with some delay in the form $\psi_1(t - \tau)$ and $\psi_2(t - \tau)$. The other delay of interaction between the populations is considered to be negligibly small. In this way we consider the control law (the law how $\dot{\psi}_1$ and $\dot{\psi}_2$ change), which incorporates an instantaneous signal of the neighboring population and the delayed signal of the population itself. Such a system models parallel work of both elbows. For example a situation where a person holds a wooden beam horizontally matches our model. Schematic representation of the model is shown in Fig. 2.2.
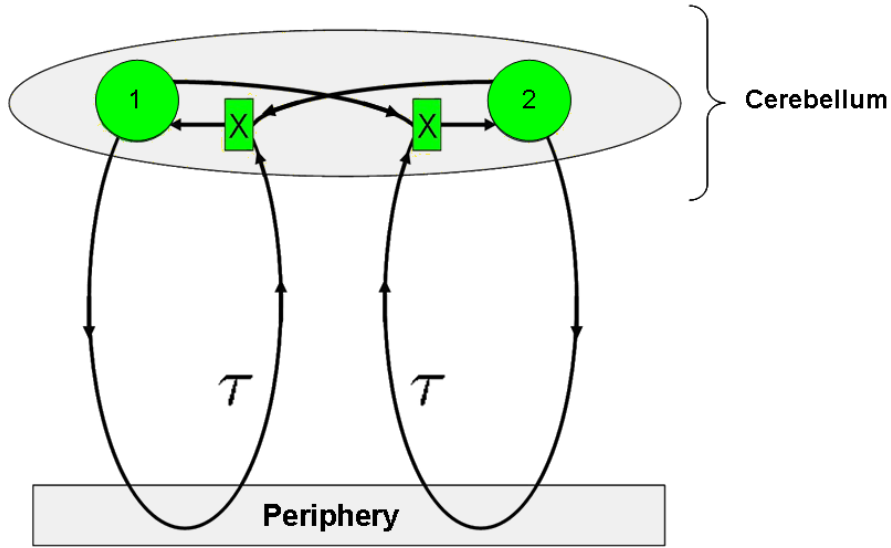

Figure 2.2: Scheme of interaction of two neuronal populations.

The "cross" blocks in Fig.2.2 denote the coupling between populations 1 and 2. The macroscopic dynamics of each population is modeled by a single phase oscillator. Thus we, consider a system of two coupled phase oscillators:

$$
\begin{cases}
\dot{\psi}_1(t) &= \omega_1 + \dfrac{K}{2} \sin[\psi_2(t) - \psi_1(t - \tau)] + X(t)I \cos(\psi_1(t) - \theta_1) + F_1(t), \\[2mm]
\dot{\psi}_2(t) &= \omega_2 + \dfrac{K}{2} \sin[\psi_1(t) - \psi_2(t - \tau)] + X(t)I \cos(\psi_2(t) - \theta_2) + F_2(t)
\end{cases}
$$

$$(2.1)$$

where K is a coupling parameter, ω_i, $i = 1, 2$ are natural frequencies of oscillators, τ is a time delay, and

$$S_i(t) = X(t)I\cos(\psi_i(t) - \theta_i) + F_i(t), \qquad (2.2)$$

$i = 1, 2$ are stimulation terms (see [57, 58]).

We study the response of system (2.1) to a strong external stimulation. Strong external stimuli are applied to each oscillator. Here, $X(t) = 1$ or 0 is a stimulus trigger controlling on- and offset of the stimulation, I is a stimulus intensity, θ_i are stimulation phase shifts, and $F_i(t)$ is a Gaussian δ-correlated noise with $\langle F_i(t) \rangle = 0$ and $\langle F_i(t)F_j(\tilde{t}) \rangle = D\delta_{ij}\delta(t - \tilde{t})$, where D is a constant noise amplitude.

Transient responses of coupled oscillators to pulsatile stimuli are relevant in several fields of the natural sciences. Such responses are typically studied by experimentalists to obtain information about dynamical systems and to characterize the system's inventory of reactions. For example, in neurology stimulus-evoked electroencephalography responses are a standard tool for diagnosis, where transient short-term brain responses evoked by sensory stimuli play a key role in the study of cerebral information processing and diagnosis [7].

2.2   Dynamics of the model: Bifurcation analysis

In this section, we explore the main dynamical regimes of the two phase oscillators coupled with delay (2.1) in the absence of stimulation.

In subsection 2.2.1, we explain the bifurcation mechanism of the delay-induced synchronization and desynchronization when the coupling strength between oscillators increases. We give numerical evidence of the coexistence of different stable synchronized regimes supported by phase-locked solutions (see below), limit cycles, or chaotic attractors, and determine the corresponding regions in the parameter space of the system (2.1).

Subsection 2.2.2 contains a detailed analysis of the appearance of phase-locked states in the system. We investigate here the structure of the parameter regions of stable phase-locked states of system (2.1) and, following smooth parameter changes (K or τ), describe bifurcations resulting in the appearance and disappearance of phase-locked states.

In the last subsection 2.2.3, we compare in detail the dynamics of two phase oscillators (2.1) with the dynamics of two coupled limit-cycle oscillators (2.33). We show that a system of two limit-cycle oscillators coupled with delay could serve as a prototype for our system of two phase oscillators coupled with delay in some interval of coupling K, but outside this interval the dynamics could be essentially different.

2.2.1 Coupled phase oscillators.

In this subsection we discuss a general bifurcation scenario in system (2.1) when the coupling strength K grows and a stimulation is not applied ($X(t) = 0$, $\forall t \geq 0$). For a further analysis, additionally to the phase variables ψ_j, we introduce a phase difference φ_1 and a mean phase φ_2:

$$\begin{cases} \varphi_1(t) &= \psi_2(t) - \psi_1(t), \\ \varphi_2(t) &= (\psi_2(t) + \psi_1(t))/2, \end{cases} \tag{2.3}$$

so that system (2.1) without the stimulation reads

$$\begin{cases} \dot{\varphi}_1(t) &= \Delta_1 - K \sin\left(\dfrac{\varphi_1(t) + \varphi_1(t-\tau)}{2}\right) \cos(\varphi_2(t) - \varphi_2(t-\tau)), \\ \dot{\varphi}_2(t) &= \Delta_2 + \dfrac{K}{2} \cos\left(\dfrac{\varphi_1(t) + \varphi_1(t-\tau)}{2}\right) \sin(\varphi_2(t) - \varphi_2(t-\tau)). \end{cases} \tag{2.4}$$

Here, $\Delta_1 = \omega_2 - \omega_1$ is a natural frequency mismatch, and $\Delta_2 = (\omega_2 + \omega_1)/2$ is a mean natural frequency. In the uncoupled regime for $K = 0$ each phase ψ_j grows with its own frequency ω_j such that the phase difference $\varphi_1(t)$ has the frequency Δ_1.

As the coupling strength grows in the system different dynamical regimes appear in the dynamics. An exemplary one dimensional bifurcation diagram is plotted in Fig.2.3(a) where the phase difference φ_1 is shown versus K. Here stable/unstable dynamical states are depicted by solid/dashed lines, correspondingly. In the diagram phase-locked states (fixed points [see below]) appear at saddle-node bifurcations at K_{sn}, K'_{sn}, the stable ones bifurcate via Hopf bifurcations at K_H, K'_H. At K big enough chaos comes into the system. For $K < K_{sn}$ and for K big enough there are desynchronous oscillations. For further details please read the current section up to the end.

We extensively use the following definition of a phase synchronization given in [41] (chapter 4, formula (4.1)):

Definition 2.1 *We say that two oscillators (2.1) are* synchronized *if for their phases $\psi_1(t), \psi_2(t)$ holds $|\varphi_1(t)| = |\psi_2(t) - \psi_1(t)| < $ C, where C is some constant.*

A desynchronous dynamics, where the phase difference φ_1 exhibits unbounded rotations, is preserved in system (2.4) for small values of K provided that $\Delta_1 \neq 0$. In what follows we will use the notion of a phase-locked state, which one finds in the book [41] (chapter 3, formula 3.1).

Definition 2.2 *A solution $(\varphi_1(t), \varphi_2(t))$ of system (2.4) is called a phase-locked state if the phase difference φ_1 is constant and if the mean phase φ_2 grows linearly with the frequency Ω (Ω is constant):*

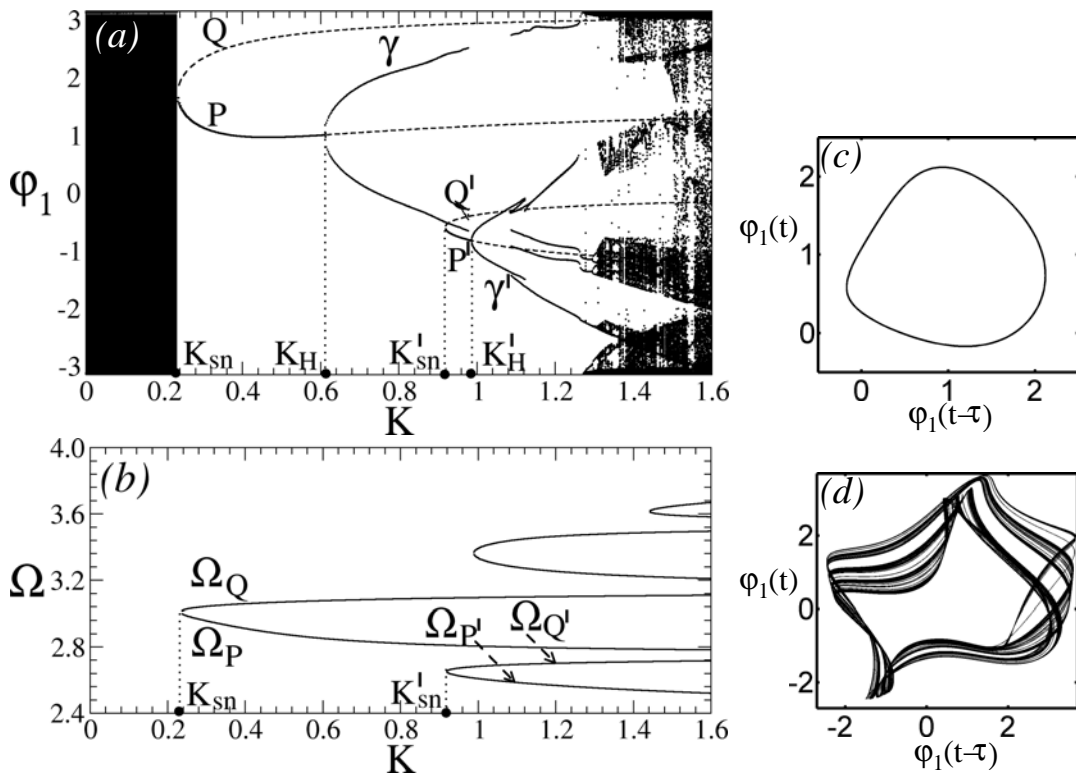$$\varphi_1(t) = \varphi_1^* = \text{const}, \quad \varphi_2(t) = \Omega t + \text{Const.} \tag{2.5}$$

Figure 2.3: (a) Dynamical regimes of the phase difference φ_1 in system (2.4) versus the coupling strength K. When the coupling increases, system (2.4) undergoes a sequence of bifurcation transitions from the desynchronization via stable phase-locked and periodically modulated synchronized states to the chaotic phase synchronization and, finally, to the desynchronization again. The stable and unstable phase-locked states are depicted by solid and dashed curves, respectively. For oscillatory regimes (limit cycles and chaotic attractors) only local maxima and minima of trajectories are plotted. K_{sn}, K'_{sn} and K_H, K'_H are the bifurcation values of K of the saddle-node (sn) and Hopf (H) bifurcations.
(b) Corresponding frequencies Ω of the phase-locked states (2.5) versus K.
In plots (c) and (d) examples of limit-cycle oscillations for $K = 0.8$ and a chaotic attractor for $K = 1.34$ are shown in the $(\varphi_1(t - \tau), \varphi_1(t))$-phase space, respectively. Parameters $\Delta_1 = 0.2$, $\Delta_2 = 3.0$, and $\tau = 4.0$.

We also call the phase-locked states *fixed points* denoted by (φ_1^*, Ω). Evidently if the oscillators (2.1) are in a phase-locked state they are synchronized.

As shown in Fig. 2.3(a), when the coupling parameter K increases, a stable phase-locked state P and a saddle phase-locked state Q are born in a saddle-node bifurcation (see below) at $K = K_{sn}$, where $K_{sn} \approx 0.235$ in Fig. 2.3(a).

The birth of the phase-locked states P and Q is induced by an emergence

of a pair of frequencies Ω_P and Ω_Q see Fig. 2.3(b). According to Eq. (2.5), Ω_P and Ω_Q are the mean frequencies of the two oscillators (2.1) in the phase-locked states P and Q, respectively. Numerical evidence suggests that the fixed point P is stable for $K \in (K_{sn}, K_H)$, where at $K_H \approx 0.61$ a Hopf bifurcation occurs [Fig. 2.3(a)]. At $K = K_H$ the fixed point P looses its stability and a stable limit cycle γ emerges [Figs. 2.3(a) and 2.3(c)]. After the bifurcation, the phase difference $\varphi_1(t)$ of trajectories attracted by γ is not constant any more and exhibits periodic oscillations. It is still bounded and, thus, a regime of *a periodically modulated phase synchronization* is established in system (2.1).

The number of different fixed points (φ_1^*, Ω) grows as the parameter K increases. For example, after the emergence of the first pair of frequencies Ω_P and Ω_Q corresponding to the phase-locked states P and Q, the second pair $\Omega_{P'}$ and $\Omega_{Q'}$ appears at $K = K'_{sn} \approx 0.92$ giving birth to a new stable phase-locked state P' and a saddle phase-locked state Q' of system (2.1) [Figs. 2.3(a) and 2.3(b)]. The fixed point P' is stable for $K \in (K'_{sn}, K'_H)$ and loses its stability with increasing K at $K = K'_H \approx 0.985$ via a Hopf bifurcation. In this bifurcation a stable limit cycle γ' emerges [Fig. 2.3(a)]. With a further increase of the coupling new pairs of stable and saddle phase-locked states appear. The stable phase-locked states exist in narrow intervals of the parameter K values, and bifurcate with increasing K via a supercritical Hopf bifurcations, lose their stability, and give birth to stable limit cycles.

At larger values of K the periodic motion in system (2.4) turns into a chaotic motion [Fig. 2.3(a) and 2.3(d)]. The phase difference φ_1 still remains bounded, which indicates an emergence of *a chaotic phase synchronization* according to the definition in Ref. [49]. Further, if K reaches some critical value $K = K_{cr}$, an attractor of the chaotic phase synchronization undergoes a crisis and the system (2.1) returns to a desynchronized state, where the phase difference $\varphi_1(t)$ displays unbounded rotations [Fig. 2.3(a)].

Stable phase-locked states of system (2.1) may coexist, leading to multistability. This takes place when the next stable phase-locked state, say P', is born before the previously emerged phase-locked state, say P, loses its stability via a Hopf bifurcation. An example of two coexisting stable phase-locked states is illustrated in Fig. 2.4.

Here, both states P and P' are in-phase locked states with $\varphi_1^* = 0$ with different frequencies $\Omega_P = 5.12$ and $\Omega_{P'} = 3.96$, respectively. Both states are realized in system (2.1) for the same parameter values but for different initial conditions.

The multistability phenomenon emerges in system (2.1) not only between stable phase-locked states, but also between other synchronous and desynchronous states. For instance, in Fig. 2.3(a) one can see that the stable fixed point P' can coexist with the stable limit cycle γ and also two stable limit cycles γ, and γ' can coexist.

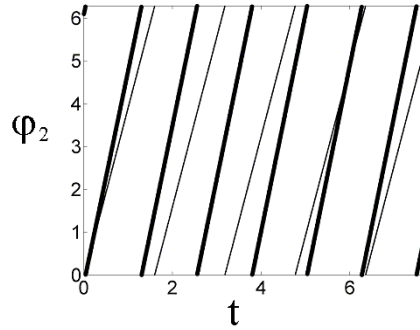For some other set of parameter values, a stable desynchronous dynamics,

Figure 2.4: Coexistence of two stable in-phase-locked states P and P' with the same phase difference $\varphi_1^* \equiv 0$, but with the different frequencies $\Omega_P = 5.12$ and $\Omega_{P'} = 3.96$, respectively. Time courses of the mean phase φ_2 are shown for stable states P (bold line) and P' (thin line). Parameters $\Delta_1 = 0.0$, $\Delta_2 = 4.5$, $\tau = 1.4$, and $K = 1.6$.

where the phase difference φ_1 exhibits unbounded rotations, and a stable synchronous state with bounded φ_1 can coexist in system (2.1), as illustrated in Fig. 2.5. A region in (τ, K)-parameter plane, where a stable synchronous state coexists with a stable desynchronous limit cycle is depicted in Fig. 2.5(a). The lowest curve corresponds to the moment of the birth of a stable phase-locked state P. As K increases this point then bifurcates into a stable synchronous limit cycle γ via a Hopf bifurcation (middle curve). For parameter values of the gray region between the "Phase-locking" and the "Desynchronization" curves, system (2.1) displays a stable synchronized motion, where the phase difference φ_1 is bounded.

On the other hand, the hatched region corresponds to parameter values, where a stable desynchronous limit cycle μ exists, characterized by unbounded rotations of φ_1 on the torus. An example of the stable fixed point P coexisting with the stable desynchronous limit cycle μ is illustrated in Fig. 2.5(b) for parameter values indicated by the point A in Fig. 2.5(a). Depending on initial conditions, system (2.1) displays one or the other stable dynamics.

In sections 3.2, 3.3, 3.4 we study responses of system (2.1) under stimulation in the following four dynamical regimes: *(i)* a single stable phase-locked state (section 3.2), *(ii)* a stable, periodically modulated synchronization (section 3.3), *(iii)* bistability of two phase-locked states, and *(iv)* a regime of bistability of a phase-locked state and a desynchronous limit cycle (section 3.4).

For the stable phase-locked state we explore the intertrial clustering of the oscillators' responses emerging during in- and post-stimulus transients. Optimal parameter values are detected, where a recovery time (i.e. a duration) of the
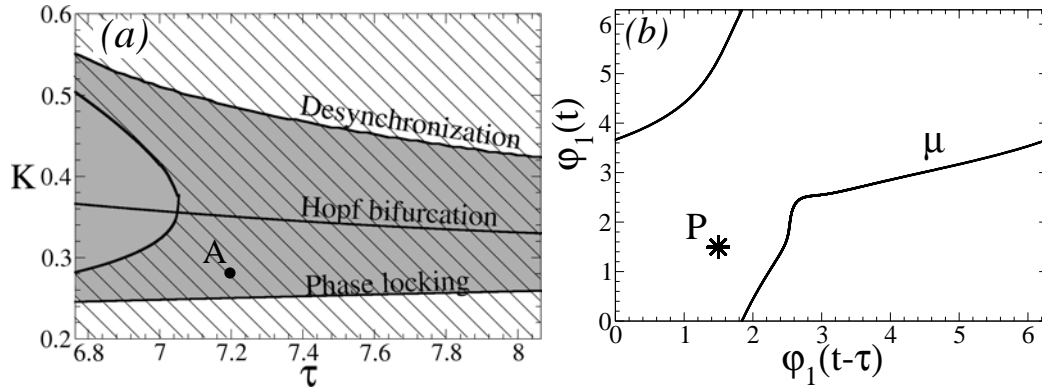
Figure 2.5: Coexistence of stable synchronized and desynchronized states.
(a) The bifurcation diagram in (τ,K)-parameter plane. The gray and hatched regions correspond to an existence of stable synchronized and desynchronized states, respectively.
(b) Example of the coexistence of the stable desynchronous limit cycle μ and the stable phase-locked state P (asterisk) for parameters $K = 0.28$ and $\tau = 7.2$ indicated by the point A in (a). Other parameters $\Delta_1 = 0.2$ and $\Delta_2 = 0.1$.

post-stimulus transient gets maximal. We also uncover the mechanism of such a maximal transient. For the periodically modulated synchronized state we analyze the post-stimulus transient and compare it with that of the phase-locked state. Finally, for the stimulated multistable regimes we provide an evidence of a stimulus-induced switching between synchronized and desynchronized motions.

2.2.2 Phase-locked states

In the previous subsection we gave a brief review of the main dynamical regimes in our system. The purpose of this subsection is to investigate under which conditions phase-locked states appear in the system, to determine their stability, to describe bifurcations which occur if we change the main parameters K and τ. In the first part we classify fixed points of system (2.1) and describe a structure of their stability regions in (τ, K) plane. The second part contains a detailed study of bifurcation mechanisms causing appearance, loss of stability and disappearance of fixed points.

2.2.2.1 Stability regions of stable phase-locked states in K-τ plane.

Substituting expressions defining a phase-locked state (2.5) into Eqs. (2.4) of the initial system in variables φ_1, φ_2, and solving them for φ_1^* and Ω one obtains that phase-locked states of system (2.1) have the following coordinate φ_1^*

$$\varphi_1^* = \begin{bmatrix} \arcsin\left[\dfrac{\Delta_1}{K\cos(\Omega\tau)}\right] \\ \pi - \arcsin\left[\dfrac{\Delta_1}{K\cos(\Omega\tau)}\right] \end{bmatrix} \,, \text{ with } \varphi_2^* = \Omega t + \text{Const}, \qquad (2.6)$$

where the mean frequency Ω is determined by the following transcendental equation:

$$f(\Omega) := -\Omega + \Delta_2 \pm \frac{K}{2}\sin(\Omega\tau)\sqrt{1 - \frac{\Delta_1^2}{K^2\cos^2(\Omega\tau)}} = 0. \qquad (2.7)$$

Later we will refer to the branch of $f(\Omega)$ with the plus sign at the term starting with K as $f^+(\Omega)$ and to the branch with the minus sign as $f^-(\Omega)$, correspondingly. In this way, any frequency Ω found from Eq. (2.7) defines a single phase-locked state with φ_1^* of the form (2.6), where the first and the second values in the expression for φ_1^* correspond to the sign "+" and "-" in Eq. (2.7), respectively. We also call solutions (2.6) of system (2.4) fixed points or steady states because the phase difference $\varphi_1(t) = \varphi_1^*$ remains constant. Note that the mean phase φ_2 can also be constant only for the case $\Delta_2 = 0$, where the trivial solutions $\Omega = 0$ of Eq. (2.7) exists for $K \geq \Delta_1$. Only under this condition, system (2.1) can exhibit an oscillation death, where both phases would stop to rotate if they were attracted by a steady-state solution (2.6) with $\Omega = 0$.

A detailed analysis of Eq. (2.7) shows that an increase of the coupling K or the delay τ leads to an emergence of new solutions Ω and, as a result, to the emergence of new fixed points (2.6) [see also Ref. [52]]. To illustrate the existence of multiple solutions of Eq. (2.7) the graphs of the function $f(\Omega)$ are shown in Fig. 2.6(a) for a few values of K. One can see that with increasing K new solutions of Eq. (2.7) appear in pairs, where the loops of the graphs, first, touch and then intersect the zero axis $f(\Omega) = 0$ in two points which are solutions of Eq. (2.7). This is caused by increase of the "amplitude" of loops, which is induced by an increase of K. On the other hand, for a given K, an increase of delay τ results in an increase of the "frequency" of the loops, where the number of loops increases with increasing τ. This leads to the appearance of new intersections of the graphs with the zero axis and, as a result, to the emergence of new phase-locked states of system (2.1).

Each new frequency Ω gives birth to a new phase-locked state (2.6). Since the frequencies emerge in pairs, the same also holds for the phase-locked states. In other words, the fixed points (2.6) appear in pairs via saddle-node bifurcations as parameter K increases. This process is illustrated in Figs. 2.6(b) and 2.6(c), where the frequencies Ω, solutions of Eq. (2.7), and coordinates φ_1^* of the corresponding fixed points (2.6) are depicted versus K, respectively. As numerical evidence suggests, in saddle-node bifurcations one stable and one unstable fixed
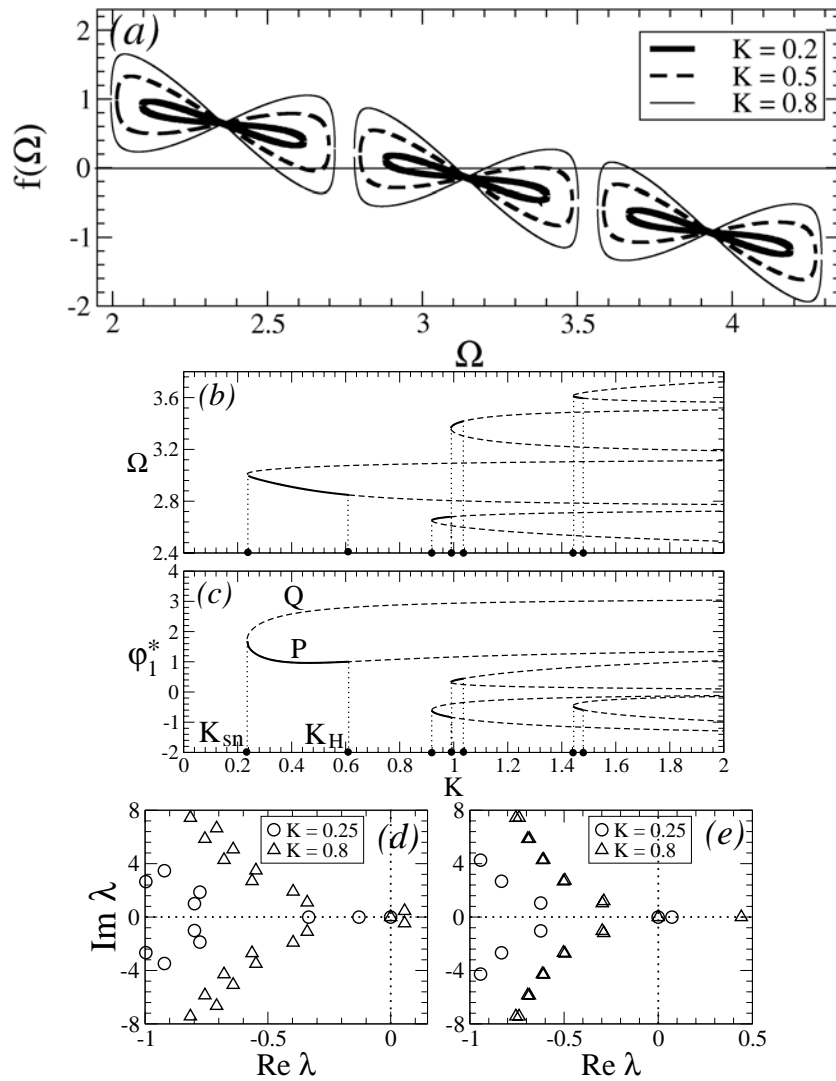
Figure 2.6: Phase-locked states of system (2.1). (a) Graphs of the function $f(\Omega)$ (2.7) for three values of K. (b),(c) Phase-locked states (Ω, φ_1^*) of system 2.1 appears in pairs. Stable ones are depicted by bold lines, unstable- by dashed lines. (d),(e) Eigenvalues for the fixed point P, Q, respectively. Eigenvalues are shown for two coupling strength $K = 0.25$ and $K = 0.8$. Parameters $\Delta_1 = 0.2$, $\Delta_2 = 3$, and $\tau = 4$.

points are born [Fig. 2.11].

We address a stability issue of the fixed point with the use of the linear stability theory [20, 2]. For this, we consider a characteristic equation for fixed points (2.6) of system (2.4). We follow the equation (4.2) on the page 17 in [20] (see also Lemmas and Theorems there after)

$$\det[\lambda I - A - Be^{-\lambda\tau}] = 0, \tag{2.8}$$

where I is the identity matrix, and A and B are the Jacobian matrices of Eq. (2.4) with respect to the instant and delayed variables, accordingly. Solutions λ of Eq. (2.8) are complex eigenvalues of the corresponding fixed points. The signs of real parts of λ determine the stability of the fixed points such that a fixed point is stable if all its eigenvalues have negative real parts. If a fixed point has an eigenvalue with a positive real part, it is unstable [2]. Calculating the matrices A and B in Eq. (2.8) on the coordinates (φ_1^*, Ω) of fixed points (2.6) we obtain the following characteristic equation:

$$\begin{aligned}\lambda^2 + \ & K\cos(\varphi_1^*)\cos(\Omega\tau)\lambda e^{-\lambda\tau} + \\ & \frac{K^2}{4}\cos(\Omega\tau - \varphi_1^*)\cos(\Omega\tau + \varphi_1^*)(e^{-2\lambda\tau} - 1) = 0.\end{aligned} \tag{2.9}$$

One can see that $\lambda = 0$ always is a solution of Eq. (2.9). However, this eigenvalue is connected with an invariance of phase-locked states (2.6) with respect to a constant shift in the variable φ_2, and, thus, it does not influence the stability of the fixed points. The other solutions of Eq. (2.9) can be calculated numerically.

Let us consider, for example, the first pair of the fixed points, denoted by P and Q, which are born in the first saddle-node bifurcation as K grows. For the parameter values as in Fig. 2.6 the bifurcation takes place at $K = K_{sn} \approx 0.236$ [Fig. 2.6(b) and 2.6(c)]. We found that P is stable and the other fixed point Q is unstable. Just after the bifurcation, the stable fixed point has three real eigenvalues: one eigenvalue is zero and the other two are negative [circles in Fig. 2.6(d) for $K = 0.25$]. The remaining eigenvalues (infinitely many) are complex conjugate with negative real parts.

The unstable fixed point Q is of a saddle-focus type having one real positive eigenvalue, one zero eigenvalue (see above), and the others are complex conjugate with negative real parts [circles Fig. 2.6(e) for $K = 0.25$]. With further increase of the coupling strength K, the two negative real eigenvalues of P approach each other, meet, diverge from the real axis, and become complex conjugate with negative real parts. Further, these eigenvalues cross imaginary axis at $K = K_H \approx 0.61$, and attain positive real parts. Therefore, the fixed point P undergoes Hopf bifurcation at $K = K_H$ and becomes an unstable focus. The eigenvalues of the fixed points P and Q after the bifurcation are depicted for $K = 0.8$ by triangle marks in Fig. 2.6(d) and Fig. 2.6(e), respectively.

The same bifurcation scenario takes place for other fixed points emerging in consecutive saddle-node bifurcations as K further increases. The newly-born stable fixed points, have the corresponding K-intervals of stability, after they undergo Hopf bifurcations and become unstable foci. The intervals of stability of a few fixed points are indicated in Figs. 2.6(b) and 2.6(c) by the bold solid curves and the vertical dotted lines. One can see that these intervals shrink in size and

become smaller for each next pair of fixed points born for larger K. In particular, the stability intervals are difficult to resolve with the resolution in Figs. 2.6(b) and 2.6(c) already for the third, the fourth, etc. pairs of fixed points.

To explore a structure of stable phase-locked states of system (2.1) we calculate regions of stability of fixed points (2.6) versus the parameters τ and K. The stability regions are shown in Fig. 2.7.

The whole complicated set of parameters (τ, K), where system (2.1) has stable phase-locked states can be classified into infinitely many separated regions which are depicted by gray of different intensity in Fig. 2.7(a).

A single stability region is depicted in Fig. 2.7(b). Its shape strongly resembles the form of stability regions of periodic cycles in cubic and quadratic two-dimensional maps called *swallows or shrimps* [36, 14]. However, the novelty and difference of the "swallows" shown in Fig. 2.7(b) is that *(i)* they represent stability regions of phase-locked states of the system of two coupled phase oscillators with delay and *(ii)* their individual structure and their global arrangement with respect to each other are different from those observed in maps.

The lowest curve in Fig.2.7(b) represents the appearance of a pair of fixed points in the τ-K plane resulting from saddle-node bifurcations which occur in the system (2.1). For $\tau = \dfrac{3}{2}T$ and $K = \Delta_1$ the point (τ, K) (the lowest point of the "swallow") belongs this curve.

Definition 2.3 *For each "swallow" and $\forall \tau_f$ fixed $\exists K_c$ that K_c is infimum on K of all points which belong to the "swallow". These points (τ_f, K_c) form curves which are called* swallow birth curves. *The points (τ_v, K_v) $(\tau_v = \dfrac{T}{2}n$, $n \in Z$ and $K_v = \Delta_1)$ belong to the swallow birth curves and we will refer to them as to the* vertexes of the "swallows" *(see diagram Fig.2.7(a),(b)).*

To find a moment of bifurcation (parameters τ and K) we need to find those parameters when maxima or minima of f touch Ω-axis. Then one needs to solve the following system of equations:

$$\begin{cases} f(\Omega) & = 0, \\ f'(\Omega) & = 0. \end{cases} \tag{2.10}$$

Its solutions (if there are some) are points of a birth of new pairs of phase-locked states. Thus we get sufficient condition of the appearance of phase-locked states belonging to the swallow birth curves. If we solve first the second of Eqs.(2.10) and find its solutions Ω_f and substitute them into the first of Eqs.(2.10) then the latter will be the equation defining the swallow birth curves. Doing this, after some algebra we end up with the following equation for the extrema of f:

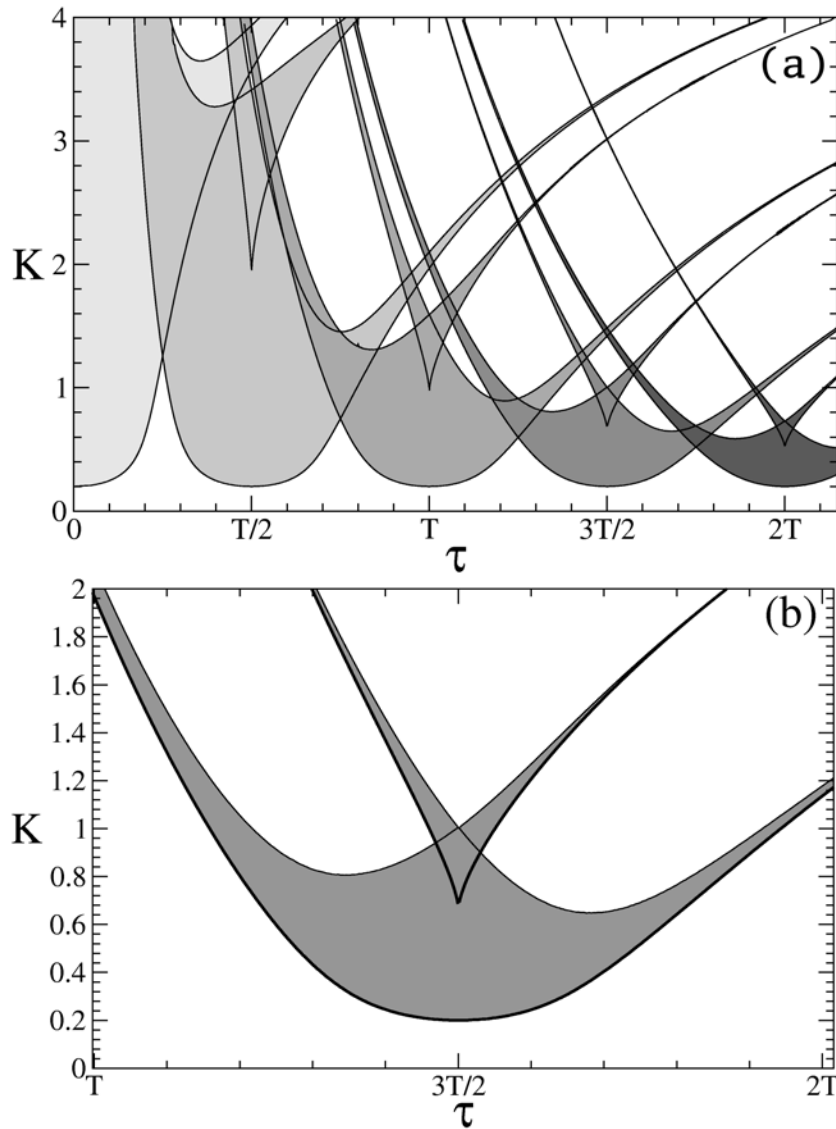$$t^4 K^4 - t^3 K^4 - t^2 K^2 \Delta_1^2 + \Delta_1^2 = 0, \tag{2.11}$$

Figure 2.7: (a) The first five "swallows" of stability regions' family are shown. Each region of the same color starts from below with a curve of a birth of a stable phase-locked state and is bounded from above with a curve, when stable fixed point loses its stability. (b) One exemplary "swallow" is shown in details. Parameters $\Delta_1 = 0.2$, $\Delta_2 = 3.0$.

where $t = \cos^2(\Omega\tau)$. As it is known the equation of forth degree could always be solved analytically. Since analytics in this case is too cumbersome, we just remark that in the general case solutions Ω_f could be derived analytically and, thus, we could get at least implicit equation for parameters of the appearance of stable phase-locked states.

Instead we find a good approximate solution of this problem. The following theorem is valid:

Theorem 2.1 *Let $g(\Omega) = f(\Omega) + \Omega - \Delta_2$, where f is defined by Eq. (2.7). Let Ω_f denote an exact solution of the Eq. (2.10) which corresponds to some of the phase-locked states belonging to one of the swallow birth curves. Then there exists a solution Ω_g of the equation $g'(\Omega) = 0$ which approximates Ω_f, satisfying the estimate:*

$$|\Omega_g - \Omega_f| \leq \frac{1}{\tau} \left| \arccos\left(\frac{\Delta_1}{K}\right) - \arccos\left(\sqrt{\frac{\Delta_1}{K}}\right) \right|. \qquad (2.12)$$

Using this theorem, we build approximate swallow birth curves in the following way: we find Ω_g, which are solutions of $g' = 0$, and after that substitute them into the first of Eqs.(2.10) and get formula $f(\Omega_g) = 0$. Having done this we obtain that the approximate curves are written:

$$\tau = \frac{\left(\pm \cos^{-1}\left(\sqrt{\frac{\Delta_1}{K}}\right) + \pi n\right)}{\pm \frac{\Delta_1 - K}{2} - \Delta_2}, \qquad (2.13)$$

where $n \in \mathbb{Z}$. In Fig.2.8 for the first five "swallows" we compare the approximate curves from (2.13) (inner dashed curves) with the numerically determined ones (solid curves).

Proof: To prove the fact stated in the theorem, we need first to consider the properties of functions f and g. The function g reads

$$g(\Omega) := \pm \frac{K}{2} \sin(\Omega\tau)\sqrt{1 - \frac{\Delta_1^2}{K^2 \cos^2(\Omega\tau)}}. \qquad (2.14)$$

Later we will refer to the branch of $g(\Omega)$ with the plus sign at the coupling term K as $g^+(\Omega)$ and to the branch with the minus sign as $g^-(\Omega)$, correspondingly. Evident is that $g(\Omega)$ is periodic with period $2\pi/\tau$. The branch g^- is shifted on π/τ in comparison to g^+. Indeed $-\sin((\Omega + \pi/\tau)\tau) = \sin(\Omega\tau)$. So to gain a full information about $g^+ = 0$ one could consider it together with g^- on a half-period interval. Also g^+ and g^- are symmetric around abscissa $\Omega = 0$ what implies $g^- = -g^+$. This also means that maximal points of g^+ are minimal point of g^- and vice versa. And absolute values of corresponding maximum and minimum are equal. The domain of definition of g are those intervals of Ω where under-root expression is non-negative. This give us
$\Omega \in [(-\arccos(\Delta_1/K) + \pi n)/\tau; (\arccos(\Delta_1/K) + \pi n)/\tau] \cup$
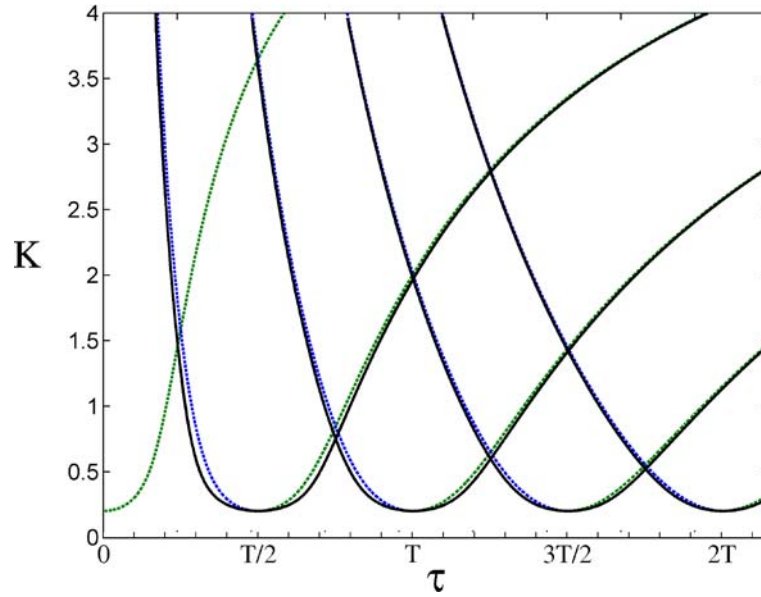
Figure 2.8: An analytical approximation of the swallows birth curves. The black solid curves represent experimental values. The green and blue curves are approximate values. Parameters $\Delta_1 = 0.2$, $\Delta_2 = 3.0$.

$$[(-\arccos(\Delta_1/K) + \pi(n+1))/\tau; (\arccos(\Delta_1/K) + \pi(n+1))/\tau],$$

n is any even integer ($n \in 2\mathbb{Z}$). For every n a junction of two intervals above gives a whole one-period interval of Ω. As we consider both branches of the g only on a half-period interval we put for simplicity $n = 0$ and take just the first interval from domain: $[-\arccos(\Delta_1/K)/\tau; \arccos(\Delta_1/K)/\tau]$. Then in this interval the function g^+ crosses $\Omega = 0$ axis at the points $\Omega_l = -\arccos(\Delta_1/K)/\tau$, $\Omega_z = 0$, $\Omega_l = -\arccos(\Delta_1/K)/\tau$, where letters l, c and r denote left, center and right, correspondingly. For $\Omega \in (\Omega_l; \Omega_c)$ and $\Omega \in (\Omega_c; \Omega_r)$ g^+ (g^-) preserve its sign. At the central point $g^+{}'(\Omega_c) > 0$ ($g^-{}'(\Omega_c) < 0$), what means g^+ increases (g^- decreases) in the central point (see equation for $g'(\Omega)$ below).

$$g'(\Omega) = \pm \frac{K\tau(K^2\cos^4(\Omega\tau) - \Delta_1^2)}{2K^2\cos^3(\Omega\tau)\sqrt{1 - \Delta_1^2/(K^2\cos^2(\Omega\tau))}} \tag{2.15}$$

Moreover, in each interval $(\Omega_l; \Omega_c)$ and $(\Omega_c; \Omega_r)$ there exists exactly one solution of equation $g^+{}'(\Omega) = 0$ ($g^-{}'(\Omega) = 0$) which gives us extremal points of g^+ (g^-). Taking into consideration that on the ends of interval $[\Omega_l; \Omega_c]$ $g^+(.) = 0$ and at the center it is increasing then an extremum in this interval is a minimum (for g^- maximum). In a similar way in the interval $[\Omega_c; \Omega_r]$ function g^+ has a maximum (g^- has a minimum). The graphs of the both branches of g are shown in Fig. 2.9 and join each other in the horizontal "eight". For example g^+ starts at Ω_l, goes down to the minimum and after that increases up to the maximum

passing through zero at Ω_c. From the maximum the function decreases again and is zero at Ω_r.
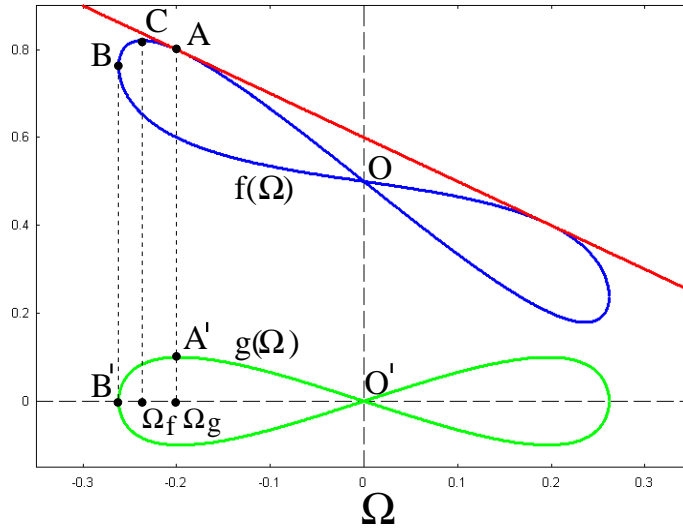

Figure 2.9: Two "eights" are depicted, which are the graphs of the functions $f(\Omega)$ and $g(\Omega)$. The invariant in abscissa points are shown: centers O and O' coincide in abscissa, the length of both "eights" is the same (points B and B' lie on the same vertical line), extremal points of $g(\Omega)$ are also abscissa of the tangent points (points A and A') of $f(\Omega)$ with the lines $l(\Omega) = -\Omega + \Delta_2 \pm (K/2 - \Delta_1/2)$ (one of these lines is depicted in red). Parameters $\Delta_1 = 0.2$, $\Delta_2 = 0.5$, $\tau = 4.0$ and $K = 0.4$.

Let us denote a minimal point of g^+ by Ω^+_{min} and its maximal point Ω^+_{max}. Analogously Ω^-_{min} and Ω^-_{max} are minimal and the maximal points of g^-. It is true that $\Omega^-_{min} > \Omega^+_{min}$ and $\Omega^-_{max} < \Omega^+_{max}$, $g^+(\Omega^+_{min}) = g^-(\Omega^-_{min})$ and $g^+(\Omega^+_{max}) = g^-(\Omega^-_{max})$. For every point $g(\Omega)$ it is valid that $f(\Omega) = -\Omega + \Delta_2 + g(\Omega)$, where for Ω with upper index $+$ is taken the function g^+, and for Ω with upper index $-$ - the function g^-, respectively. Then for all four extremal points of g we have:

$$
\begin{aligned}
f(\Omega^-_{min}) &= -\Omega^-_{min} + \Delta_2 + g(\Omega^-_{min}) \\
f(\Omega^+_{min}) &= -\Omega^+_{min} + \Delta_2 + g(\Omega^+_{min}) \\
f(\Omega^-_{max}) &= -\Omega^-_{max} + \Delta_2 + g(\Omega^-_{max}) \\
f(\Omega^+_{max}) &= -\Omega^+_{max} + \Delta_2 + g(\Omega^+_{max})
\end{aligned}
\tag{2.16}
$$

and we have that $f(\Omega^-_{min}) < f(\Omega^+_{min}) < f(\Omega^+_{max}) < f(\Omega^-_{max})$. Now we come back to the primary problem to find solutions of the equation $f(\Omega) = 0$, which denote an appearance of phase-locked states belonging the swallow birth curves. At these points extrema of f touches abscissa. Points $f(\Omega^+_{min})$ and $f(\Omega^+_{max})$ would not touch it before the other two points $f(\Omega^-_{min})$ and $f(\Omega^-_{max})$ would do

(see the relationship between them above). So they could give birth only to the second or further pairs of phase-locked states which can not be on the any of the swallow birth curves, and, thus, we exclude these two points from the further consideration.

Let function f attain the maximal value at some Ω_f, $\Omega_f \in [\Omega_l; \Omega_r]$. For every Ω is true: $g(\Omega) \leq g(\Omega^+_{max})$, where $g(\Omega^+_{max}) = K/2 - \Delta_1/2$. Let us take the upper line $l_g(\Omega) = K/2 - \Delta_1/2$, which bounds horizontal "eight". It is true that $g(\Omega) \leq l_g(\Omega)$, $\forall \Omega \in [\Omega_l; \Omega_r]$. Then $g(\Omega) + \Omega - \Delta_2 = f(\Omega) \leq l_f(\Omega) = l_g(\Omega) + \Omega - \Delta_2$ and function $f(\Omega)$ is under the line $l_f(\Omega)$, which again bounds the whole inclined "eight" (see Fig. 2.9). It holds that $l_f(\Omega_c) > l_f(\Omega)$, $\forall \Omega \in (\Omega_c; \Omega_r]$ and $l_f(\Omega^-_{max}) = f(\Omega^-_{max}) > l_f(\Omega_c)$. The last inequalities mean that the maximal point lies somewhere in $[\Omega_l; \Omega_c)$. Moreover as $f'(\Omega^-_{max}) = -1 < 0$ and f is smooth, then Ω_f lies to the left from Ω^-_{max}. The domain of definition of f is the same like for g and function f is defined at Ω_l as at the most left point. We call $\Omega^-_{max} = \Omega_g$, substitute the value of Ω^-_{max} (which immediately follows from Eq. 2.15), and get the following formula:

$$|\Omega_g - \Omega_f| \leq \frac{1}{\tau} \left| \arccos\left(\frac{\Delta_1}{K}\right) - \arccos\left(\sqrt{\frac{\Delta_1}{K}}\right) \right|. \tag{2.17}$$

As one can see $\Omega_g \to \Omega_f$ as $K \to \infty$ or $\tau \to \infty$.

An estimate for a minimal point of $f(\Omega)$ is obtained in a similar way. On the next half-period interval graphs of g^+ and g^- interchange and extremal points of g^+ will play a role of estimates of some other Ω_f. The theorem is proved.

It is possible to find Ω_f and its φ_1^*, i.e. to determine phase-locked states analytically, for some certain pairs of (τ, K). The following theorem solves this problem for the minimal points of the swallow birth curves (see Fig.2.7).

Theorem 2.2 *For $\tau = \dfrac{Tn}{2}, n = 0, 1, \ldots$ and $|K| \geq |\Delta_1|$ in the dynamics of system (2.4) two phase-locked states $S=(\varphi_1^S, \Omega_S)$ and $R=(\varphi_1^R, \Omega_R)$ exist. Here $\Omega_S = \Omega_R = \Delta_2$ and $\varphi_1^S = (-1)^n \arcsin[\Delta_1/K]$ and $\varphi_1^R = \pi - (-1)^n \arcsin[\Delta_1/K]$. Furthermore for n even S is stable for $K \in [\Delta_1, K_{pf}]$ and for n odd R is stable for $K \in [\Delta_1, K_{pf}]$, where K_{pf} is given by the following formula:*

$$K_{pf} = \sqrt{\frac{4}{\tau^2} + \Delta_1^2}. \tag{2.18}$$

The fixed point R is unstable for n even, and the fixed point S is unstable for n odd.

Proof: We remark first that $\tau = \dfrac{Tn}{2} = \dfrac{2\pi}{\Delta_2} \dfrac{n}{2} = \pi n$. To check if Ω_S and Ω_R are solutions of Eq. (2.7) we put $\Omega = \Delta_2$ and substitute all other parameters into

it. Then noting $\tau\Omega = \pi n$ and $\cos(\pi n) = (-1)^n$ we have:

$$f(\Delta_2) := -\Delta_2 + \Delta_2 \pm \frac{K}{2}\sin(\pi n)\sqrt{1 - \frac{\Delta_1^2}{K^2(-1)^{2n}}}. \tag{2.19}$$

and thus Δ_2 are solutions of f^+ and f^-, what implies an existence of two phase-locked states S and R with the same frequency for $|K| \geq |\Delta_1|$. Moreover, it is easy to see that Eq. (2.7) has no solutions for $|K| < |\Delta_1|$ and for any $\tau \geq 0$. Therefore, with increasing $|K|$ from zero, the very first pair of the phase-locked states (2.6) S and R emerges. Substituting the values of the frequencies Ω_S and Ω_R into 2.6 we obtain the phase differences φ_1 of these states $\varphi_1^S = (-1)^n\arcsin\left[\Delta_1/K\right]$ and $\varphi_1^R = \pi - (-1)^n\arcsin\left[\Delta_1/K\right]$. Existence of the phase-locked states mentioned in the theorem is proved.

To investigate their stability we consider characteristic equation 2.9 computed using coordinates of the phase-locked states and parameters as in the theorem:

$$\lambda^2 + \ K\cos(\varphi_1^*)(-1)^n\lambda e^{-\lambda\tau} + \frac{K^2}{4}\cos^2(\varphi_1^*)(e^{-2\lambda\tau} - 1) = 0. \tag{2.20}$$

The further analysis we provide in the case $\Delta_1 \geq 0$ and $K \geq 0$. The other cases can be treated with the same arguments used below. We see that equation 2.20 is dependent on a value of n. So in following we consider two cases n is even and n is odd. It is so that for both n (even and odd) $\cos(\varphi_1^S) \geq 0$ and $\cos(\varphi_1^R) \leq 0$.

For the case n is even the characteristic equation is split into two:

$$\left[\begin{array}{ll} \lambda & = -\dfrac{K}{2}\cos(\varphi_1^*)(e^{-\lambda\tau} + 1), \\ \lambda & = -\dfrac{K}{2}\cos(\varphi_1^*)(e^{-\lambda\tau} - 1). \end{array}\right. \tag{2.21}$$

For the case n is odd the characteristic equation also is split into two:

$$\left[\begin{array}{ll} \lambda & = \dfrac{K}{2}\cos(\varphi_1^*)(e^{-\lambda\tau} + 1), \\ \lambda & = \dfrac{K}{2}\cos(\varphi_1^*)(e^{-\lambda\tau} - 1). \end{array}\right. \tag{2.22}$$

From now on we consider the case n is even only. The case n is odd is treated analogously.

Representing complex variable λ as $\lambda = x + iy$, where $x, y \in \mathrm{R}^1$, we rewrite the first of the two complex variable equations (2.21) as a system of two real variable equations:

$$\left\{\begin{array}{ll} x & = -\dfrac{K}{2}\cos(\varphi_1^*)(e^{-x\tau}\cos(y\tau) + 1), \\ y & = \dfrac{K}{2}\cos(\varphi_1^*)e^{-x\tau}\sin(y\tau). \end{array}\right. \tag{2.23}$$

If we now examine stability of the fixed point S and remember $\cos(\varphi_1^S) \geq 0$ we obtain that for all $x \geq 0$ and any K r.h.s. of the first of Eqs. (2.23) is non-positive. Indeed for $x \geq 0$ $e^{-x\tau}\cos(y\tau) + 1 \geq 0$ and stated above becomes true for any $K \geq 0$. So no eigenvalue with positive real part for the phase-locked state S satisfies the first of Eqs. (2.21).

Now we show that from the second equation of Eqs. (2.21) for the phase-locked state S an eigenvalue with a positive real part can exist only from $K \geq K_{pf}$. For this we rewrite this equation as a system of two real variable equations:

$$\begin{cases} x & = -\dfrac{K}{2}\cos(\varphi_1^*)(e^{-x\tau}\cos(y\tau) - 1), \\ y & = \dfrac{K}{2}\cos(\varphi_1^*)e^{-x\tau}\sin(y\tau). \end{cases} \tag{2.24}$$

The fixed point S can lose stability via two scenario:
a) one real eigenvalue crosses the imaginary axis, in this case $y = 0$ holds;
b) two complex conjugated eigenvalues cross the imaginary axis.
Consider first the case a). $y = 0$ satisfies the second equation of Eqs. (2.24). We denote $h(x) = 2x + K\cos(\varphi_1^*)(e^{-x\tau} - 1)$ and then the first of Eqs. (2.24) becomes $h(x) = 0$. The last equation has always a trivial root $x = 0$. To find other possible roots we need to analyze the function $h(x)$. Its extremal points are solutions of $h'(x) = 0$ so we have:

$$h'(x) = 2 - \tau K\cos(\varphi_1^*)e^{-x\tau} = 0 \tag{2.25}$$

and an extremal point is $x_* = -\dfrac{1}{\tau}\ln\dfrac{2}{\tau K\cos(\varphi_1^*)}$. The point x_* is a minimal point of $h(x)$ because $h''(x_*) > 0$. Moreover:

$$h(x_*) = -\dfrac{2}{\tau}\ln\dfrac{2}{\tau K\cos(\varphi_1^*)} + \dfrac{2}{\tau} - K\cos(\varphi_1^*) \leq 0 \tag{2.26}$$

The last inequality is equivalent to $1 + \ln(x) \leq x$ which is a standard one. So the minimum of $h(x)$ lies below or on the line $x = 0$. The position of x_* provides an answer how many roots the equation $h(x) = 0$ has. Thus if $x_* < 0$ there is one negative root besides the trivial root. If $x_* > 0$ there is one positive root besides the trivial root. This means that the phase-locked state S loses its stability. At $x_* = 0$ $h(x_*) = 0$ and there is no root except the trivial one. So the value $x_* = 0$ is critical, after which S loses its stability. To find K_{pf} one needs to solve the equation $x_* = -\dfrac{1}{\tau}\ln\dfrac{2}{\tau K\cos(\varphi_1^*)} = 0$. This results in the equation:

$$\dfrac{2}{\tau K\cos(\varphi_1^*)} = 1 \tag{2.27}$$

Remembering that $\varphi_1^S = (-1)^n\arcsin\left[\Delta_1/K\right]$ and that n is even we come to the following equation:

$$K\sqrt{1 - \frac{\Delta_1^2}{K^2}} = \frac{2}{\tau} \qquad (2.28)$$

and finally we have:

$$K_{pf} = \sqrt{\frac{4}{\tau^2} + \Delta_1^2} \qquad (2.29)$$

Therefore for $K > K_{pf}$ $x_* > 0$ and S loses stability.

Now we return to the case b) where S could lose its stability by means of a couple of complex conjugate eigenvalues crossing the imaginary axis. To check this we substitute into the second of Eqs. (2.24) $x = 0$ and try to find a non-trivial solution for $y > 0$:

$$y = \frac{K}{2}\cos(\varphi_1^*)\sin(y\tau) \qquad (2.30)$$

Let us consider the function $w(y) = y - \frac{K}{2}\cos(\varphi_1^*)\sin(y\tau)$. The equation Eq. (2.30) has more than one solution (non-trivial solution) if the function w(y) is non-monotonic and has extrema. It is true because $w(y) = 0$ is equivalent to Eq. (2.30) and $w(0) = 0$. The extrema of $w(y)$ are determined by $w' = 0$:

$$1 - \frac{K\tau}{2}\cos(\varphi_1^*)\cos(y\tau) = 0 \quad \text{or} \quad \cos(y\tau) = \frac{2}{K\tau\cos(\varphi_1^*)} \qquad (2.31)$$

The last equation imposes a constraint $\frac{2}{K\tau\cos(\varphi_1^*)} \leq 0$. If we compare it to Eq. (2.27) we immediately get that the constraint above means $K \geq K_{pf}$. So we come to the conclusion that for the Eq. (2.30) to have a non-trivial solution the coupling should be at least $K = K_{pf}$. Summarizing we see that the fixed point S does not lose its stability either via scenario a) or b) before coupling strength reaches K_{pf}.

If we now examine the stability of the fixed point R and remember $\cos(\varphi_1^R) \leq 0$ we obtain that the r.h.s. of the first of Eqs. (2.23) is nonnegative. So x could be only equal or greater then zero. If we consider just the case $y = 0$ then even schematic graphs of the functions $-\frac{K}{2}\cos(\varphi_1^*)(e^{-x\tau} + 1)$ and x and their monotonicity reveal a presence of a non-trivial solution $x > 0$ for $K > \Delta_1$.

The case n is odd is treated in a similar manner. The theorem is proved.

2.2.2.2 The bifurcation mechanisms of the birth and destabilization of the phase-locked states.

In this part of the current subsection we explore in detail the bifurcation mechanisms of the birth and the destabilization of phase-locked states of system
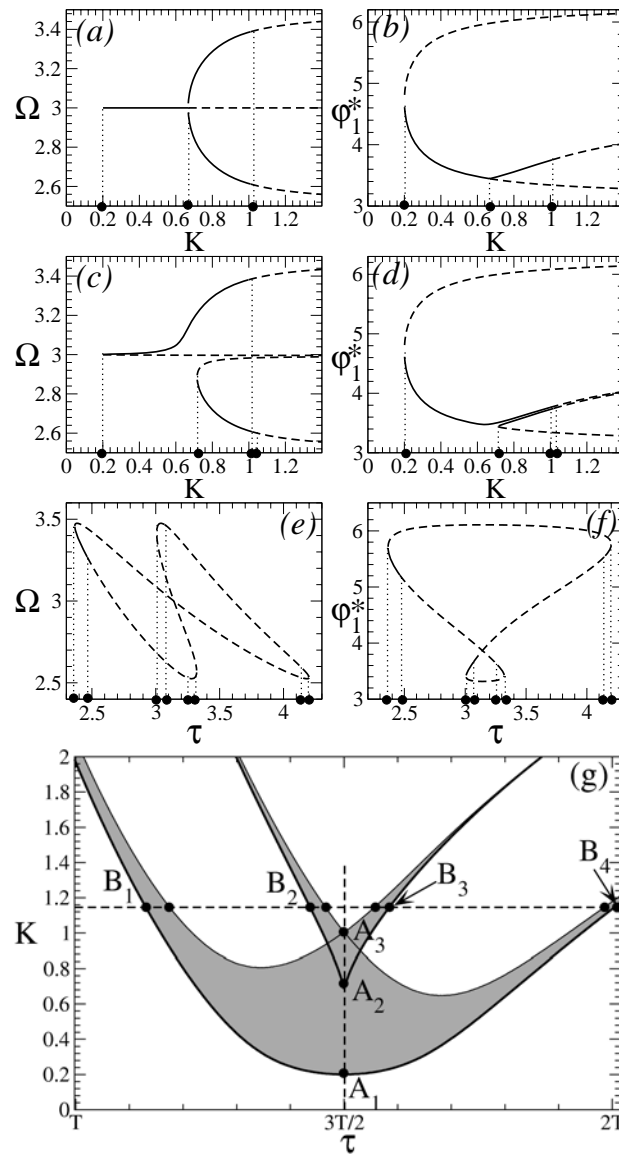
Figure 2.10: A few one-parameter bifurcation diagrams for Ω (left column) and φ_1^* (right column) versus parameters K and τ are shown. Stable and unstable phase-locked states depicted by black solid and dashed curves, respectively. (a),(b) K is changed from 0 to 1.4 for fixed $\tau = 3T/2 = \pi$. (c),(d) K is changed from 0 to 1.4 for fixed $\tau = 3.18 > \pi$. (e),(f) τ is changed from 2.2 o 4.2 for fixed $K = 1.15$. (g): one of the "swallows" (with the vertex $\tau = \frac{3}{2}T$ and $K = \Delta_1$) is shown. The lines A_1A_3 and B_1B_4 demonstrate how parameters K and τ are varied in (a),(b) and (e),(f), respectively. The other parameters $\Delta_1 = 0.2$ and $\Delta_2 = 3.0$.

(2.1). For this, we describe the bifurcations which occur at the entering or leaving the "swallow" stability regions.

In Fig. 2.10, a few one-parameter bifurcation diagrams are shown, which correspond to various parameter pathways crossing the "swallow" region in different places as indicated by the dashed lines in Fig. 2.10(g). The first pair of bifurcation diagrams is plotted in Figs.2.10(a),(b) for fixed $\tau = \pi$ and varying $K \in (0, 1.4)$ [line $A_1 A_3$ in Fig. 2.10(g)]. For the case $\Delta_2 = 3.0$ the value of τ is $\tau = \pi = 3T/2$, where $T = 2\pi/\Delta_2$ is the mean period of system (2.1) without coupling ($K = 0$). The second pair of diagrams is plotted in Figs.2.10(c),(d) for fixed $\tau = 3.148$ and varying $K \in (0, 1.4)$ [not shown in Fig. 2.10(g)]. The latter calculation is performed to show how the bifurcation scenario changes if the values of the parameter τ slightly differ from the former, "special" value of $\tau = \pi = 3T/2$. The third pair of diagrams is plotted in Figs.2.10(e),(f) for the fixed $K = 1.15$ and varying $\tau \in (2.2, 4.2)$ [line $B_1 B_4$ in Fig. 2.10(g)]. For all three parameter scans we only consider the fixed points connected with the "swallow" shown in Fig. 2.10(g). The other fixed points which the system (2.4) can have for these parameter values will be ignored.

For the first run for fixed $\tau = 3T/2 = \pi$, the bifurcation diagrams are shown in Fig. 2.10(a) and 2.10(b), where the frequencies Ω and coordinates φ_1^* of the fixed points (2.6) are depicted versus K, respectively. To find the first bifurcation moment as K increases, we substitute $\tau = 3T/2 = 3\pi/\Delta_2$ into Eq. (2.7). Then one finds that for $K \geq \Delta_1$ Eq. (2.7) has two solutions $\Omega_S = \Omega_R = \Delta_2$ (see the theorem 2.2). So we found that the fixed point S is born stable for even $n = 0, 2, 4, \ldots$, whereas the fixed point R is born stable for odd $n = 1, 3, 5, \ldots$. Further, the corresponding fixed point remains stable for $K \in (K_{sn}, K_{pf})$, where $K_{sn} = \Delta_1$, as mentioned above. Substituting the corresponding values of the delay $\tau = \pi n/\Delta_2$, $n = 0, 1, 2, \ldots$ into the equation for K_{pf}, we obtain the bifurcation values of $K = K_{pf}$, where the corresponding phase-locked state S (for even n) or R (for odd n) loses its stability (e.g., $K_{pf} \approx 0.66$ in Fig. 2.10(a) and 2.10(b)). This value of $K = K_{pf}$ defines the K-coordinate of the point A_2 in Fig. 2.7(b).

At the bifurcation at $K = K_{pf}$, a real negative eigenvalue of the stable fixed point S (or R) crosses zero and becomes positive. The fixed point undergoes a pitchfork bifurcation and loses its stability, and two new phase-locked states, denoted by S' and R', are born. These newly-born states are depicted in Fig. 2.10(a) and 2.10(b) for $K > K_{pf}$. Note that S' and R' have different frequencies $\Omega_{S'}$ and $\Omega_{R'}$ symmetrically located with respect to $\Omega = \Delta_2$ [Fig. 2.10(a)]. On the other hand, the φ_1-coordinates of S' and R' are the same [Fig. 2.10(b)], which also follows from Eq. (2.6) provided that $|\Omega_{S'} - \Delta_2| = |\Omega_{R'} - \Delta_2|$ and $\tau = \pi n/\Delta_2$. Depending on the initial conditions, the trajectories of system (2.4) will be attracted to the stable phase-locked state S' or R' exhibiting the same φ_1 but rotating with

distinct frequencies $\Omega_{S'}$ or $\Omega_{R'}$, respectively.

If the coupling K further increases, the fixed points S' and R' also lose their stability. This takes place at $K = K_H$, where two complex conjugate eigenvalues of each point S' and R' cross the imaginary axis and attain positive real parts. For parameter values as in Fig. 2.10(a) and 2.10(b), $K_H \approx 1.0$ defines the K-coordinate of the point A_3 in Fig. 2.7(b). At $K = K_H$, the fixed points S' and R' simultaneously undergo supercritical Hopf bifurcations and two stable limit cycles are born. After the bifurcation the phase difference $\varphi_1(t)$, attracted by the stable limit cycle, exhibits periodic oscillations and remains bounded.

The occurrence of the pitchfork bifurcation in system (2.4) is strongly connected to the particular values of $\tau = Tn/2$, $n = 0, 1, 2, \ldots$. The bifurcation scenario described above will change for other values of τ, where the pitchfork bifurcation will be replaced by a generic saddle-node bifurcation. This is illustrated in Fig. 2.10(c) and 2.10(d), where one-parameter bifurcation diagrams are presented for fixed $\tau = 3.148$ and varying K. One can see that two fixed points, denote the stable fixed point P and unstable fixed point Q, are born at $K = K_{sn} \approx 0.21$ in a saddle-node bifurcation. These fixed points correspond to the fixed points R and S above. The difference is that P and Q already have distinct frequencies Ω_P and Ω_Q, respectively [Fig. 2.10(c)].

With increasing K, the stable fixed point P does not destabilize via a pitchfork bifurcation [like R does as shown above, see Fig. 2.10(b)], but remains stable up to the moment of a Hopf bifurcation at $K = K_H \approx 0.998$. Instead of the pitchfork bifurcation, a saddle-node bifurcation occurs at $K = K'_{sn} \approx 0.72$, where an unstable Q' and a stable P' fixed points are born [Fig. 2.10(c) and 2.10(d)]. The latter is then stable up to $K = K'_H \approx 1.16$, where it undergoes a Hopf bifurcation in its turn. With even larger deviations of τ from $Tn/2$, $n = 0, 1, 2, \ldots$, the bifurcation sequence of the phase-locked states attains the form as illustrated in Fig. 2.6. With increasing K, an unstable and a stable phase-locked states emerge in pairs via saddle-node bifurcations, and then the stable states lose their stability via Hopf bifurcations.

Following the evolution (birth, (de)stabilization, and disappearance) of phase-locked states connected with the "swallow" region shown in Fig. 2.10(g), we perform the third parameter scan for the fixed $K = 1.15$ and varying τ [line B_1B_4 in Fig. 2.10(g)]. The evolutions of the frequencies Ω and the phase differences φ_1^* of the corresponding phase-locked states are illustrated in one-parameter bifurcation diagrams in Fig. 2.10(e) and 2.10(f) versus τ, respectively. With increasing delay τ, the scanning (K, τ)-parameter point enters the "swallow" through the point B_1 [Fig. 2.10(g)], where two fixed points, one stable P and one unstable Q are born via a saddle-node bifurcation at $\tau = \tau_{sn} \approx 2.366$ [Fig. 2.10(e) and 2.10(f)]. The fixed point P then loses its stability via a supercritical Hopf bifurcation at $\tau = \tau_H \approx 2.463$, where the scanning parameter point leaves the left "wing" of

the "swallow" region. After the bifurcation, the parameters are located out of the stability region and both fixed points are unstable.

With further increase of τ the next pair of the fixed points, stable P' and unstable Q', emerges via a saddle-node bifurcation at $\tau = \tau'_{sn} \approx 3.01$. At this moment the scanning parameter point enters the "swallow" through the point B_2 of the left branch of the "tail" [Fig. 2.10(g)]. The fixed point P' is stable up to $\tau = \tau'_H \approx 3.07$, where it undergoes supercritical Hopf bifurcation corresponding to the moment, where the scanning parameter point leaves the left branch of the "swallow's tail".

The fixed points P, Q, P', and Q' of the system (2.4) can exist only for parameter values within the inner domain of the "swallow" region confined between the left and right "wings" of the "swallow" [Fig. 2.7(b)]. More precisely, all four points exist only for parameter values within the inner domain of the "swallow's tail" confined between left and right branches of the it. This is illustrated in Fig. 2.10(e) and 2.10(f), where the interconnections between the fixed points are shown.

With increasing τ the fixed point P stabilizes via an inverse supercritical Hopf bifurcation, approaches Q' and then both fixed points meet and annihilate in inverse saddle-node bifurcation. These bifurcations take place when the point (K, τ) first enters the right branch of the "tail" and then escapes from it through point B_3 [Fig. 2.10(g)]. The analogous bifurcations take place for the remaining fixed points Q and P' with the further increase of τ: P' gets stabilized in its turn via an inverse Hopf bifurcation and then the fixed points Q and P' meet and disappear in inverse saddle-node bifurcation. These bifurcations take place when the scanning parameter point first enters the right "wing" of the "swallow" and then escapes from it through point B_4 [Fig. 2.10(g)]. None of the fixed points above exists out of the inner domain of the "swallow".

2.2.3 Coupled limit-cycle oscillators

Looking for a generalization of the system of two coupled phase oscillators (2.1) we come to the following system of two coupled limit-cycle oscillators:

$$
\begin{cases}
\dot{Z}_1(t) \;=\; (a_1 + i\omega_1 - |Z_1(t)|^2)Z_1(t) \;+\; \dfrac{K}{2}Z_1(t)Z_2(t)Z_1^*(t-\tau), \\[4mm]
\dot{Z}_2(t) \;=\; (a_2 + i\omega_2 - |Z_2(t)|^2)Z_2(t) \;+\; \dfrac{K}{2}Z_2(t)Z_1(t)Z_2^*(t-\tau).
\end{cases}
\tag{2.32}
$$

Here, Z_1, Z_2 are complex variables. The first part of the right-hand side is a normal form of the supercritical Hopf bifurcation ([29]). The second part starting from $\frac{K}{2}$ is a coupling in the system. In the absence of the coupling, i.e., $K = 0$, Z_j uniformly rotate over circles with radii $\sqrt{a_j}$ and with natural frequencies ω_j. The coupling term consists of a cubic non-linearity where instantaneous signals

of both oscillators are multiplied by a delayed feedback signal of the oscillator itself. The asterisk denotes complex conjugacy.

We have chosen such a special form of the non-linearity because the phase dynamics of the two limit-cycle oscillators will be similar to the one of the system (2.1). In polar coordinates the complex variable of each oscillator can be rewritten as: $Z_j(t) = R_j(t)e^{i\psi_j(t)}$, where $R_j(t)$ denotes the amplitude, $\psi_j(t)$ is the phase. If we write the above system in new coordinates we get for the first oscillator:

$$\begin{cases} \dot{R}_1 &= (a_1 - R_1^2)R_1 + \dfrac{K}{2}R_1R_2R_1(t-\tau)\cos[\psi_2(t) - \psi_1(t-\tau)] \\ \dot{\psi}_1 &= \omega_1 + \dfrac{K}{2}R_2R_1(t-\tau)\sin[\psi_2(t) - \psi_1(t-\tau)] \end{cases} \tag{2.33}$$

The equation for the phase ψ_1 repeats in its form the one for the first phase oscillator from Eqs. (2.1). However, in the equations 2.33 amplitudes of both oscillators additionally amplify the coupling strength K. Therefore, the phase dynamics of the two systems (2.1) and (2.33) can be equivalent if $R_1 = \text{const}$ and $R_2 = \text{const}$. Assuming that the amplitudes $R_j(t)$ of the limit-cycle oscillators remain constant or close to that, one can neglect the amplitude dynamics and consider the phase equations only. The latter then attain the form (2.1). However, the above assumption does not hold always and the amplitudes play an essential role in the dynamics of system (2.32). Nevertheless, as we show below, the system of two coupled limit-cycle oscillators reflects essential dynamical features of the system of two coupled phase oscillators.

In Fig. 2.11, one-parameter bifurcation diagrams of systems (2.32) [Fig. 2.11(a)] and (2.1) [Fig. 2.11(b)] are presented. More precisely, the local extrema (maxima and minima) of the trajectories $\varphi_1(t)$, $t > 0$ considered on the interval $[-\pi, \pi]$ (mod 2π) are depicted versus the coupling parameter K. Analyzing the diagrams one concludes that two coupled oscillators of both systems remain desynchronized for small values of the coupling parameter $0 \leq K < K_{sn}$, which is because of the different natural frequencies. With increasing K, a saddle-node bifurcation occurs at $K = K_{sn}$ [$K_{sn} \approx 0.235$ in Fig. 2.11], where a stable phase-locked state is born. One can see in Fig. 2.11 that for $K \in (K_{sn}, K_H)$ [$K_H \approx 0.58$ in Fig. 2.11(a) and $K_H \approx 0.6$ in Fig. 2.11(b)] the phase difference $\varphi_1(t)$ approaches stationary regimes of phase-locked states in systems (2.32) and (2.1).

Further, the phase-locked states lose their stability at $K = K_H$ (K_H as above) via a Hopf bifurcation and stable limit cycles are born. The phase difference periodically oscillates and remains bounded. Therefore, the systems of coupled phase and limit-cycle oscillators exhibit regimes of the periodically modulated phase synchronization.

The limit cycles of the phase difference φ_1 undergo a series of bifurcations as K increases, which are different for systems (2.32) and (2.1) (see the diagrams in Figs. 2.11(a) and 2.11(b)). For example, in system (2.32), the limit cycle undergoes a cascade of period-doubling bifurcation [Fig. 2.11(a), range of $K \in$
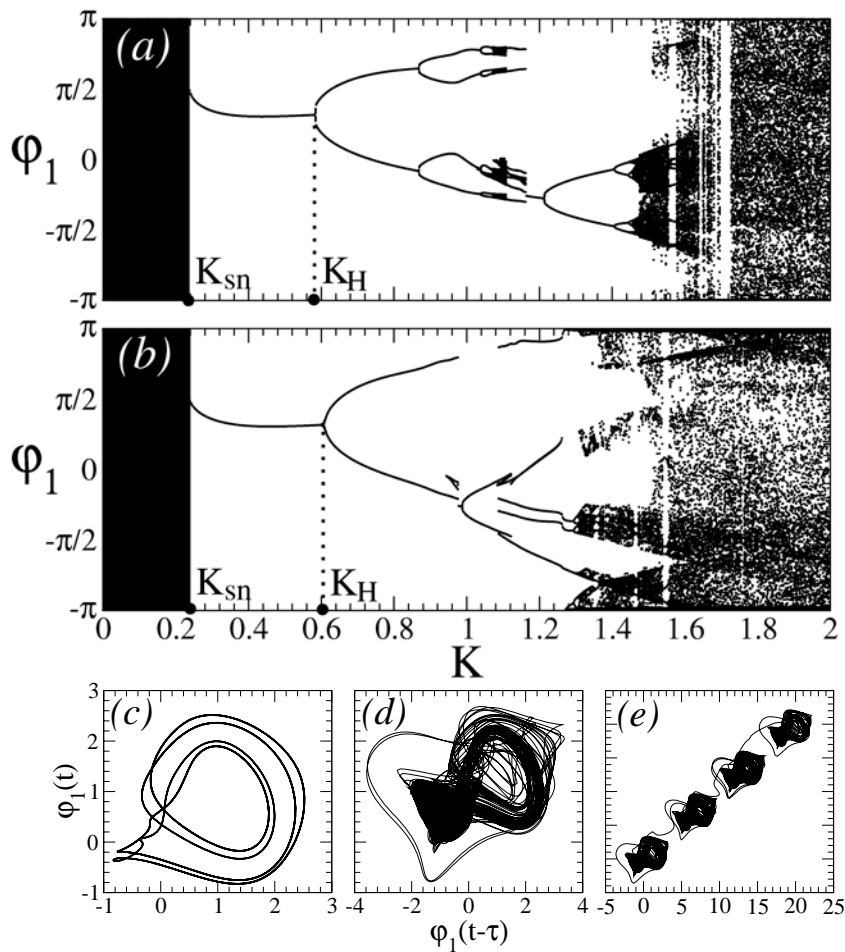
Figure 2.11: Attracting states of (a) system (2.32) and (b) system (2.1) are depicted in the phase difference variable $\varphi_1 = \psi_2 - \psi_1$ versus the coupling parameter K. The only local maxima and minima of the trajectories $\varphi_1(t)$ are plotted after a skipped transient. K_{sn} and K_H denote parameter K values of the saddle-node and the Hopf bifurcations of phase-locked states, respectively. In (c)-(e) attractors of system (2.32) are shown in $(\varphi_1(t - \tau), \varphi_1(t))$-plane for (c) $K = 1.02$, (d) $K = 1.58$, and (e) $K = 1.6$. System (2.32) is simulated using the amplitude (R_1 and R_2) and phase (ψ_1 and ψ_2) variables. Parameters $\tau = 4.0$, $\Delta_1 = 0.2$, $\Delta_2 = 3.0$.

$(0.8, 1.2)$] transforming into a chaotic attractor. The "period-4" limit cycle of system (2.32) born after the second period-doubling bifurcation is depicted in Fig. 2.11(c) for $K = 1.02$. In the phase dynamics given by system (2.1) there are no corresponding bifurcations of period-doubling cascade [Fig. 2.11(b)].

Nevertheless, as K further increases, both systems exhibit a similar jump in the φ_1 variable to a stable phase-locked state at $K \approx 1.164$ in Fig. 2.11(a) and at

$K \approx 0.978$ in Fig. 2.11(b). This indicates that one stable state of the periodically modulated phase synchronization and one stable phase-locked state can coexist. The latter, in its turn, undergoes a Hopf bifurcation and loses its stability as K increases. The newly born limit cycle initiates a cascade of period-doubling bifurcations in both system and a chaotic attractor is born.

An example of the chaotic attractor in system (2.32) is illustrated in Fig. 2.11(d) for $K = 1.58$. One can see that, in-spite of a chaotic dynamics of the phase difference φ_1, it remains bounded. Therefore, a regime of the chaotic phase synchronization takes place. A similar regime of the chaotic phase synchronization is observed in the coupled phase oscillators.

The next important bifurcation transition takes place in the system of coupled limit-cycle oscillators as well as in the system of coupled phase oscillators when the coupling grows again. The chaotic attractor undergoes a boundary crisis and the phase difference starts to exhibit unbounded rotations. This indicates an onset of the desynchronization in both systems. An example of desynchronized dynamics in system (2.32) is illustrated in Fig. 2.11(e) for $K = 1.6$.

Summarizing to this moment, we note that the impact of the delayed feedback in the form (2.32) on the dynamics of coupled oscillators has a twofold effect. On the one hand, the coupling between the oscillators leads to the synchronization and a stable phase-locked state emerges for an intermediate range of the coupling strength. On the other hand, if the coupling strength increases further, the phase-locked states lose stability via Hopf bifurcations giving birth to states of the periodically modulated phase synchronization and then to the chaotic phase synchronization. The latter undergoes crisis bifurcation at a larger value of the coupling parameter and the coupled oscillators desynchronize. Such synchronization-desynchronization transitions take place in the system of the coupled limit-cycles oscillators (2.32) as well as in the system of the coupled phase oscillators (2.1).

In what follows, we focus on the dynamics of system (2.1). The next chapter answers the question how the stimulation effects our model. There it will be shown that a strong and sufficiently long stimulus resets phases of both oscillators. Moreover, the stimulation causes clustering of trials; hence the stimulation enables switching between stable regimes in multistable cases.

Chapter 3

Stimulation in different regimes

This chapter describes the results of a stimulation of system (2.1) in different dynamical regimes. By means of the stimulation we model a situation where two neuronal populations undergo an external stimulation (visual, audio, and etc.). In this way we study responses of the brain and obtain conclusions about a propagation of signals in the brain. First in the section (3.1) we study in theory how a strong and sufficiently long stimulus influences the dynamics of our system. The next three sections are dedicated to the consideration how the stimulation effects the system in a regime of a stable phase-locked state (section 3.2), in a regime of a periodically modulated phase synchronization (section 3.3) and in multistable regimes (section 3.4). These sections include results of computer simulations of system (2.1) at the presence of stimuli.

3.1 Effect of stimulation (theory)

In this section we consider system (2.1) when the stimulation is turned on ($X(t) = 1$):

$$\begin{cases} \dot{\psi}_1(t) &= \omega_1 + \dfrac{K}{2}\sin[\psi_2(t) - \psi_1(t - \tau)] + X(t)I\cos(\psi_1(t) - \theta_1) + F_1(t), \\[2mm] \dot{\psi}_2(t) &= \omega_2 + \dfrac{K}{2}\sin[\psi_1(t) - \psi_2(t - \tau)] + X(t)I\cos(\psi_2(t) - \theta_2) + F_2(t). \end{cases}$$

$$(3.1)$$

The stimulation signals

$$S_j(t) = X(t)I\cos(\psi_j(t) - \theta_j) + F_j(t),$$

$j = 1, 2$, govern the dynamics in the system when the stimulation is strong ($I \gg K$, $I \gg \omega_1$ and $I \gg \omega_2$) and long (at least $T_{st} > \tau$) enough, as we see later. Here, $X(t) = 1$ or 0 is a stimulus trigger controlling on- and off-set of the

stimulation, I is the stimulus intensity, θ_j are stimulation phase shifts, and $F_i(t)$ is a Gaussian δ-correlated noise.

Without loss of generality, in this work we consider the case $\theta_1 = 0$ (a simple change of variables $\varphi_1^{new} = \varphi_1 + \theta_1$ and $\varphi_2^{new} = \varphi_2 + \theta_1$ let's neglect in S_1 the phase shift θ_1 and we could consider equivalent system with one parameter of the stimulation $\theta = \theta_2 - \theta_1$). In this case only the second oscillator ψ_2 is stimulated with the non-vanishing phase shift $\theta = \theta_2 \in [0, 2\pi]$ which is considered below to be a main stimulation parameter.

Such a stimulation is supposed to effect the primary system, and evokes changes in its dynamics (responses). Strong external stimuli are administered to each oscillator. If a strong stimulus (2.2) ($I \gg \omega_j, I \gg K$) is applied to system (2.1), a phase reset occurs. This means that in a short transient after onset of the stimulus, the stimulation shifts both phase oscillators to a stimulus-locked state, where both phases (ψ_1 and ψ_2) become constant. Consider system (2.1) in variables φ_1 (the difference of phases), φ_2 (the mean phase) when stimulation is on ($X(t) = 1$):

$$
\begin{cases}
\dot{\varphi}_1(t) & = \Delta_1 - K \sin\left(\dfrac{\varphi_1(t) + \varphi_1(t - \tau)}{2}\right) \cos(\varphi_2(t) - \varphi_2(t - \tau)) - \\
& \qquad\qquad\qquad\qquad -2I \sin(\dfrac{\varphi_1(t) - \theta}{2}) \sin(\varphi_2(t) - \dfrac{\theta}{2}), \\
\dot{\varphi}_2(t) & = \Delta_2 + \dfrac{K}{2} \cos\left(\dfrac{\varphi_1(t) + \varphi_1(t - \tau)}{2}\right) \sin(\varphi_2(t) - \varphi_2(t - \tau)) + \\
& \qquad\qquad\qquad\qquad +I \cos(\dfrac{\varphi_1(t) - \theta}{2}) \cos(\varphi_2(t) - \dfrac{\theta}{2}).
\end{cases}
\tag{3.2}
$$

Phase reset by the stimulation means nothing else that system 3.2 has stable fixed point(s). Let us show that the condition that stimulus is strong ($K \ll I$ and $\Delta_j \ll I$) allows to neglect own dinamics of the system performing the analysis for coordinates of the stable reset states. Suppose the system above has some fixed point $(\varphi_1, \varphi_2) = (C_1, C_2)$. Substituting the coordinates of this point into 3.2 we obtain:

$$
\begin{cases}
0 & = \Delta_1 - K \sin(C_1) - 2I \sin(\dfrac{C_1 - \theta}{2}) \sin(C_2 - \dfrac{\theta}{2}), \\
0 & = \Delta_2 + I \cos(\dfrac{C_1 - \theta}{2}) \cos(C_2 - \dfrac{\theta}{2}).
\end{cases}
\tag{3.3}
$$

Remembering now that the stimulus is strong and dividing both parts of 3.3 on I we easily notice that during the stimulation one can neglect terms with the coupling and the natural frequencies. Therefore coordinates of the reset states could be found from a new system, where only stimulation terms are preserved

from 3.2:

$$\begin{cases} \dot{\tilde{\varphi}}_1(t) &= -2I\sin(\dfrac{\tilde{\varphi}_1(t) - \theta}{2})\sin(\tilde{\varphi}_2(t) - \dfrac{\theta}{2}), \\ \dot{\tilde{\varphi}}_2(t) &= I\cos(\dfrac{\tilde{\varphi}_1(t) - \theta}{2})\cos(\tilde{\varphi}_2(t) - \dfrac{\theta}{2}), \end{cases} \tag{3.4}$$

where the variables $\tilde{\varphi}_i$ approximate the variables φ_i defined by Eq. (3.2). For a strong enough stimulus (2.2), system (3.4) governs the in-stimulus dynamics of Eq. (2.1). To be able to estimate to what reset state a trajectory comes after a stimulus onset we investigate steady states of system (3.4).

Lemma 3.1 *System (3.4) has the following steady states* $(\tilde{\varphi}_1(t), \tilde{\varphi}_2(t)) = (\tilde{\varphi}_1^*, \tilde{\varphi}_2^*)$:

$$\tilde{\varphi}_1^* = \theta + 2\pi n, \qquad \tilde{\varphi}_2^* = \frac{\theta}{2} + \frac{\pi}{2} + \pi m,$$

$$and \tag{3.5}$$

$$\tilde{\varphi}_1^* = \theta + \pi + 2\pi n, \qquad \tilde{\varphi}_2^* = \frac{\theta}{2} + \pi m, \qquad n, m \in \mathbb{Z}.$$

All steady states can be split into two groups:

a) $\tilde{\varphi}_1^* = \theta + 2\pi n$ *and* $\tilde{\varphi}_2^* = \dfrac{\theta}{2} + \dfrac{\pi}{2} + \pi m$. *For* $n + m$ *is even the fixed points of the first family are stable nodes, otherwise* ($n + m$ *is odd) they are unstable nodes.*

b) $\tilde{\varphi}_1^* = \theta + \pi + 2\pi n$ *and* $\tilde{\varphi}_2^* = \dfrac{\theta}{2} + \pi m$. *The second family of fixed points consists of saddles only.*

Proof: To find steady states of system 3.4 one puts the r.h.s. of these equations equal to zero. After straight forward calculations one obtains the coordinates of fixed points as in Eqs. (3.5).

To determine if some of these phase locked solutions are stable we solve the characteristic equation for system 3.4. For this purpose we calculate the Jacobi matrix:

$$J(\tilde{\varphi}_1(t), \tilde{\varphi}_2(t)) = \begin{pmatrix} f_{1,1}(t) & f_{1,2}(t) \\ f_{2,1}(t) & f_{2,2}(t) \end{pmatrix} \tag{3.6}$$

Where:

$$f_{1,1}(t) = -I\cos(\frac{\tilde{\varphi}_1(t) - \theta}{2})\sin(\tilde{\varphi}_2(t) - \frac{\theta}{2}),$$

$$f_{1,2}(t) = -2I\sin(\frac{\tilde{\varphi}_1(t) - \theta}{2})\cos(\tilde{\varphi}_2(t) - \frac{\theta}{2}),$$

$$f_{2,1}(t) = -\frac{I}{2}\sin(\frac{\tilde{\varphi}_1(t) - \theta}{2})\cos(\tilde{\varphi}_2(t) - \frac{\theta}{2}),$$

$$f_{2,2}(t) = -I\cos(\frac{\tilde{\varphi}_1(t) - \theta}{2})\sin(\tilde{\varphi}_2(t) - \frac{\theta}{2}).$$

Examining first the points $\tilde{\varphi}_1^* = \theta + 2\pi n$ and $\tilde{\varphi}_2^* = \dfrac{\theta}{2} + \dfrac{\pi}{2} + \pi m$ for a stability

we find that: $J(\tilde{\varphi}_1^*, \tilde{\varphi}_2^*) = \begin{pmatrix} I(-1)^{n+m+1} & 0 \\ 0 & I(-1)^{n+m+1} \end{pmatrix}$.

In this case both eigenvalues of the system are equal $\lambda_{1,2} = I(-1)^{n+m+1}$. For $n + m$ even they are negative and thus the corresponding fixed point $(\tilde{\varphi}_1, \tilde{\varphi}_2)$ is of a stable node type, then all points corresponding to $(n, m-1)$, $(n, m+1)$, $(n-1, m)$ and $(n+1, m)$ are unstable nodes.

In opposite, the second family of fixed points (3.5) $\varphi_1^* = \theta + \pi + 2\pi n$ and $\varphi_2^* = \dfrac{\theta}{2} + \pi m$ consists only of saddles. In fact we have:

$J(\tilde{\varphi}_1^*, \tilde{\varphi}_2^*) = \begin{pmatrix} 0 & 2I(-1)^{n+m+1} \\ I/2(-1)^{n+m+1} & 0 \end{pmatrix}$ and $\lambda_{1,2} = \pm I$. The lemma is proved.

Since system (3.4) is 4π-periodic in $\tilde{\varphi}_1$ and 2π-periodic in $\tilde{\varphi}_2$, it has 8 different fixed points (3.5) in the $[0; 4\pi) \times [0; 2\pi)$-phase space ($n = 0, 1$ and $m = 0, 1$). Therefore in a basic rectangle $[0; 4\pi) \times [0; 2\pi)$ in $(\tilde{\varphi}_1, \tilde{\varphi}_2)$ plane there are two stable nodes A=$(\theta, \theta/2 + \frac{\pi}{2})$ and B=$(\theta + 2\pi, \theta/2 + \frac{3\pi}{2})$, two unstable nodes $(\theta, \theta/2 + \frac{3\pi}{2})$ and $(\theta + 2\pi, \theta/2 + \frac{5\pi}{2})$, and four saddles $(\theta + \pi + 2\pi n, \theta/2 + \pi m)$ with $n, m = 0, 1$ (the coordinates should be normed to the range above).

For the following analysis we give definitions of stable and unstable manifolds of a saddle fixed point, which one finds in [63], pages 94-96.

Definition 3.1 *The stable manifold $\mathcal{M}^{(s)}$ of a saddle point S is a differentiable manifold that is tangent to the stable subspace E^s at S and such that all orbits in $\mathcal{M}^{(s)}$ are asymptotic to S as $t \to +\infty$. The stable subspace E^s is a subspace spanned by those eigenvectors $s_1, s_2, \ldots, s_{n_s}$ of S whose eigenvalues have a negative real part.*

Definition 3.2 *The unstable manifold $\mathcal{M}^{(u)}$ of a saddle point S is a differentiable manifold that is tangent to the unstable subspace E^u at S and such that all orbits in $\mathcal{M}^{(u)}$ are asymptotic to S as $t \to -\infty$. The unstable subspace E^u is a subspace spanned by those eigenvectors $u_1, u_2, \ldots, u_{n_u}$ of S whose eigenvalues have a positive real part.*

In Fig. 3.1 the phase portrait of system the (3.4) with fixed points (3.5) and with stable and unstable manifolds of the saddles is shown for $\theta = 4.11$. The grid formed by the stable manifolds of the saddle points (dashed lines with arrows [see theorem 3.2 below]) divides the whole $(\tilde{\varphi}_1, \tilde{\varphi}_2)$-phase plain into basins of attraction of the stable fixed points A (white regions) and B (gray regions). Therefore, for $t \geq 0$ a generic trajectory $(\tilde{\varphi}_1(t), \tilde{\varphi}_2(t))$ of system (3.4) will be attracted by either the stable fixed point A or B, depending on the basin of attraction in which the trajectory starts, as given by initial conditions $(\tilde{\varphi}_1(0), \tilde{\varphi}_2(0))$. During stimulation

the phases ψ_i of system (2.1), (2.2) approach a stationary reset state: both phases become approximately constant The corresponding coordinates (φ_1, φ_2) in the reset state are approximated by the coordinates of the stable fixed points A and B of the approximate system (3.4).

We give two following definitions used in the theorem about stable and unstable manifolds of the saddle points of system (3.4).

Definition 3.3 The nearest unstable nodes *to the saddle point* $S = (\tilde{\varphi}_1^S, \tilde{\varphi}_2^S)$ *of system (3.4) are two unstable nodes* $U1$ *and* $U2$ *whose coordinates differ from* $\tilde{\varphi}_1^S$ *on* $\pm\pi$ *and from* $\tilde{\varphi}_2^S$ *on* $\pm\pi/2$.

Definition 3.4 The nearest stable nodes *to the saddle point* $S = (\tilde{\varphi}_1^S, \tilde{\varphi}_2^S)$ *of system (3.4) are two stable nodes* $S1$ *and* $S2$ *whose coordinates differ from* $\tilde{\varphi}_1^S$ *on* $\pm\pi$ *and from* $\tilde{\varphi}_2^S$ *on* $\pm\pi/2$.
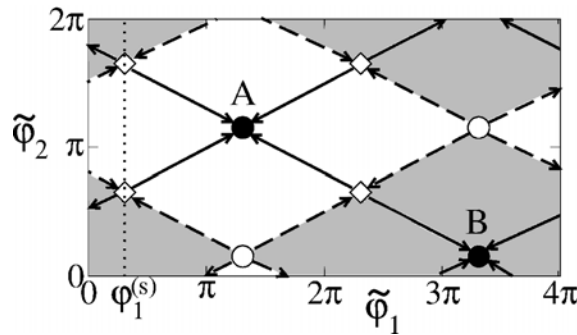
Figure 3.1: Fixed points of system (3.4) induced by the stimulation. Black filled circles (points A and B) indicate stable nodes, empty circles indicate unstable nodes, and diamonds indicate saddles. Dashed and solid lines depict stable and unstable manifolds of the saddles, respectively. Basins of attraction of the stable fixed points A and B are indicated by white and gray areas, respectively. The vertical dotted line shows the φ_1-coordinate $\varphi_1^{(s)}$ of the stable phase-locked state of system (2.1) and corresponds to the initial conditions of system (2.4) at stimulus onset. Parameters: $\theta = 4.11$, $\Delta_1 = 0.2$, $\Delta_2 = 3.0$, $K = 0.4$, and $\tau = 4.0$.

We also shall need some known fact about a saddle equilibrium formulated in the following theorem (see [42], pp.209-217):

Theorem *Consider a system of differential equations of the form*

$$\begin{cases} \dot{x} & = f(x, y), \\ \dot{y} & = g(x, y). \end{cases} \qquad (3.7)$$

where $f(x,y)$ and $g(x,y)$ are at least twice differentiable. Let the equilibrium point $O = (0,0)$ of this system be a saddle (see Fig.3.2). Let P be the line passing through O in direction of the eigenvector of the matrix A (the matrix of r.h.s. of linearized system (3.7)) which corresponds to the negative eigenvalue, and let Q be the line passing through the point O in direction of the eigenvector of the matrix A which corresponds to the positive eigenvalue. Then there exist exactly two trajectories U_1 and U_2 of system (3.7) which for $t \to \infty$ asymptotically approach to the point O. These trajectories compose together with the point O continuous differentiable curve U which is tangent to the line P at O. Similar there exist exactly two trajectories V_1 and V_2 of system (3.7) which for $t \to -\infty$ asymptotically approach the point O. In their turn these trajectories compose together with the point O continuous differentiable curve V which is tangent to the line Q at O. The other trajectories of system (3.7) near the point O behave essentially in the same way like in a case of a linear system

$$\begin{cases} \dot{x}^1 & = a_1^1 x^1 + a_2^1 x^2, \\ \dot{x}^2 & = a_1^2 x^1 + a_2^2 x^2. \end{cases} \tag{3.8}$$

where a_1^1, a_1^2, a_2^1 and a_2^2 are constant coefficients.
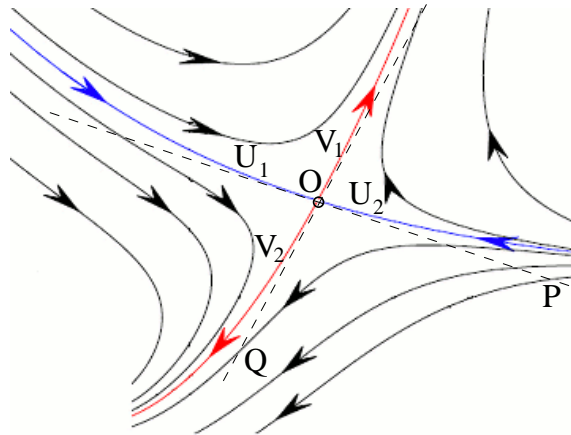
Figure 3.2: Illustration to the theorem about trajectories near a saddle.

Exploiting the theorem above and given definitions we formulate and prove the following theorem:

Theorem 3.2 *Let the point S be a saddle point of system (3.4) (see Fig.3.3). Then the stable and unstable manifolds of S in the phase space $(\tilde{\varphi}_1, \tilde{\varphi}_2)$ are segments of straight lines connecting S with the nearest unstable nodes $U1$ and $U2$ (stable manifolds) and connecting S with the nearest stable nodes $S1$ and $S2$ (unstable manifolds), correspondingly.*
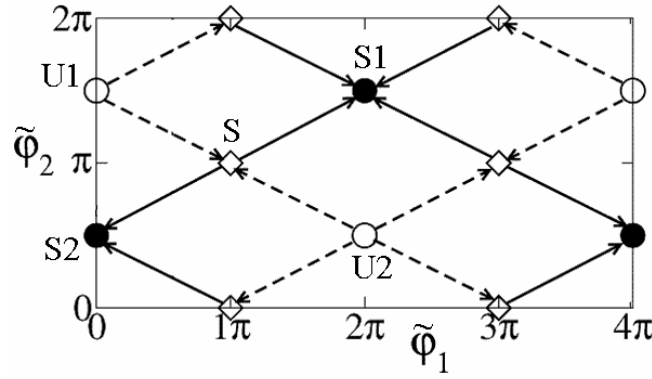
Figure 3.3: Illustration to the theorem about manifolds of a saddle.

Proof: Since the right-hand side of system (3.4) is 4π-periodic in $\tilde{\varphi}_1$ and 2π-periodic in $\tilde{\varphi}_2$, it is sufficient to consider the system in its phase space in the basic rectangle $[0; 4\pi) \times [0; 2\pi)$. In this rectangle there are eight fixed points. Let us consider a saddle $S = (\theta + \pi + 2\pi, \theta/2 + \pi)$ and a stable node $S1 = (\theta + 2\pi, \theta/2 + \frac{3\pi}{2})$ (see lemma 3.1). and suppose that $\theta \in [0, \pi]$. For such θ points S and $S1$ lie in the basic rectangle. For other θ either S or $S1$ (or both) is out of the rectangle and we need to take some other pair of saddle and stable fixed points inside the basic rectangle. But the whole algorithm of the proof is the same. Moreover from now we concentrate our attention on the segment $SS1$ only, the other segments $SS2$, $SU1$ and $SU2$ are to be considered in the similar manner.

We need to prove that $SS1$ segment of the line $SS1$ belongs to the unstable manifold $\mathcal{M}^{(u)}$ of saddle S. All points on the line $SS1$ satisfy the equation: $\tilde{\varphi}_2 = -\dfrac{\tilde{\varphi}_1}{2} + \theta + \dfrac{5}{2}\pi$. We supplement by this equation system 3.4 and solving the system of three equations come to a new system:

$$\begin{cases} \dot{\tilde{\varphi}}_1(t) & = -2I \sin(\dfrac{\tilde{\varphi}_1(t) - \theta}{2}) \cos(\dfrac{\tilde{\varphi}_1(t) - \theta}{2}), \\[2mm] -\dfrac{1}{2}\dot{\tilde{\varphi}}_1(t) & = I \sin(\dfrac{\tilde{\varphi}_1(t) - \theta}{2}) \cos(\dfrac{\tilde{\varphi}_1(t) - \theta}{2}), \\[2mm] \tilde{\varphi}_2 & = -\dfrac{\tilde{\varphi}_1}{2} + \theta + \dfrac{5}{2}\pi \end{cases} \tag{3.9}$$

The first two equations of system (3.9) are the same. Thus, we end up with equations:

$$\begin{cases} \dot{\tilde{\varphi}}_1(t) & = -2I \sin(\dfrac{\tilde{\varphi}_1(t) - \theta}{2}) \cos(\dfrac{\tilde{\varphi}_1(t) - \theta}{2}), \\[2mm] \tilde{\varphi}_2 & = -\dfrac{\tilde{\varphi}_1}{2} + \theta + \dfrac{5}{2}\pi. \end{cases} \tag{3.10}$$

They have continuous right parts, which also have continuous derivative of an arbitrary order. That means that for any initial conditions which are on the line $SS1$ there exist a solution of system 3.4 which belongs the line $SS1$. If we take initial conditions on the segment $SS1$ at a point $S_\varepsilon = (\theta + \pi + 2\pi - 2\varepsilon, \theta/2 + \pi + \varepsilon)$, where $0 < \varepsilon < \pi/2$ (excluding S and $S1$), then a solution from S_ε stays on $SS1$ forever and $SS1$ segment is invariant. To determine asymptotic behavior of this solution we just solve system (3.10) for initial conditions $(\tilde\varphi_1^0, \tilde\varphi_2^0) = S_\varepsilon$ then we get:

$$\begin{cases} \tilde\varphi_1(t) = 2\arctan(e^{-I(C+t)}) + \theta + 2\pi n, \\ \tilde\varphi_2(t) = -\dfrac{\tilde\varphi_1}{2} + \theta + \dfrac{5}{2}\pi. \end{cases} \quad (3.11)$$

where $C(\tilde\varphi_1^0) = -\dfrac{1}{I}\ln\tan(\pi + \pi/2 - \varepsilon)$ is constant and $-\infty < C < +\infty$ ($0 < \varepsilon < \pi/2$) and $n \in \mathbb{Z}$. If we take limit $t \to -\infty$ then $\tilde\varphi_1(t) \to \theta + \pi + 2\pi n$. We saw that the point $(\tilde\varphi_1(t), \tilde\varphi_2(t))$ should belong the segment $SS1$ that is why we take $n = 1$. Therefore we obtain that $(\tilde\varphi_1(t), \tilde\varphi_2(t)) \to S$ as $t \to -\infty$.

The saddle S according to the lemma above has a positive eigenvalue I and an eigenvector corresponding to it is a solution of the equation:

$$J(S)\mathbf{x} = \begin{pmatrix} 0 & -2I \\ -\dfrac{I}{2} & 0 \end{pmatrix}\mathbf{x} = I\mathbf{x} \quad (3.12)$$

where x is the required eigenvector. We obtain $x_2 = -x_1/2$, where x_1, x_2 are the components of x. Evidently the line $SS1$ touches x at S. According to the definition above the segment $SS1 \in \mathcal{M}^{(u)}$. Furthermore according to theorem above there are only two trajectories approaching S in reverse time. The second one is the segment $SS2$ (the proof is very similar). Therefore unstable manifold of the saddle S is a junction of two segments $\mathcal{M}^{(u)} = SS1 \cup SS2$. An existence and a structure of the stable manifold $\mathcal{M}^{(s)}$ is proved analogously. Since the saddle S was arbitrary in the basic rectangle the theorem is proved.

Studying the stimulation of our system in a stable phase-locked state (see subsection 3.2.1) we shall use the result, formulated in the theorem below. Namely, if we have that trajectories (trials) split into clusters (for example two clusters) then we introduce the clustering number H defined as:

Definition 3.5 The clustering number H *is a quantity defined as a relative number of trajectories (trials) within the smallest cluster over the number of all trajectories (trials).*

If for example we have two clusters only with N_1 and N_2 trials, correspondingly, then $H = \min\left\{\dfrac{N1}{N1 + N2}; \dfrac{N2}{N1 + N2}\right\}$. Evidently, $H \in [0; 0.5]$ for two

clusters. The following theorem gives us an estimate of the clustering number H for trials of system (3.4) for the case when number of trials goes to infinity:

Theorem 3.3 *If initial conditions $\tilde{\varphi}_1(0), \tilde{\varphi}_2(0)$ of all trajectories of system (3.4) belong to the segment $\varphi_1^{(s)} \times [0; 2\pi)$ in the basic rectangle in the phase space $(\tilde{\varphi}_1, \tilde{\varphi}_2)$, where $\varphi_1^{(s)} \in [0; 2\pi]$ and is constant, and there are N trials, $N \to \infty$, and all N initial conditions are uniformly distributed over the whole segment, then all N trajectories, originating from these initial conditions, split into two clusters and clustering number $H(\theta)$ is given by the following formula:*

$$H(\theta) = -\left| \frac{-[(\theta - \varphi_1^{(s)}) \ mod \ 2\pi] + \pi}{2\pi} \right| + \frac{1}{2} \tag{3.13}$$

Proof: In the dynamics of system 3.4 there are two stable fixed points A and B in the basic rectangle (see above). The other stable nodes in the $(\tilde{\varphi}_1, \tilde{\varphi}_2)$ space are mapped by transform modulo 2π either to A or to B.

Points A and B have their own basins of attraction. Vertical line of initial conditions $\varphi_1^{(s)} \times [0; 2\pi]$ (see Fig.3.4) crosses both basins. The clustering number $H(\theta)$ of system 3.4 is calculated trough determining the relative number of trials attracted by different fixed points (A or B). For uniformly distributed magnitude a number of trials in a certain range is proportional to the length of the range and, thus, a relative number of trials in this range is equal to the ratio of the length of the range over 2π (the whole interval of changes of variable $\tilde{\varphi}_2$). As $N \to \infty$ this trials fill dense range $[0; 2\pi]$ and instead of relative number of trials we are able to use relative range length. All we need now is to find the low how relative range lengths in φ_2 variable corresponding to the fixed points A and B depend on θ.

In the figure below we show all fixed points and stable/unstable manifolds connecting them for system 3.4 in the basic rectangle in $(\tilde{\varphi}_1, \tilde{\varphi}_2)$ plane where $\theta = 0$. For positive θ the whole picture (except the initial segment) is shifted linearly to the right and up. Let us also fix first $\varphi_1^{(s)} = 0$ and consider $H_0(\theta) = H_{\varphi_1^{(s)}=0}(\theta)$. Then for $\theta = 0$ line $\varphi_1^{(s)} \times [0; 2\pi]$ lies completely in a basin of attraction of A and no clustering occurs. This imposes $H_0(0) = 0$. For $\theta = \pi$ the line of initial conditions would be divided into halves between A and B basins and $H_0(\pi) = 0.5$. For intermediate values of $\theta \in [0; \pi]$ values of $H_0(\theta)$ would belong to the line connecting $H_0(0)$-$H_0(\pi)$ because the structure of fixed points moves linearly in dependence on θ. Further consideration gives us for the clustering number periodic curve shown bold in the Fig. 3.5. As one notices $H_0(\theta)$ is 2π periodic, that is why $H_0(\theta) = H_0(\theta \mod 2\pi)$. We obtain that $H_0(\theta)$ is piecewise linear for the case $\varphi_1^{(s)} = 0$.

For non-zero $\varphi_1^{(s)}$ the line of initial conditions shifts horizontally, but this shift does not influence the structure of fixed points of system 3.4 and, thus,
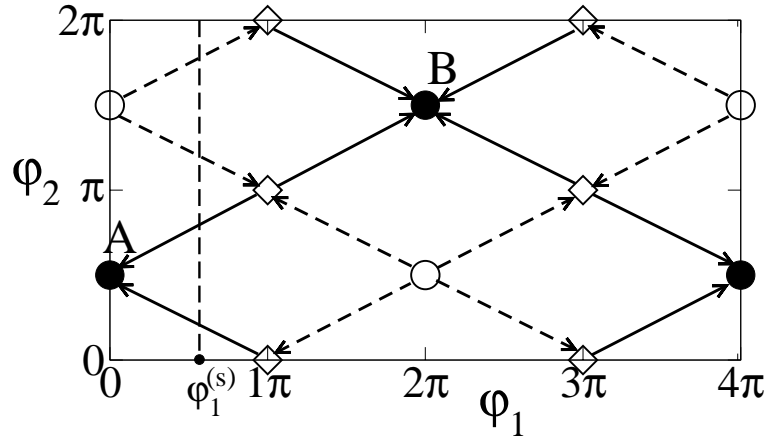
Figure 3.4: Fixed points of system (3.4) induced by stimulation. Black filled circles (points A and B) indicate stable nodes, empty circles indicate unstable nodes, and diamonds indicate saddles. Dashed and solid incline lines depict stable and unstable manifolds of the saddles, respectively. The vertical dashed line represents the initial segment for non-zero $\varphi_1^{(s)}$. Parameters: $\theta = 0.0$, $\Delta_1 = 0.2$, $\Delta_2 = 3.0$, $K = 0.4$, and $\tau = 4.0$.
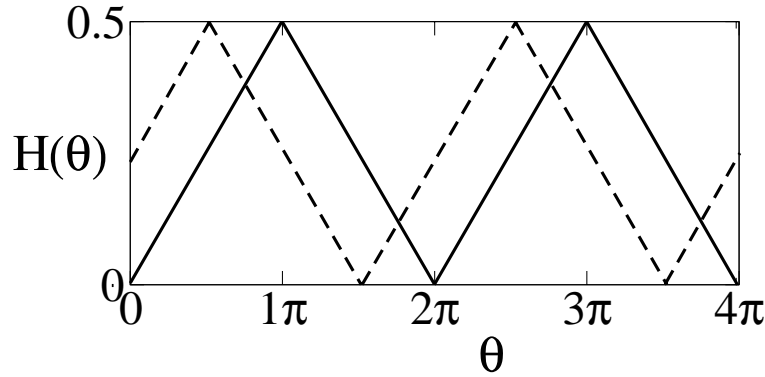

Figure 3.5: The clustering number $H(\theta)$ for the cases $\theta = 0$ (bold line) and $\theta > 0$ (dashed line). Other parameters as in Fig.3.4.

$H_{\varphi_1^{(s)}}(\theta)$ should be also piecewise linear and 2π periodic. For example for positive $\varphi_1^{(s)} \in (\pi; 2\pi)$ and for $\theta = 0$ from the Fig. 3.4 the line of initial conditions crosses both basins of attractions of A and B, respectively, and thus $H_{\varphi_1^{(s)}}(0) > 0$, but for $\theta = \varphi_1^{(s)}$ $H_{\varphi_1^{(s)}}(\theta) = 0$ and from those θ value on $H_{\varphi_1^{(s)}}(\theta)$ again is 2π periodic (see dashed line in Fig. 3.5). In this case $\varphi_1^{(s)}$ plays a role of a phase along cyclic $H_{\varphi_1^{(s)}}(\theta)$ function and the following equality holds:

$$H(\theta) = H_{\varphi_1^{(s)}}(\theta) = H_0(\theta - \varphi_1^{(s)}).$$
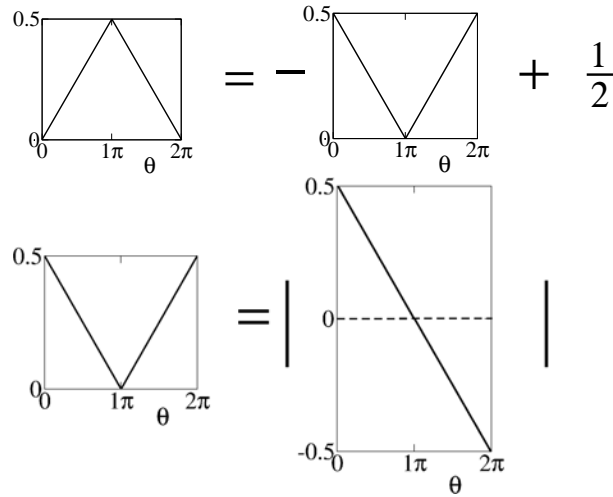
Figure 3.6: Geometrical (and algebraic) identities for a piecewise linear function.

Eventually, knowing form and properties of $H(\theta)$, we come to the final formula through a chain of simple geometric transformations (see figure 3.6). Here we first obtain formula for $H_0(\theta)$ on interval $\theta \in [0; 2\pi]$ (one period).

For that we just notice that according to the geometric identities (Figs. 3.6) both linear pieces of $H_0(\theta)$ could be given by one formula including the absolute value operation: $H_0(\theta) = -\left|\dfrac{-\theta + \pi}{2\pi}\right| + \dfrac{1}{2}$. Incorporating now the periodicity of $H(\theta)$ and its dependence on non-zero $\varphi_1^{(s)}$ we come to the formula:

$H(\theta) = -\left|\dfrac{-[(\theta - \varphi_1^{(s)}) \bmod 2\pi] + \pi}{2\pi}\right| + \dfrac{1}{2}$. The theorem is proved.

3.2 Stimulation of phase-locked states

This section deals with a stimulation of system (2.1) in a phase-locked state. We discuss results of numerical simulation of system (2.1) and their agreement with the theory (see chapter 2 and section 3.1). The resetting effect of the stimulation is explained in detail. The clustering processes of trials during the stimulation (in-stimulus) and after the stimulation (post-stimulus) are qualified and the mechanisms underlying them are investigated. Moreover, we obtain an optimal value of stimulation parameter $\theta = \theta_{max}$ necessary for the longest

transient time from a perturbed state back to a synchronous one.

In the framework of a statistical approach to a transient stimulus-locked dynamics [55], [57] (see also Appendix) we consider the following stimulation protocol: a series of N identical stimuli (2.2) is administered consecutively one stimulus after the other (see Fig.3.7(a)). Each stimulus acts only during a short time in-
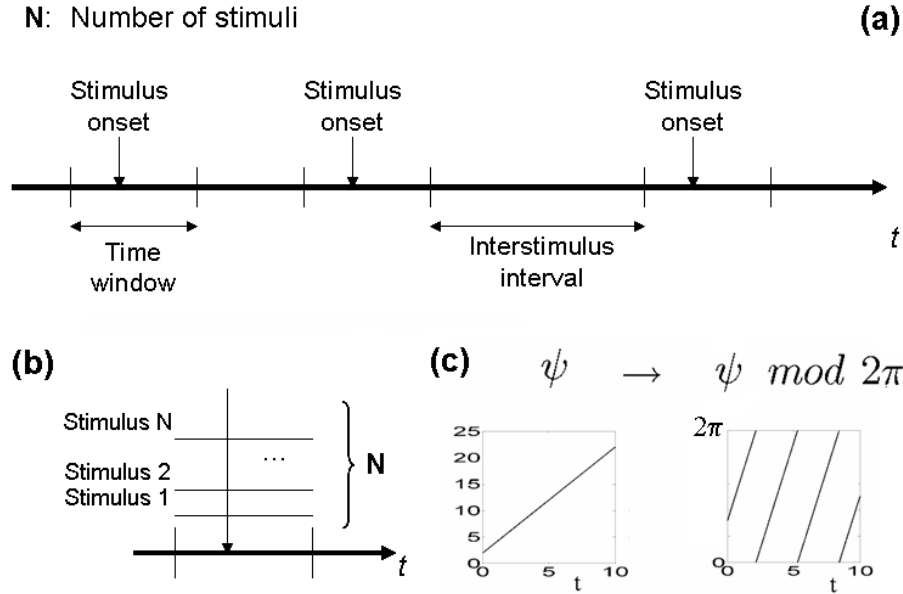

Figure 3.7: Schematic representation of a stimulation protocol. (a): Repetitive application of N stimuli is shown. This protocol holds for all phases. (b): The process of cross-trial diagram formation is illustrated. All N trials of each phase are depicted simultaneously versus time. (c): In a cross trial diagram every phase ($\psi \in \psi_1, \psi_2, \varphi_1, \varphi_2$) is normed to the range $[0; 2\pi]$. After this operation one exemplary trial is transformed as it is shown in the plot (c).

terval of duration T_{st}. The length of the interstimulus intervals is stochastically varied from one stimulus to another and is large enough to let the system return to its own dynamical regime, before the next stimulus is applied. Around each stimulus a time window of the length T_w is attached, in which the evaluation of the trajectories of system (2.1) is performed across trials (see Fig.3.7(a),(b)). During a post-stimulus transient, when stimulation is off ($X(t) = 0$), system (2.1) relaxes towards its stable state displaying different kinds of responses to the stimulation. These post-stimulus responses are the subject of our study.

Let system (2.1) be first stimulated in a regime, with only one stable phase-

locked state. For this, the values of the parameters are chosen such as in Fig. 2.11(a), where a stable fixed point P and a saddle point Q exist. Generic system responses extracted from $N = 300$ stimulation trials with a stochastic phase resetting analysis [58] are presented in Fig. 3.8. In this figure one can see typical diagrams how
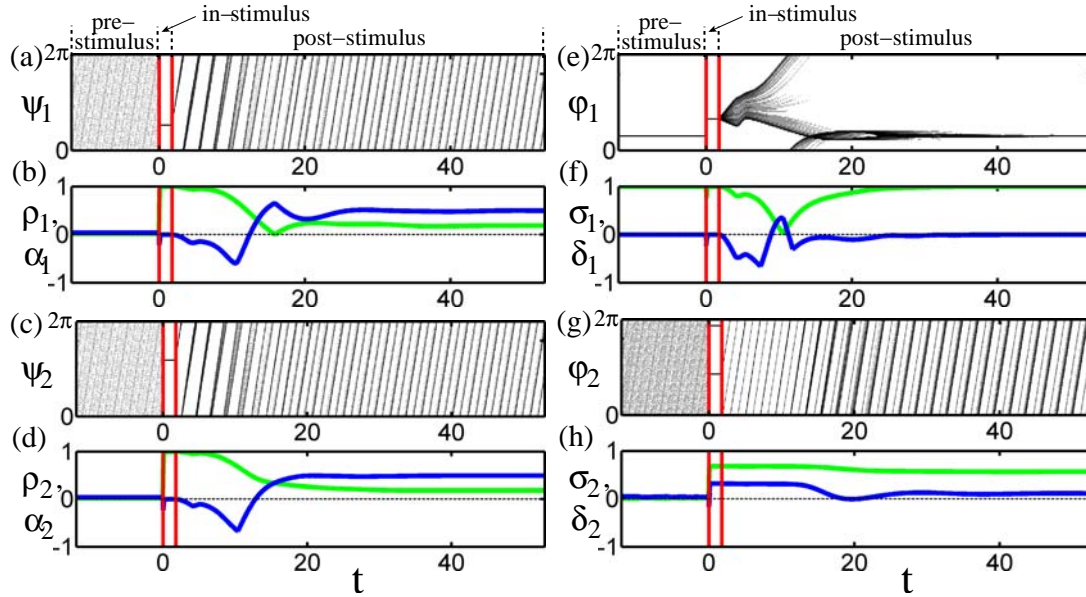

Figure 3.8: Stimulus-locked responses of system (2.1) stimulated in the phase-locked regime. Cross-trial distributions of the phases ψ_1, ψ_2, the phase difference φ_1, and the mean phase φ_2 are shown in (a), (c), (e), and (g), respectively, where the density of trajectories is encoded by a gray scale (minimum is white, maximum is black). All phases are taken modulo 2π. Onset (at time $t = 0$) and offset of the stimuli are indicated by vertical red lines. Characteristic features of the stimulus-locked dynamics as revealed by cross-trail indices (see Appendix and Ref. [58]): The resetting indices ρ_1 and ρ_2 and the clustering indices α_1 and α_2 of the phases ψ_1 and ψ_2 are shown in (b) and (d); the synchronization indices σ_1 and σ_2 and the clustering indices δ_1 and δ_2 of the phase difference φ_1 and the mean phase φ_2 are shown in (f) and (h). The resetting/synchronization indices (green curves) and the clustering indices (blue curves) detect whether the corresponding cross-trial distribution has one pronounced peak or two pronounced anti-phase peaks. Number of stimuli $N = 300$. Parameters: $\Delta_1 = 0.2$, $\Delta_2 = 3.0$, $K = 0.4$, $\tau = 4.0$, and $\theta = 2.075$.

the phases behave before, during and after stimuli during time window T_w. We use cross-trial distributions of the variables $\psi_{1,2}$ and $\varphi_{1,2}$ [Fig. 3.8(a),(c),(e),(g)] and the corresponding stimulus-locked indices [Fig.3.8(b),(d),(f),(h)] (see Appendix) to study the stimulus-locked dynamics. The phases $\psi_{1,2}$ and $\varphi_{1,2}$ are

taken modulo 2π and belong to the interval $[0; 2\pi)$.

Before stimulus onset the phases ψ_1 and ψ_2 are uniformly distributed in $[0, 2\pi)$ since stimuli are administered at random times which obey uniform distribution. Accordingly, both resetting indices ρ_j and clustering indices α_j, $j = 1, 2$, are close to 0.

A stimulus rapidly resets the phase of the jth *oscillator to the phase ψ_1^{res} and ψ_2^{res}, in such a way, that the phase difference $\varphi_1 = \psi_2^{res} - \psi_1^{res}$ and the mean phase $\varphi_1 = (\psi_2^{res} + \psi_1^{res})/2$ are equal to the coordinates of the stable fixed points A or B (see Fig. 3.1 and description there) of system (3.4).*

Hence, at stimulus offset the resetting indices ρ_1 and ρ_2 are close to 1, which indicates a complete reset of the phases. The phases ψ_1 and ψ_2 are reset to particular values $\psi_1^{res}(t_E)$ and $\psi_2^{res}(t_E)$ irrespective of their initial values at stimulus onset, where t_E denotes time moments of stimulus offset. Note, $\psi_1^{res}(t_E) \neq \psi_2^{res}(t_E)$ due to the non-vanishing shift term θ of the stimulus.

Before stimulus onset the two oscillators are strongly synchronized with a non-vanishing phase difference φ_1 [Fig. 3.8(e)]. This stereotypical phase relationship between the two oscillators shows up as a dirac-type pre-stimulus distribution of φ_1 and, thus, the synchronization index σ_1 is close to 1, where the value of the phase difference φ_1 remains fixed within the entire pre-stimulus interval. The stimuli reset the oscillators in a way that their phase difference is set to a value different to that of the pre-stimulus range [Fig. 3.8(e)]. This processes is reflected by a quick decrease and subsequent reincrease of the synchronization index σ_1, which occurs directly after stimulus onset [Fig. 3.8(f)].

After the stimulus offset the oscillators relax back to their stable pre-stimulus phase difference. This is achieved in two different ways: one of the oscillators speeds up relative to the other one [Fig. 3.8(a),(c)]. Accordingly, the phase difference either increases (mod 2π) or decreases [Fig. 3.8(e)]. This two-branch type resynchronization process of φ_1 shows up as a transient epoch of desynchronization, where the synchronization index σ_1 of φ_1 decreases [Fig. 3.8(f)]. The clustering index δ of the phase difference φ_1 gets maximal when the two branches are in anti-phase position.

A further consequence of the two branches of transient trajectories is the emergence of a response clustering of both oscillators ψ_1 and ψ_2: After stimulus offset the oscillators restart from the reset state [Fig. 3.8(a),(c)], the resetting indices ρ_1 and ρ_2 decrease, whereas the clustering indices α_1 and α_2 increase above the pre-stimulus level, indicating an anti-phase response clustering [Fig. 3.8(b),(d)]. Put otherwise, after an initial reset each oscillator displays two anti-phase types of responses across trials. This corresponds to the cross-trail distribution of ψ_j having two anti-phase peaks [Fig. 3.8(a),(c)] (see Appendix).

Additionally, there is a clustering process of the mean phase φ_2 [Fig. 3.8(g),(h)].

As one can see in Fig. 3.8(g), this clustering process occurs already during stimulation, directly after stimulus onset, where two anti-phase clusters of the variable φ_2 are formed. During the post-stimulus transient these clusters get slightly smeared. Correspondingly, the pre-stimulus resetting and clustering indices σ_2 and δ_2 of the mean phase are close to zero because of the randomized stimulus administration [Fig. 3.8(g)]. The clustering index δ_2 first quickly increases after stimulus onset, and then, after a transient slight decrease, finally remains above the prestimulus level, as soon as the resynchronization is achieved [3.8(e),(f)].

The combination of increased σ_2 and δ_2 is indicative of two asymmetric anti-phase peaks of the cross-trial distributions of φ_2 with one peak being large, the other one being small [Fig. 3.8(g), see also [58]]. The numbers of trials in each cluster (i.e. peak of the bimodal cross-trial distribution of φ_2) are 252 and 48, out of a total $N = 300$ stimulation trials. In contrast, in [Fig. 3.8(a), 3.8(c), and 3.8(e)] the phase variables ψ_1 and ψ_2, and the phase difference φ_1 simultaneously split into two anti-phase clusters with 143 and 157 trials, respectively. Therefore, the clustering of the variable φ_2 does not correspond to the post-stimulus clustering of the other variables, as we will also show below (see the subsection 3.2.2).

We consider the formation of the response clusters in more detail in the subsections 3.2.1, 3.2.2. We show that the response clustering of the phase difference φ_1 plays an important role in the formation of the response clustering of the phases ψ_1 and ψ_2. For this, we first investigate the dynamics of system (2.1) during stimulation, i.e., the in-stimulus dynamics. Secondly, we study the post-stimulus transient.

3.2.1   In-stimulus clustering

In the current and in the next subsections we discuss two types of a clustering of response trials observed in our system due to the stimulation. First we define and investigate an in-stimulus clustering.

Definition 3.6 In-stimulus clustering *is a clustering of trials into two clusters during the stimulation. Two trajectories* $Tr^a(t) = (\varphi_1^a(t), \varphi_2^a(t))$ *and* $Tr^b(t) = (\varphi_1^b(t), \varphi_2^b(t))$ *belong to different clusters if at the end of the strong and long enough stimulation at the time* t_E $Tr^a(t_E) \approx (\tilde{\varphi}_1^A, \tilde{\varphi}_2^A)$ *and* $Tr^b(t_E) \approx (\tilde{\varphi}_1^B, \tilde{\varphi}_2^B)$, *where* $A = (\tilde{\varphi}_1^A, \tilde{\varphi}_2^A)$ *and* $B = (\tilde{\varphi}_1^B, \tilde{\varphi}_2^B)$ *are stable steady states induced by the stimulation (see Fig. 3.1).*

The splitting of the trajectories of system (2.1) between the basins of attraction of the reset states A and B is the mechanism which causes the in-stimulus clustering (see Fig. 3.1).

The clustering phenomenon for the in-stimulus transient of system (2.1) is illustrated in Fig. 3.9, where transients towards A and B are shown for a few

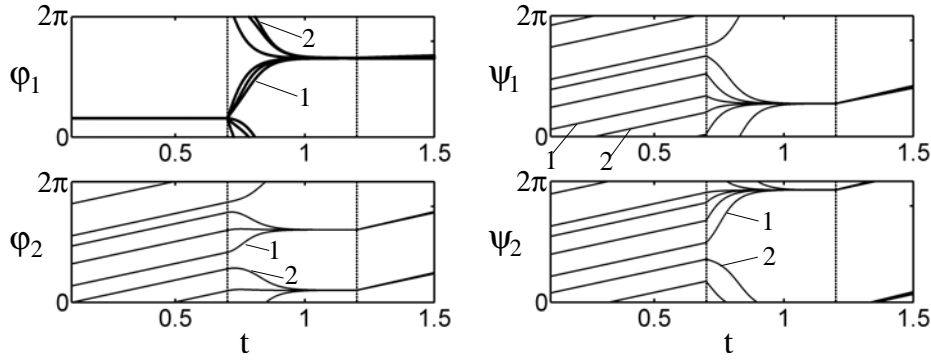selected trajectories of Eqs. (2.1).

Figure 3.9: The in-stimulus clustering illustrated for a few trajectories of the stimulated system (2.1) with different initial conditions. Variables $\varphi_1(t)$, $\varphi_2(t)$, $\psi_1(t)$, and $\psi_2(t)$ are separately shown on each plot. The in-stimulus clustering is induced by an attraction of different reset states A or B [Fig. 3.1]. Two selected trajectories belonging the different clusters are denoted by numbers 1 and 2. The on- and off-sets of stimulation are indicated by vertical dashed lines. $\theta = 4.11$ and the other parameters are as in Fig. 3.8.

Trajectories like #1 are attracted by A and their coordinate φ_1 increases, whereas trajectories like #2 are attracted by B and φ_1 decays. Note, the two reset states given by the fixed points A and B of Eq. (3.4) are indistinguishable when considering cross-trial distributions of the variables ψ_i, $j = 1, 2$, and φ_1 taken modulo 2π [Fig. 3.8]:

$$
\begin{aligned}
(\psi_1, \psi_2) &\approx (\pi/2, \theta + \pi/2) && \text{corresponds to} \\
(\varphi_1, \varphi_2) &\approx (\theta, \theta/2 + \pi/2) && \text{(A) and} \\
(\varphi_1, \varphi_2) &\approx (\theta, \theta/2 + 3\pi/2) && \text{(B)}
\end{aligned}
\tag{3.14}
$$

The twofold convergence of trajectories of system (2.1) to the reset states A and B constitutes the in-stimulus response clustering of the mean phase φ_2 [Fig. 3.8(g)].

Moreover, we are able to estimate analytically the clustering number $H(\theta)$ for trials of system (2.1) for in-stimulus clustering.

As interstimulus interval is uniformly varied, that means, that in a stable phase-locked state at the beginning of the stimulus each trial has the following coordinates: $\varphi_1(t_0^j) = \varphi_1^{(s)}$ and $\varphi_2(t_0^j) \sim \Omega t_0^j$, where t_0^j is the begin time of a stimulus number j. The value $\varphi_2(t_0^j)$ is proportional to the time t_0^j and for uniformly distributed t_0^j the phase $\varphi_2(t_0^j)$ is also uniformly distributed. If we take $\varphi_2(t)$ mod 2π then normed $\varphi_2(t)$ is also uniformly distributed in the $[0; 2\pi]$ interval. This situation was modelled in our simulations. At the beginning and during the

stimulation the dynamics in system (2.1) is approximated by the dynamics in system (3.4) (see the section 3.1). The initial conditions $(\tilde{\varphi}_1(0), \tilde{\varphi}_2(0))$ of system (3.4) equal to the values of the variables $(\varphi_1^{(s)}, \varphi_2(t_0^j))$ at the stimulus onset.

For all N trials (N tends to ∞) initial conditions $(\tilde{\varphi}_1(0), \tilde{\varphi}_2(0))$ fill uniformly the vertical segment (an initial segment) $\varphi_1^{(s)} \times [0; 2\pi)$ in the phase space (see in Fig. 3.1 dotted line). The fixed points A and B of Eq. (3.4) are located on different sides with respect to the initial segment above (when consider a lift of the torus $[0; 2\pi) \times [0; 4\pi)$ to $\mathbb{R}^2$), i.e., on different sides with respect to the initial phase shift $\tilde{\varphi}_1(0) = \varphi_1^{(s)}$. Therefore, during in-stimulus transient on the way towards the fixed point A (B), the phase difference $\tilde{\varphi}_1(t)$ increases (decreases). Furthermore, during the in-stimulus transient $\tilde{\varphi}_2$ approaches either A or B, accordingly.

We are able to apply the theorem 3.3 and the in-stimulus clustering number $H(\theta)$ for the in-stimulus clustering in dependence on the parameter θ reads

$$H(\theta) = - \left| \frac{-[(\theta - \varphi_1^{(s)}) \bmod 2\pi] + \pi}{2\pi} \right| + \frac{1}{2}.$$

As a result we observe that the graph of the theoretical in-stimulus clustering number H given by Eq. (3.13) (solid line in Fig. 3.10) is in a good agreement with the values of H obtained by simulating system (2.1) (crosses in Fig. 3.10).
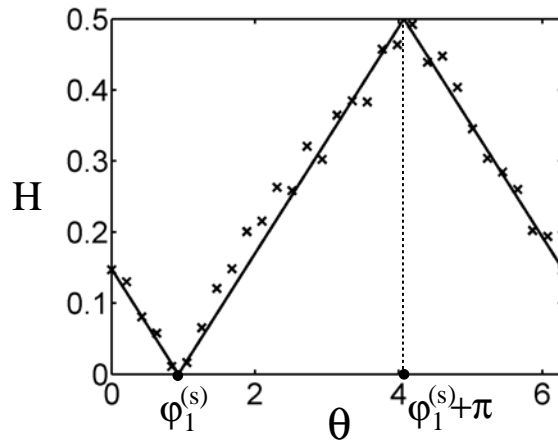
Figure 3.10: The clustering number H, i.e., the relative number of trajectories in the smallest cluster during in-stimulus clustering versus stimulation phase shift θ. Solid line shows the theoretical estimation according to Eq. (3.13) and crosses show results of series of numerical simulations for different values of θ. $\varphi_1^{(s)}$ denotes the φ_1-coordinate of the stable fixed point of system (2.4). Parameters: $\Delta_1 = 0.2$, $\Delta_2 = 3.0$, $K = 0.4$, $\tau = 4.0$ and $N = 1300$.

There is an optimal value of the parameter $\theta = \theta_{cl} = (\varphi_1^{(s)} + \pi) \bmod 2\pi$, where the in-stimulus clustering is maximal, i.e., the two emerging clusters are of equal size. This situation occurs if the $\tilde{\varphi}_1$-coordinates of the saddle fixed points of system (3.4), which are $\theta + \pi + 2\pi n$, $n = 0, 1$, coincide with the φ_1-coordinate $\varphi_1^{(s)}$ of the stable fixed point P. In this case equally long fractions of the segment $\varphi_1^{(s)} \times [0; 2\pi)$ belong to the basins of attractors A and B, respectively, as shown in Fig. 3.1.

The in-stimulus clustering determines the post-stimulus clustering of the mean phase φ_2 [Fig. 3.8], where the clusters of trajectories emerging during the stimulation are preserved during the post-stimulus transient.

Below we explore in which way the global structure of the phase space of system (2.4) influences the post-stimulus clustering in system (2.1).

3.2.2   Post-stimulus clustering

Definition 3.7 Post-stimulus clustering *is a clustering of trials into two clusters after the stimulation offset. Two trajectories $Tr^a(t) = (\varphi_1^a(t), \varphi_2^a(t))$ and $Tr^b(t) = (\varphi_1^b(t), \varphi_2^b(t))$ belong to two different clusters if $|\varphi_1^b(t) - \varphi_1^a(t)| \to 2\pi$ as $t \to +\infty$ and $\varphi_1^a(t) \bmod 2\pi \to \varphi_1^{(s)}$ and $\varphi_1^b(t) \bmod 2\pi \to \varphi_1^s$ as $t \to +\infty$, where φ_1^s is the phase difference of the stable phase-locked state of system (2.1).*

The clustering of post-stimulus responses can easily be seen in Figs. 3.8(a), 3.8(c), 3.8(e), and 3.16(b). The clustering number H in variable φ_1 for the post-stimulus transient is plotted in Fig. 3.11 versus the stimulation phase shift θ. Maximal clustering is attained at $\theta = 1.87$ which we also call θ_{max}. One notices that $\theta_{max} \neq \varphi_1^{(s)}$. This phenomenon is connected with the properties of the stable manifold $\mathcal{M}^{(s)}$ of the saddle-focus fixed point Q. This manifold serves as a separator between two different kinds of the post-stimulus transients of system (2.4). In this connection, the optimal value θ_{max} can also be referred to as a separator of the post-stimulus trajectories of system (2.4) and θ_{max} is very close to $\mathcal{M}^{(s)}$ (see the next section).

Indeed, as mentioned below, for the stimulation phase shift $\theta \approx \theta_{max}$ the trajectories starting very close to $\mathcal{M}^{(s)}$ approach $\mathcal{M}^{(s)}$, follow it towards Q and stay there for a long time. After a long attraction stage they will be repelled from Q and attracted by the stable fixed point P.

On the other hand, if $\theta \neq \theta_{max}$ then the trajectory will be directly attracted by P or by a copy of P shifted by 2π without or with an additional rotation on the torus, respectively. For example, for parameter values as in Fig. 3.11, stimulation with $\theta < \theta_{max}$ leads to a simple post-stimulus transient, where trajectories are directly attracted by P. In contrast, stimulation with $\theta > \theta_{max}$ results in that post-stimulus trajectories perform one rotation in φ_1 on the torus and will be attracted by a copy of P shifted by 2π and, thus, the post-stimulus clustering
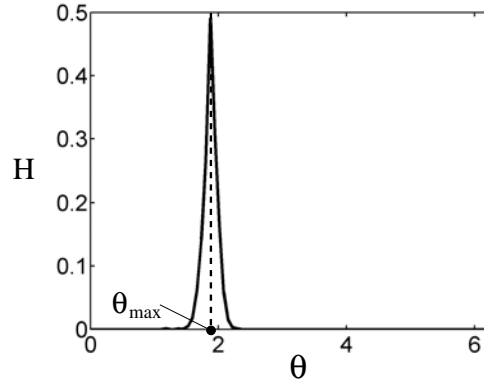
Figure 3.11: Post-stimulus clustering number H in variable φ_1 versus the stimulation phase shift θ. System (2.1) is simulated with Gaussian white noise of an amplitude $D = 0.002$. The width of the peak of the clustering number depends on the amplitude of the noise and grows with an increase of the noise amplitude. Number of stimuli $N = 100$, stimulus length $T_{st} = 5$, and other parameters: $\Delta_1 = 0.2$, $\Delta_2 = 3.0$, $\tau = 4.0$, and $K = 0.4$.

takes place (see definition above). In this way, when stimulating with $\theta \approx \theta_{max}$ in the presence of noise, there will be trajectories relaxing to P after a stimulus offset according to the first scenario ($\theta < \theta_{max}$), and there will be trajectories relaxing to P according to the second scenario ($\theta > \theta_{max}$).

This explains the formation of the post-stimulus clustered responses of the variable φ_1 (see Fig. 3.8). Simultaneously with the formation of the post-stimulus response clusters for the variable φ_1, clusters also emerge for the phase variables ψ_1 and ψ_2, see Fig. 3.8. Variable φ_2, in its turn, gets clustered during stimulation and keeps being clustered after the stimulus offset. In the time course after the stimulus offset, the response clusters in variable φ_1 are suppressed when the trajectories are attracted by the stable phase-locked state, see also Fig. 3.16(b). In contrast, the clusters in the phase variables ψ_1 and ψ_2 are preserved for the whole post-stimulus transient period.

The clustering of the variable φ_1 means that some trajectories are approaching the value $\varphi_1^{(s)}$, and the others are approaching $\varphi_1^{(s)} \pm 2\pi$, where $\varphi_1^{(s)}$ is the φ_1-coordinate of the stable fixed point P. Taken mod 2π these clusters are not seen in Figs. 3.8(e) and 3.16(b). Simultaneously, across trials the variable φ_2 attains two different values from Eq. (3.14) at stimulus offset. Assuming that the clustering in φ_2 is preserved, with a simple calculation one arrives at the conclusion that the clustering in variable φ_1 determines the clustering of the phase variables ψ_1

and ψ_2:

    Two trajectories from different clusters in φ_1 are also from different clusters in the phase variables $\psi_{1,2}$ and vice versa.

Moreover, the "distance" between the clusters in the phase variables is π and the clusters are clearly observed in the cross-trial diagram in Fig. 3.8(a) and 3.8(c).

Therefore, the optimal stimulation phase shift θ_{max} serves for the maximal post-stimulus response clustering of the system (2.1), but as well it serves for the maximal post-stimulus transient time of trials (see the next section).

3.2.3 Maximal transient time

Stimuli of sufficient strength and duration shift the trajectories of system (2.1) very close to the reset state (3.14), where they remain till the end of the stimulation. After the stimulus offset system (2.1) returns to its own stable state. In this section we are continuing to study the post-stimulus transients of the system in the phase-locked regime. Surprisingly we found out that the phase shift θ_{max} besides the feature that it is the point of the maximal post-stimulus clustering has another important property. This value of θ is an optimal parameter which allows the stimulation to evoke the longest transient of perturbed trajectories to a synchronized state.

This optimal value θ_{max} is very important for applications in practice. If an external stimulation of a patient shifts his/her nervous system functioning closer to its normal regime, then the duration how this state is preserved after a stimulus offset determines an efficiency of the stimulation.

Let us, as before, consider the case, where system (2.1) has just one stable phase-locked state P. After a stimulus offset, trajectories relax from the stimulus-induced reset state (3.14) towards the phase-locked state P. An example of such a transient is shown in the cross-trail distributions in Fig. 3.8.

We define the transient time T_{tr} as the time it takes a trajectory after the stimulus offset to permanently enter an ε-vicinity of the stable phase-locked state, averaged over the ensemble of N stimuli. We study how T_{tr} depends on the stimulation phase shift θ for long and strong enough stimuli.

An example of the transient time T_{tr} calculated for the stimulated system (2.1) without delay, i.e., for $\tau = 0$, is shown in Fig. 3.12(a) versus θ. One can see that there are two critical values of the stimulation phase shift θ_{max} and θ_{min}, where the transient time attains its maximum and minimum, respectively. Moreover, the stimulus length T_{st} has a minor influence on the transient time T_{tr},
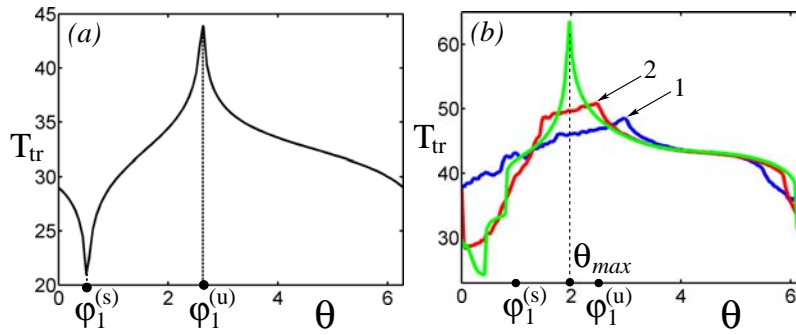
Figure 3.12: Transient time T_{tr} for the post-stimulus relaxation of system (2.1), necessary to reestablish its stable phase-locked state, versus stimulation phase shift θ. Delay: (a) $\tau = 0$ and (b) $\tau = 4.0$. In both plots three graphs are shown for different stimulus lengths $T_{st} = 0.75$ (blue), $T_{st} = 2.25$ (red) and $T_{st} = 4.75$ (green). Coinciding curves in (a) are indicated by a black curve. Maxima of blue and red curves in (b) are indicated by "1" and "2", respectively. $\varphi_1^{(s)}$ and $\varphi_1^{(u)}$ indicate the φ_1-coordinates of the stable and unstable fixed points of system (2.4), respectively. Number of stimuli $N = 200$ and $\varepsilon = 0.05$. Parameters: $\Delta_1 = 0.2$, $\Delta_2 = 3.0$, $K = 0.4$, $I = 30.0$.

as demonstrated for $T_{st} = 0.75$, 2.25, and 4.75 in Fig. 3.12(a) three curves for the different stimulation times just coincide.

The critical values θ_{min} and θ_{max} correspond to the stable P and the unstable Q fixed points of system (2.4) without delay with φ_1-coordinates $\varphi_1^{(s)} \approx 0.52$ and $\varphi_1^{(u)} \approx 2.62$, respectively. Evidently, in order to obtain the longest post-stimulus transient in system (2.1) without delay, the stimulation has to shift the trajectories towards the unstable fixed point of Eq. (2.4). This can be done by a proper choice of the stimulus phase shift θ, namely, θ has to be taken equal to the φ_1-coordinate $\varphi_1^{(u)}$ of the unstable fixed point Q.

The situation is different if the stimulated system has a significant time delay. This is illustrated in Fig. 3.12(b), where the transient time T_{tr} is plotted versus θ for the delay $\tau = 4.0$ and for the same three values of the stimulus length as above $T_{st} = 0.75$, 2.25, and 4.75. For the parameter values as in Fig. 3.12(b), system (2.4) has two fixed point: stable P and saddle Q with coordinates $\varphi_1^{(s)} \approx 0.997$ and $\varphi_1^{(u)} \approx 2.583$, respectively, see Fig. 2.11(a).

If the stimulation time T_{st} is relatively small (in comparison with the delay τ), the transient time T_{tr} still has a maximum, which is not directly located at the coordinate $\varphi_1^{(u)}$ of Q but close to it [maximum 1 in Fig. 3.12(b)]. The dependence of the transient time on the phase shift θ undergoes a significant change when T_{st} increases: The maximum of T_{tr} is shifted to the left [maximum 2 in Fig. 3.12(b)]

and finally saturates at a critical point θ_{max}, located between the stable fixed point P and the unstable fixed point Q [Fig. 3.12(b)].

Therefore, in order to obtain the maximal post-stimulus transient time in system with delay (2.1), one has to stimulate the system into a neighborhood of an optimal point θ_{max} which is different from the φ_1-coordinate of the unstable fixed point.

We investigate the properties of this optimal point of the maximal transient in more detail. Let us consider a stimulation which is long and strong enough. If system (2.1) is reset for a time longer than the delay τ, the initial condition of system (2.1) at stimulus offset can be approximated by constants of the form (3.14) [see Sec. 3.1]. Thus, the strong reset constitutes an initial value problem for system (2.4) with initial values (3.14). Therefore we study the transient post-stimulus dynamics of the stimulus-free system (2.4) towards its stable phase-locked state for constant initial conditions $\varphi_1(t) = \varphi_1^{(0)} = \theta$ and $\varphi_2(t) = \varphi_2^{(0)} = (\theta + \pi)/2 + \pi n$, $n = 0, 1$, $t \in [-\tau; 0]$. It is easy to see that the dynamics of system (2.4) does not depend on the constant initial value $\varphi_2^{(0)}$. Hence, we fix it $\varphi_2^{(0)} = 0$.

In Fig. 3.13(a) the transient time T_{tr} is plotted versus the initial condition $\varphi_1^{(0)} = \theta$. One can see that there is one minimum and one maximum of the transient time, which correspond to those in Fig. 3.12(b). The mismatch between θ_{max} (where the maximum of T_{tr} is achieved) and coordinate $\varphi_1^{(u)}$ of the unstable fixed point Q becomes more significant with the increasing time delay τ. The difference $\varphi_1^{(u)} - \theta_{max}$ is depicted by plus signes in Fig. 3.13(b) versus τ for fixed K. One can see that the difference grows approximately proportionally to τ. The slope of the straight line Fig. 3.13(b) is $0.8/4.5$.

The coordinates $\varphi_1^{(s)}$ and $\varphi_1^{(u)}$ of the stable fixed point P and of the unstable fixed point Q of system (2.4) as well as values of θ_{max} are plotted in Fig. 3.13(c) versus τ and indicated by dots, crosses and circles, respectively. The corresponding transient time T_{tr} for constant initial conditions with $\varphi_1^{(0)} = \varphi_1^{(s)}$, $\varphi_1^{(u)}$, and θ_{max} is depicted in Fig. 3.13(d) by the same symbols, respectively.

When τ is small, the optimal value of the stimulation phase shift θ_{max} is located close to the value of $\varphi_1^{(u)}$ [see also Fig. 3.12(a)]. With increasing τ, θ_{max} moves from $\varphi_1^{(u)}$ towards the φ_1-coordinate $\varphi_1^{(s)}$ of the stable fixed point P. It is a generic situation that the values of θ_{max} separate the fixed points P and Q and can even be located closer to the stable fixed point than to the unstable one [Figs. 3.12(b) and 3.13(c)].

We explore now what a difference is in the dynamics of system (2.4) for the two distinct constant initial conditions $\varphi_1^{(0)} = \varphi_1^{(u)}$ and $\varphi_1^{(0)} = \theta_{max}$. These initial conditions corresponds to the stimulation which brings trajectories of system
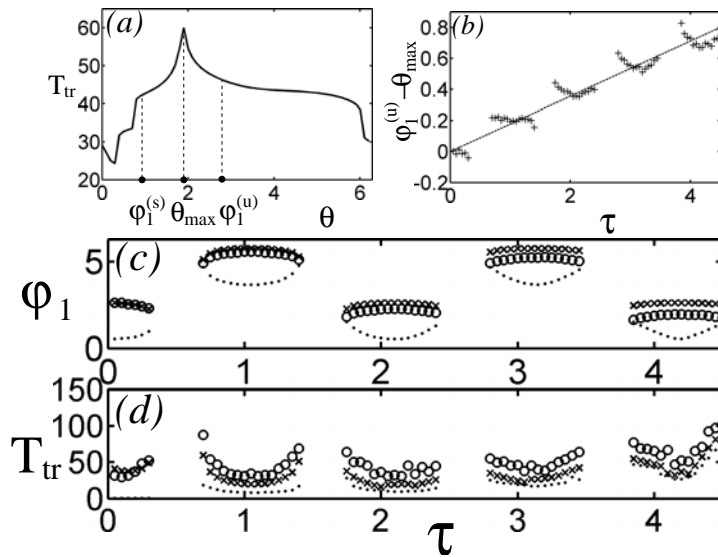
Figure 3.13: The transient time T_{tr} for system (2.4) for constant initial conditions $\varphi_1(t) = \varphi_1^{(0)}$ and $\varphi_2(t) = \varphi_2^{(0)} = 0$, $t \in [-\tau; 0]$. (a) T_{tr} versus $\varphi_1^{(0)}$ for $\tau = 4.0$. θ_{max} indicates the value of the initial phase shift $\varphi_1^{(0)}$ for a post-stimulus transient of maximal duration. (b) Differences between φ_1-coordinate $\varphi_1^{(u)}$ of the unstable fixed point Q of system (2.4) and the phase shift θ_{max} versus the delay τ. (c) Coordinates $\varphi_1^{(s)}$ and $\varphi_1^{(u)}$ of the stable fixed point P and the unstable fixed point Q of system (2.4), respectively, and the optimal initial phase shift θ_{max} are depicted versus τ by points, crosses, and circles, correspondingly. In the lower plot (d) the transient times T_{tr} are depicted by the same symbols as in (c) for initial condition $\varphi_1^{(0)} = \varphi_1^{(s)}$, $\varphi_1^{(u)}$, and θ_{max}, respectively. Parameters $\Delta_1 = 0.2$, $\Delta_2 = 3.0$, and $K = 0.4$.

(2.1) into a vicinity of the unstable phase locked state Q or the optimal point θ_{max} of the maximal transient, respectively. Figure 3.14(a) illustrates the time course of trajectories originating from such initial conditions.

The difference in the transient time for both cases is obvious: The trajectories enter an ε-neighborhood of the stable fixed point P after transient time $T_{tr} \approx 65$ for $\varphi_1^{(0)} = \varphi_1^{(u)}$ and $T_{tr} \approx 125$ for $\varphi_1^{(0)} = \theta_{max}$ (with $\varepsilon = 0.01$). Moreover, in the latter case the trajectory spends a long time in an almost stationary regime, where $\varphi_1(t)$ closely approaches the coordinate $\varphi_1^{(u)}$ of the unstable fixed point Q.

The transients in the $(\varphi_1(t - \tau), \varphi_1(t))$- projection of the phase space are illustrated in Fig. 3.14(b)-(d) for these two initial conditions. In the first case depicted in Fig. 3.14(b), where $\varphi_1^{(0)} = \varphi_1^{(u)}$, the trajectory leaves a vicinity of Q and directly spirals to the stable fixed point P which is a stable focus. In the second case depicted in Fig. 3.14(c) [with enlargements in Figs. 3.14(d) and
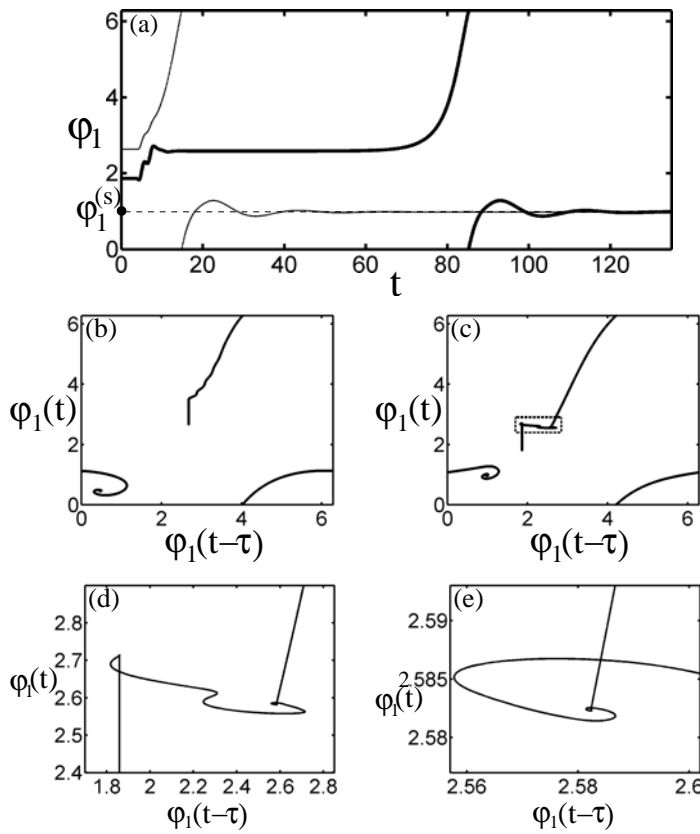
Figure 3.14: (a) Transients of system (2.4) towards the stable fixed point P occurring for two different constant initial conditions: $\varphi_1^{(0)} = 2.58 \approx \varphi_1^{(u)}$ (thin line) and $\varphi_1^{(0)} = 1.86 \approx \theta_{max}$ (bold line). $\varphi_1^{(s)}$ and $\varphi_1^{(u)}$ are the φ_1-coordinates of the stable P fixed point and the saddle fixed point Q, respectively. Transients from $\varphi_1^{(u)}$ and from θ_{max} are shown in (b) and (c), respectively, in the $(\varphi_1(t-\tau), \varphi_1(t))$-projection of the phase space. (d),(e) Successive enlargements of (c) around the φ_1-coordinate $\varphi_1^{(u)}$ of the unstable fixed point Q. Parameters: $\Delta_1 = 0.2$, $\Delta_2 = 3.0$, $\tau = 4.0$, and $K = 0.4$.

3.14(e)], where $\varphi_1^{(0)} = \theta_{max}$, the trajectory exhibits a different itinerary: The trajectory starting at the optimal value of the initial condition $\varphi_1^{(0)} = \theta_{max}$, first, very closely approaches the unstable fixed point Q and stays there for a long time before it is finally attracted by P. Such kind of a transient demands longer time than that in the first case of $\varphi_1^{(0)} = \varphi_1^{(u)}$ [Fig. 3.14(a) and 3.14(b)].

The unstable fixed point $Q = (\varphi_1(t), \varphi_2(t))$ of system (2.4) has the following coordinates in the infinite-dimensional functional phase space of Eq. (2.4): $\varphi_1(t) = \varphi_1^{(u)}$ and $\varphi_2(t) = \Omega_Q t + \text{const}$, where $\varphi_1^{(u)} \approx 2.58$ and $\Omega_Q \approx 3.06$ for parameter values as in Fig. 3.14. As mentioned above, a long and strong stim-

ulation (2.2) results in an almost complete reset of system (2.1), such that the post-stimulus transient of system (2.1) starts from almost constant initial conditions with $\varphi_1^{(0)} = \theta$ and $\varphi_2^{(0)} = Const$.

But the steady initial conditions are still far from the coordinates of the unstable fixed point Q (due to mismatch in φ_2) even if θ is taken equal to $\varphi_1^{(u)}$. Therefore, if the stimulus shifts φ_1 into a vicinity of $\varphi_1^{(u)}$, i.e., if $\theta \approx \varphi_1^{(u)}$, the fixed point Q has a minor influence on the post-stimulus dynamics of system (2.1) and the transient time appears to be relatively small [Fig. 3.14(a),(b)]. This is in contrast with the stimulation of coupled oscillators without delay, where the maximal transient time is attained for stimulation with $\theta = \varphi_1^{(u)}$ [Fig. 3.12(a) and Ref. [58]].

For system with delay (2.1), there is another optimal value of the stimulation phase shift $\theta = \theta_{max}$, at which the transient time is essentially larger than that for the other values of θ and attains its maximum [Figs. 3.13 and 3.14]. At this optimal value the unstable fixed point Q significantly affects the post-stimulus transient dynamics, although the initial conditions of system (2.1) for the post-stimulus transient for $\theta = \theta_{max}$ seem to be even more remote from Q than those for $\theta = \varphi_1^{(u)}$.

The fixed point Q of system (2.4) is of a saddle-focus type. Its eigenvalues are depicted in Fig. 3.15(a). Q has one real positive eigenvalue, one zero [62], and the others are complex conjugate with negative real parts. Therefore, the fixed point Q has a one-dimensional unstable manifold corresponding to the positive eigenvalue and an infinite-dimensional stable manifold $\mathcal{M}^{(s)}$ corresponding to the complex eigenvalues with negative real parts. If a trajectory of system (2.4) comes close to $\mathcal{M}^{(s)}$, it will then follow the manifold and approach the saddle point Q very closely, spending a long time there. Approaching the fixed point Q, the trajectory comes close to the unstable manifold of Q and, thus, it will eventually be repelled from Q by its unstable manifold and finally be attracted by the stable fixed point P.

This situation is realized during the post-stimulus transient of system (2.1) for the stimulation phase shift $\theta = \theta_{max}$ or close to that. This can be seen in Fig. 3.14(c)-(e), where the trajectory of Eq. (2.4) spirals to Q following $\mathcal{M}^{(s)}$, thereby exploring a characteristic focus shape of the stable manifold of Q, and only thereafter that being attracted by P.

The itinerary of the trajectory shown in Fig. 3.14(c)-(e) reflects the property of the saddle fixed point Q that its stable manifold $\mathcal{M}^{(s)}$ has an intersection with a class of constant initial conditions of the system (2.4).

To illustrate this fact, consider the following class of linear functions:

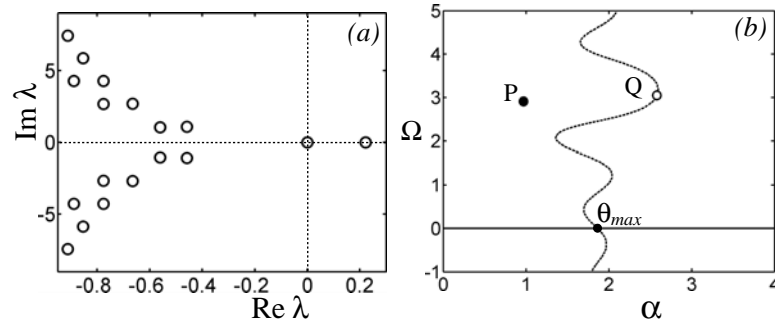$$\psi_1(t) = \Omega t - \alpha/2, \qquad \psi_2(t) = \Omega t + \alpha/2. \tag{3.15}$$

Figure 3.15: (a) A few eigenvalues λ_i with the largest real parts of the saddle-focus fixed point Q are depicted by empty circles in the complex plane. (b) Intersection of the stable manifold $\mathcal{M}^{(s)}$ of the saddle-focus fixed point Q with the class of functions (3.15) depicted by dashed curve in the (α, Ω)-parameter plane. The stable fixed point P and the saddle fixed point Q are shown by filled and empty circles, respectively. The stable manifold intersects the axis $\Omega = 0$ at the point $\theta_{max} \approx 1.86$. Parameters $\Delta_1 = 0.2$, $\Delta_2 = 3.0$, $\tau = 4.0$, and $K = 0.4$.

Taking functions (3.15) as initial conditions for system (2.1) we find regions in the (α, Ω)-parameter space, where the trajectories demonstrate different transients on their ways towards the stable fixed point P born in a saddle-node bifurcation together with Q. The transients differ with respect to whether or not the variable φ_1 rotates once through a cycle of 2π before being attracted by P. In other words, we find a boundary between the basins of attraction of P and its copy shifted by 2π. This boundary is depicted in Fig. 3.15(b) by a dotted curve in the (α, Ω)-parameter plane. It goes through the saddle fixed point Q and is the intersection of the stable manifold $\mathcal{M}^{(s)}$ of Q with the class of functions (3.15).

The manifold serves as separator between two different kinds of post-stimulus transients of system (2.1). The stable manifold also intersects with the axis $\Omega = 0$, i.e., it intersects with the class of constant initial conditions of the system (2.1), which we have at the end of each stimulus. The intersection point $\alpha = \theta_{max} \approx$ 1.86 is the phase shift of the maximal post-stimulus transient considered above [Figs. 3.13 and 3.14]. This demonstrates the central role of the stable manifold $\mathcal{M}^{(s)}$ of the saddle point Q in the post-stimulus dynamics of the stimulated system (2.1).

The existence of the intersection point θ_{max} of the line $\{\Omega = 0\}$ with the stable manifold of Q [Fig. 3.15(b)] means that for a long and strong stimulation of system (2.1) there exists an optimal value of the stimulation phase shift θ_{max} such that for $\theta \approx \theta_{max}$ a very long post-stimulus transient occurs. Theoretically, $T_{tr} \to \infty$ as $\theta \to \theta_{max}$, and when the post-stimulus initial conditions directly fit the stable manifold $\mathcal{M}^{(s)}$ of the fixed point Q. The trajectory will then be directly attracted by Q and will never relax to the stable fixed point P. Put

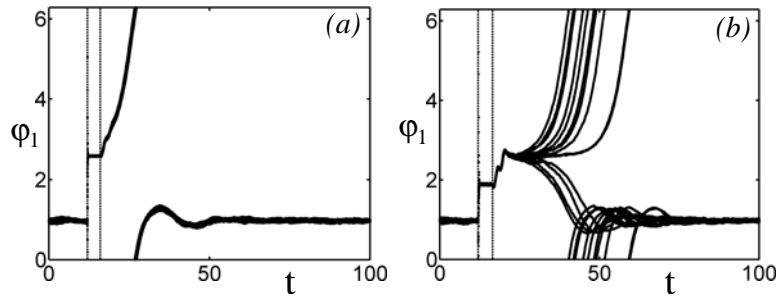otherwise, the trajectory gets trapped by the stable manifold $\mathcal{M}^{(s)}$.

Figure 3.16: Post-stimulus transients of system (2.1) stimulated with (a) $\theta = 2.583 \approx \varphi_1^{(u)}$ and (b) $\theta = 1.87 \approx \theta_{max}$ and with a Gaussian white noise with $D = 0.001$. Parameters $I = 15.0$, $T_{st} = 4.5$, $\Delta_1 = 0.2$, $\Delta_2 = 3.0$, $\tau = 4.0$, and $K = 0.4$. The number of stimuli $N = 15$ in both plots.

However, this limiting case is difficult to realize in practice, because of the inevitable noise and the mismatches in the stimulus-induced reset. Nevertheless, even with noise, the transient time at $\theta = \theta_{max}$ or close to θ_{max} is significantly larger than that for the other values of θ. This is illustrated in Fig. 3.16, where a few trajectories of the system (2.1) stimulated with noise and stimulation phase shifts $\theta = \varphi_1^{(u)}$ [Fig. 3.16(a)] or $\theta = \theta_{max}$ [Fig. 3.16(b)] are plotted. Comparing the results of the calculations shown in Fig. 3.16 with those in Fig. 3.14, one finds that the trajectories still follow the corresponding itineraries as in the case of ideal constant initial conditions, which provides an evidence for longer transients for the optimal value of the stimulation phase shift $\theta = \theta_{max}$.

At this moment we stop to consider the stimulation of our system in the stable phase-locked state and proceed to the other dynamical regimes emerging with increase of the coupling K.

3.3 Stimulation of periodically modulated synchronized states

A phase-locked state of system (2.1) is stable only for a finite interval of the parameter K values. The exemplary phase-locked states P and Q [Fig. 2.11(a)] have been considered above. When the coupling K increases, the stable fixed point P loses its stability via a supercritical Hopf bifurcation at which a stable limit cycle γ is born [Fig. 2.11(a) and 2.11(c)]. The limit cycle γ is stable within a range of the coupling strength. In this regime, called the periodically modulated phase synchronization, the phase difference φ_1, being attracted by γ, is periodically oscillating and is bounded between its maximal φ_1^{max} and minimal

φ_1^{min} values [Fig. 2.11(a),(c)]. In this section we study the influence of the stimulation in system (2.1) in the dynamical regime of periodically modulated phase synchronization.

An example of the cross-trial distributions and the corresponding stimulus locking indices typical for the stimulation in this regime is shown in Fig. 3.17. Due to the randomized stimulus administration, in the pre-stimulus time interval
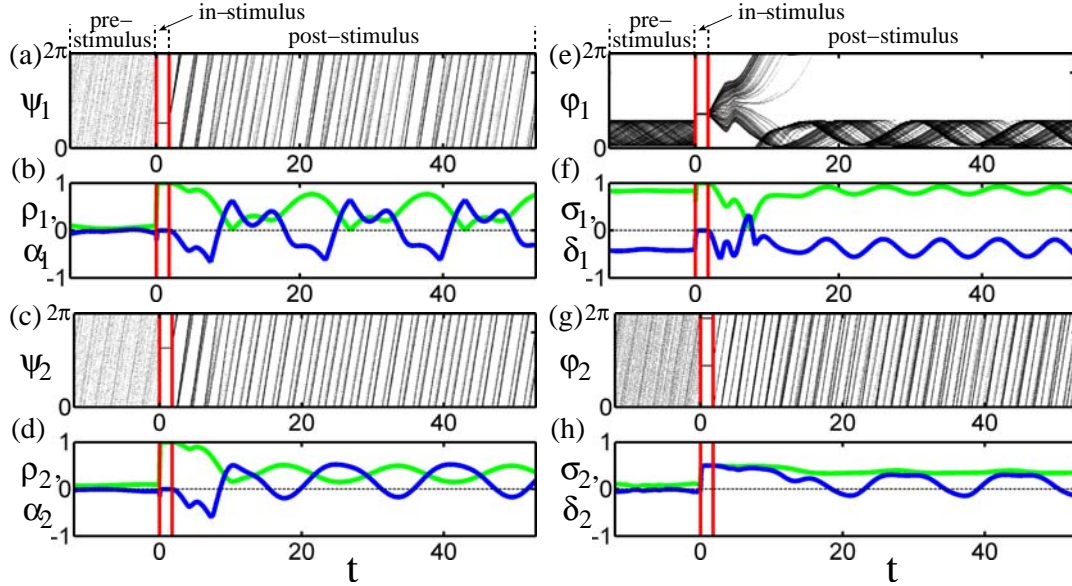

Figure 3.17: Stimulus-locked responses of system (2.1) stimulated in a periodically modulated synchronized regime. Cross-trials of the phases ψ_1, ψ_2, the phase difference φ_1, and the mean phase φ_2 are shown in (a), (c), (e), and (g), respectively, where the density of trajectories is encoded by an intensity of gray. All phases are taken modulo 2π. Onsets and offsets of stimuli are indicated by vertical red lines. The features of stimulus-locked dynamics as revealed by cross-trail indices (see Appendix and Ref. [58]): The resetting indices ρ_1, ρ_2 and the clustering indices α_1, α_2 of the phases ψ_1 and ψ_2 are shown in (b) and (d); the resetting indices σ_1 and σ_2 and the clustering indices δ_1 and δ_2 of the phase difference φ_1 and the mean phase φ_2 are shown in (f) and (h). The resetting/synchronization indices (green curves) and the clustering indices (blue curves) detect unimodal and anti-phase bimodal cross-trial distributions, respectively. The number of stimuli $N = 300$. Parameters $\Delta_1 = 0.2$, $\Delta_2 = 3.0$, $\tau = 4.0$, $K = 0.7$, and $\theta = 2.27$.

the phase difference φ_1 fills the whole segment $[\varphi_1^{min}, \varphi_1^{max}]$. A strong and long enough stimulus (2.2) results in the phase reset as described in Sec. 3.1. The coordinates of the reset states (3.14) are determined by the stimulation phase

shift θ and are independent on the underlying dynamics of system (2.1). For the considered case of a stimulated limit cycle, the in- and post-stimulus transients are more complicated than those for the case of stimulated phase-locked states considered above.

For the in-stimulus transient, for instance, the analysis similar to that from Sec. 3.1 can be applied. The difference here is that the initial conditions of system (2.4) summed over all stimulation trials at the stimulus onsets fill the whole strip $[\varphi_1^{min}, \varphi_1^{max}] \times [0, 2\pi)$ in the phase space in Fig. 3.1. This strip intersects the basins of attraction of the stable reset states A and B of system (3.4) and, hence, a more complicated clustered in-stimulus transient can be observed.

When the stimulation is off, the trajectories of system (2.1) relax from the reset state to the stable limit cycle γ. As discussed above, the stable manifold $\mathcal{M}^{(s)}$ of the saddle-focus fixed point Q of the system (2.4) serves as a separator of two kinds of a post-stimulus dynamics of system (2.1) when it is stimulated in a phase-locked state, see Sec. 3.2.3. The same holds for the stimulated regime of periodically modulated phase synchronization, since the saddle fixed point Q coexists with the limit cycle γ. The difference here is that the trajectories of Eq. (2.4) will be attracted after a stimulus offset by the limit cycle. This is illustrated by Fig. 3.17, where system (2.1) is stimulated with an optimal stimulation phase shift $\theta \approx \theta_{max}$.

One can see that there are two different groups of trajectories splitting from each other when the stimulus is off. The φ_1-coordinate of one of them is decaying, so that the trajectories are directly attracted by γ. The other group of trajectories exceeds the value $\varphi_1 = 2\pi$ and is attracted by a copy of γ shifted by 2π. This mechanism, which is similar to the case of stimulated phase-locked states, generates two stereotypical post-stimulus responses.

With a more detailed consideration of the post-stimulus dynamics of system (2.4) one observes another important phenomenon. For the post-stimulus responses, besides splitting trajectories into two post-stimulus clusters, there is also an additional spreading of them within each of the clusters of variable φ_1 [Fig. 3.17(e)]. Such a kind of a spreading can also be observed for a stimulated phase locked-state in a short time interval after stimulus offset, see Figs. 3.8(e) and 3.16(b).

However, for the stimulated phase-locked states, in the course of the post-stimulus transient these broad clusters of variable φ_1 are suppressed, when the trajectories are attracted by a stable fixed point. For the case of the stimulated periodically modulated synchronized state, the clusters of the variable φ_1 are preserved for the whole post-stimulus transient period. Moreover, the spreading of trajectories within the clusters is preserved as well [Fig. 3.17(e)]. This phenomenon is strongly related to the properties of a dynamics on the limit cycle.

The initial conditions of system (2.4) at a stimulus offset slightly differ from each other because of a noise, mismatches in reset states, and the time delay (if

the phases are reset for a time shorter than delay). Therefore, each trajectory spends a different amount of a time during a post-stimulus transient before it is attracted by the limit cycle γ. This causes the trajectories approaching γ attain different phase shifts along the limit cycle with respect to each other. Since there is no contraction or expansion along γ, the trajectories will preserve their phase shifts after a full rotation around γ, which can clearly be seen in Fig. 3.17(e). This explains the mechanism of a creation of the multicluster stimulus response of system (2.1) stimulated at the periodically modulated synchronized state.

The phenomena above are clearly reflected by the resetting and clustering indices depicted in Fig. 3.17. Indeed, these indices of the phases ψ_1 and ψ_2 as well as of the phase difference φ_1 (see Appendix) exhibit periodic oscillations preserved for the whole post-stimulus transient period. Such periodic oscillations of the stimulus locking indices are caused by periodic oscillations of clusters of trajectories of system (2.1) on the limit cycle γ. Within a period of rotation on γ, the projections of the response clusters on the corresponding axes demonstrate a subsequent gathering and separation of the clusters, leading to an anti-phase oscillation of the resetting and clustering indices, respectively. Such a dynamics of stimulus locking indices of the phases ψ_1 and ψ_2 can be seen in Fig. 3.17(b),(d). The state of clusters and values of stimulus locking indices are repeated after each period of the oscillations of trajectories on γ. In general, this results in a periodic behavior of the indices with the same period as that of the limit cycle γ [Fig. 3.17(b) and 3.17(d)].

3.4   Stimulation of multistable regimes

Multistability is a common phenomenon in complex systems, in particularly, in systems with delay [73, 11, 52, 27]. In this section we consider an impact of the stimulation on system (2.1) stimulated in dynamical regimes, where more than one stable state exists.

We are interested in the stimulation of the multistable states because of very simple reason which could be of a big use in medical applications: If in the neuronal dynamics of a brain there are several stable states which coexist, then it would be of the great benefit to be able by means of a stimulation to switch between them and thus shift the neuronal dynamics to the stable state which is the closest to the state of the normal functioning of a brain.

3.4.1   Bistability of phase-locked states

The first example is the case of the two coexisting stable phase-locked states, denoted by P and P', shown in Fig. 2.4. In both states the phases are in-phase

locked with $\varphi_1^* = 0$. However, P and P' have different frequencies: $\Omega_P \approx 5.12$ and $\Omega_{P'} \approx 3.96$, respectively. Depending on initial conditions, a trajectory of system (2.1) will be attracted either by P or by P'.

We calculate the basins of attraction of P and P' for the class of initial conditions of the form (3.15) [see also Ref. [52]]. The parameters to be varied here are the phase shift α and the frequency Ω. In Fig. 3.18, the basins of attraction of the fixed points P [white region] and P' [gray regions] are shown in
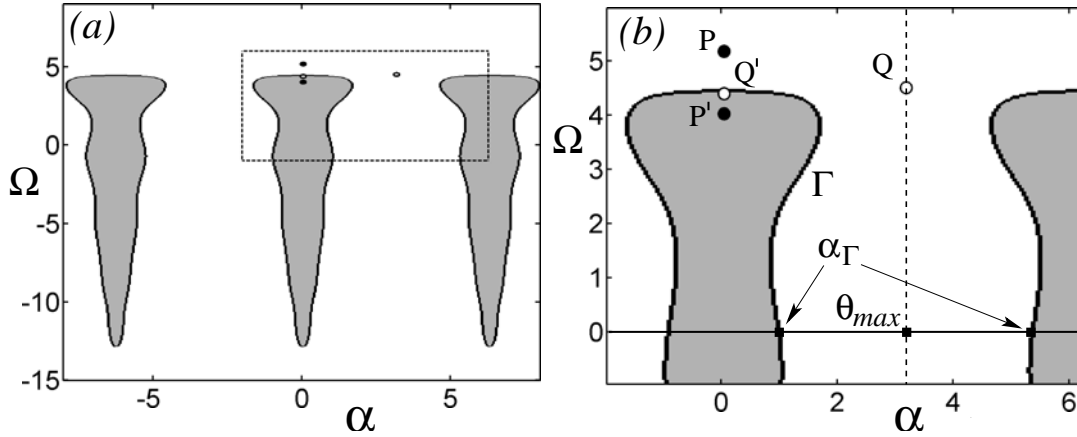
Figure 3.18: Basins of attraction of the two stable phase-locked states P (white region) and P' (gray regions) of system (2.1) calculated for initial conditions of the form (3.15) in the (α, Ω)-parameter plane. (b) Enlargement from (a). The stable fixed points P and P' are indicated by filled circles and the saddle fixed points Q and Q' are indicated by empty circles. Γ is the basin boundary of P' and $\alpha_\Gamma = \Gamma \bigcap \{\Omega = 0\}$, $\alpha_\Gamma \approx 0.95$ and $\alpha_\Gamma \approx 2\pi - 0.95$. The vertical dashed line shows the intersection of the stable manifold of Q with the class of functions (3.15), where $\theta_{max} = \pi$. Parameters: $\Delta_1 = 0.0$, $\Delta_2 = 4.5$, $\tau = 1.4$, and $K = 1.6$.

the (α, Ω)-parameter plane. The stable fixed points are depicted by black filled circles and the corresponding saddle fixed points Q and Q', which are born with P and P' in saddle-node bifurcations, respectively, are depicted by empty circles.

As mentioned above, after the long and strong enough stimulation a post-stimulus transient in system (2.1) starts from almost constant initial condition [see Sec. 3.1]. Therefore, the post-stimulus initial conditions of Eq. (2.1) are located in Fig. 3.18 within a small strip with $\Omega \approx 0$ and with the phase shift $\alpha = \theta$. By choosing an appropriate stimulation phase shift θ one can put the post-stimulus initial conditions of system (2.1) into the one or the other basin of attraction. In this way the stimulation can redirect trajectories from the one to the other stable state, e.g., from the phase-locked state P to P' and vice versa.

This is illustrated in Fig. 3.19, where the stimulation is performed with two different phase shifts $\theta = 0.9$ and $\theta = 1.0$ resulting in different synchronized dy-

namics after an stimulus offset, respectively. Note, the stimulus-induced switching between the states P and P' does not manifest itself in a change of a synchronization properties from the pre- to the post-switching dynamics of the system (2.1): In both states the oscillators are in-phase synchronized. However, after a switching of the mean frequency the synchronized state is significantly different.
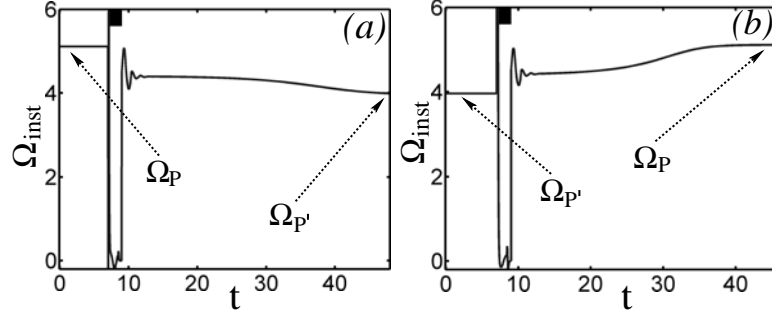

Figure 3.19: Stimulus-induced switching between the two stable in-phase-locked states P and P' from Fig. 2.4: (a) Stimulation phase shift $\theta = 0.9$ induces a transition from P with frequency $\Omega_P \approx 5.12$ to P' with frequency $\Omega_{P'} \approx 3.96$, and (b) stimulation phase shift $\theta = 1.0$ induces the inverse transition from P' to P. The vertical axis stands for the an instantaneous mean frequency $\Omega_{inst} = \dot{\varphi}_2$. Stimulation epochs are indicated by black bars at the top of the graphs. Parameters: $I = 15$, $T_{st} = 2.0$, $\Delta_1 = 0.0$, $\Delta_2 = 4.5$, $\tau = 1.4$, and $K = 1.6$.

The basin boundary Γ [boundary between gray and white regions in Fig. 3.18] plays an important role in the structure of the basin of attraction. Taking initial conditions close to Γ, one observes that the trajectory of the system (2.4) approaches very close the unstable fixed point Q'. For such initial conditions the transient dynamics is very similar to that discussed in Sec. 3.2.3, see Fig. 3.14.

As mentioned above, the fixed point Q' is born in a saddle-node bifurcation with P' and is of a saddle-focus type. Q' has one real positive eigenvalue, one zero, and the others are complex conjugate with negative real parts. The point Q' is placed on Γ and thus, its stable manifold $M^{(s)}(Q')$ contributes to the basin boundary and serves as a separator between the basins of attraction of the two different stable phase-locked states P and P'. In this way, the basin boundary Γ shown in Fig. 3.18 represents an intersection of the stable manifold $M^{(s)}(Q')$ with a class of functions (3.15). Therefore, analogously to the case considered in Sec. 3.2.3, one may expect that a very long post-stimulus transient in system (2.1) may occur also for the case illustrated in Fig. 3.18.

Indeed, from Fig. 3.18 it follows that the basin boundary Γ intersects the line $\Omega = 0$ in the points denoted by α_Γ. Since the post-stimulus initial conditions very close approach constant functions, they can be adjusted to approach very close the point $\alpha_\Gamma \in \Gamma$ [Fig. 3.18]. This can be achieved by a strong and long

enough stimulation with a phase shift $\theta \approx \alpha_\Gamma$. Then, during the post-stimulus transient, the trajectories of system (2.1) will follow the stable manifold $M^{(s)}$ of Q' approaching the saddle point Q' and spend a long time there before being attracted by one of the stable fixed points P or P'.

For the parameter values as in Fig. 3.18, there exists another saddle-focus fixed point Q which is born simultaneously with P. The stable manifold $M^{(s)}(Q)$ of the fixed point Q also has an intersection with the class of initial functions (3.15) and with the line $\Omega = 0$ [dashed line in Fig. 3.18(b)], which has been discussed in Sec. 3.2.3. Therefore, there is another optimal value of the phase shift $\alpha = \theta_{max}$ such that the stimulation with the phase shift $\theta \approx \theta_{max}$ brings the post-stimulus initial conditions of system (2.1) close to $M^{(s)}(Q)$. The corresponding post-stimulus trajectories then approach the saddle fixed point Q, which results in a long post-stimulus transient towards the stable phase-locked state P, similar to that illustrated in Fig. 3.14.
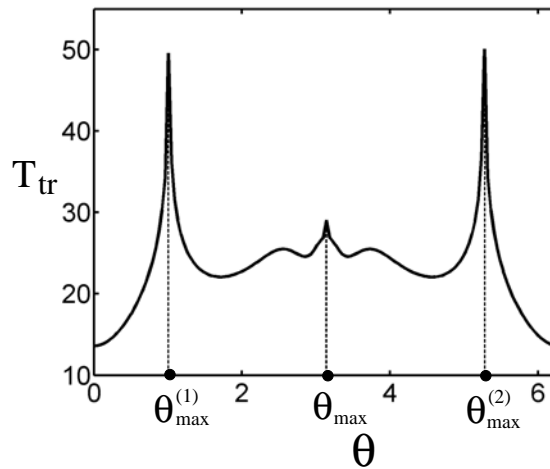
Figure 3.20: Mean post-stimulus transient time T_{tr} versus the stimulation phase shift θ calculated for system (2.1). Three local maxima are observed for $\theta = \theta_{max}^{(1)}$, θ_{max} and $\theta_{max}^{(2)}$, corresponding to the three points which closely approach the stable manifolds of the saddle fixed points Q (θ_{max}) and Q' ($\theta_{max}^{(1)}$ and $\theta_{max}^{(2)}$) [see also Fig. 3.18]. The number of stimuli $N = 100$. Parameters $\Delta_1 = 0.0$, $\Delta_2 = 4.5$, $\tau = 1.4$, $K = 1.6$, $I = 25$, and $T_{st} = 2.5$.

The length of the mean post-stimulus transient time T_{tr} calculated for system (2.1) for parameter values from Fig. 3.18 is depicted in Fig.3.20 versus stimulation phase shift θ. One can see that there are three optimal values of $\theta = \theta_{max}^{(1)}$, $\theta_{max}^{(2)}$, and θ_{max}, where the transient time T_{tr} attains local maxima. These are the points, where the post-stimulus initial conditions of system (2.1) come close to the stable manifolds $M^{(s)}(Q')$ and $M^{(s)}(Q)$ of the fixed points Q' and Q, respectively.

More precisely, the optimal phase shifts $\theta_{max}^{(1,2)}$ correspond to the phase shifts α_Γ [Fig. 3.18], which are placed on the basin boundary Γ and, thus, belong to the stable manifold $\mathcal{M}^{(s)}(Q')$. The stimulation with such phase shifts directs the trajectories during the post-stimulus transient to the saddle fixed point Q'. The optimal phase shift θ_{max} corresponds to the stable manifold $M^{(s)}(Q)$, and a stimulation with such a phase shift directs the trajectories to the saddle fixed point Q, see also Sec. 3.2.3.

3.4.2 Bistability of synchronous and desynchronous dynamics

Multistability occurs not only between synchronized states, but also between synchronized and desynchronized states, as shown in Sec. 2.2 [see Fig. 2.5]. An example of a stable phase-locked state P which coexists with the stable desynchronized limit cycle μ is shown in Fig. 2.5(b). In this section we consider the impact of the stimulation (2.2) on the dynamics of system (2.1) when it exhibits a multistable regime with the stable point P and a cycle μ. We consider parameter values indicated by the point A in Fig. 2.5(a).
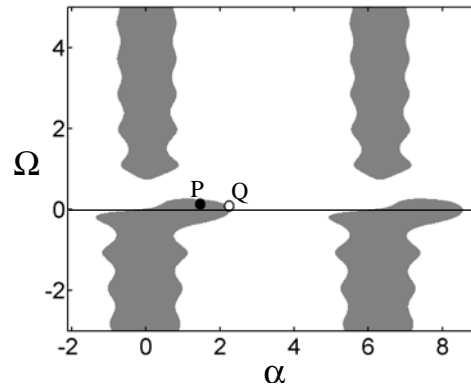
Figure 3.21: Basins of attraction of the stable phase-locked state P (gray regions) and the stable desynchronous limit cycle μ (white regions) [Fig. 2.5(b)] calculated for initial conditions of the form (3.15) in the (α, Ω)-parameter plain. The black filled circle indicates the stable fixed point P and the empty circle indicates the saddle fixed point Q. Parameters $\Delta_1 = 0.2$, $\Delta_2 = 0.1$, $\tau = 7.2$, and $K = 0.28$.

With the use of the class of linear functions (3.15), in Fig. 3.21 the basins of attraction of the stable phase-locked state P (gray regions) and the desynchronous limit cycle (white region) are shown in the (α, Ω)-parameter plane. Stimulation resets the variables of system (2.1) to the almost constant functions (Sec. 3.1). Therefore, as before, the initial conditions for the post-stimulus transient are

located close to the line $\Omega = 0$ with $\alpha = \theta$ in the (α,Ω)-parameter plane in Fig. 3.21. By varying the stimulation phase shift $\theta \in [0; 2\pi)$, the initial conditions can be placed at any point on the horizontal axis $\Omega = 0$. As one can see, this line intersects both basins of attraction in Fig. 3.21 and, thus, the stimulation with an appropriate phase shift θ can redirect the dynamics of the system from one stable state to the other.
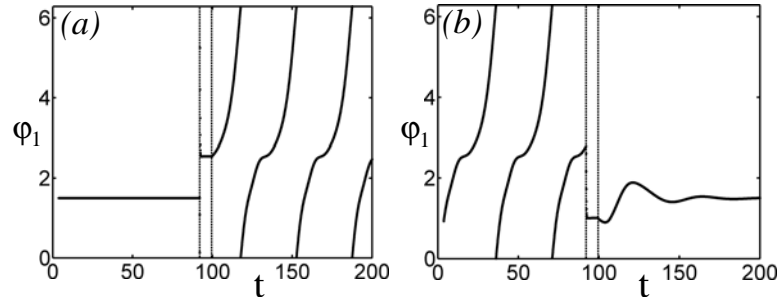

Figure 3.22: Stimulus-induced switching between the stable phase-locked state P and the stable desynchronous limit cycle μ [Fig. 2.5(b)]: (a) Stimulation phase shift $\theta = 2.3$ induces a transition from P to μ, and (b) stimulation phase shift $\theta = 2.2$ induces an inverse transition from μ to P. Stimulation onsets and offsets are indicated by vertical dashed lines. Parameters: $I = 15.0$, $T_{st} = 8.0$, $\Delta_1 = 0.2$, $\Delta_2 = 0.1$, $\tau = 7.2$, and $K = 0.28$.

The switching between synchronized and desynchronized states caused by the stimulation is illustrated in Fig. 3.22. Starting in a synchronized phase-locked regime, stimulation can effectively desynchronize system (2.1) [Fig. 3.22(a)]. On the other hand, starting from the desynchronized dynamics, the stimulation can also induce phase-locked synchronization [Fig. 3.22(b)].

Applying multiple stimuli one can end up with two different situations: *(i)* All trajectories before and after stimulation will exhibit the same synchronized or desynchronized dynamics, respectively; or *(ii)* there will be a mixture of trajectories, attracted by both stable synchronized and desynchronized states. In the case *(i)* the stimulation phase shift θ has to be chosen from the inner part of the corresponding basin of attraction. In the case *(ii)* the switching between different stable states can be achieved by values of θ close to the basin boundary, and enforced by noise which is inevitably present in natural systems.

Chapter 4

System of two phase oscillators coupled with delay

The communication among elements of complex systems inevitably takes place with some delay in time. This might be caused by the finite transmission speed of the signals, non-zero activation time of the elements of the system and many other factors. Transmission time is always of great interest, but it is often difficult to determine. The usually unknown structure of the system, communication paths between elements, latency times necessary for an element to respond to a transmitted signal, and many other confounding factors interplay with each other and make it impossible to reveal true sources of a delay in the system. Little is known about the transmission of stimulus effects in oscillators coupled with delay. To approach this issue, we study the transmission of stimulus-locked responses in a generic model studied by Schuster and Wagner [52]. This model consists of two phase oscillators interacting through a delay in time. We add a standard stimulation term S [Winfree 1980, Tass 1999] to one of the oscillators proposed by Schuster&Wagner [52] and, therefore, obtain Eq. (4.1)

$$
\begin{cases}
\dot{\psi}_1(t) = \omega_1 + \dfrac{K}{2} \sin\left[\psi_2(t - \tau) - \psi_1(t)\right] + S(\psi_1, t), \\[2mm]
\dot{\psi}_2(t) = \omega_2 + \dfrac{K}{2} \sin\left[\psi_1(t - \tau) - \psi_2(t)\right].
\end{cases}
\tag{4.1}
$$

where K is a coupling parameter, ω_1 and ω_2 are natural frequencies of the oscillators, and τ is a time delay.

$$
S(\psi_1, t) = X(t) I \cos(\psi_1(t) - \theta)
\tag{4.2}
$$

$S(\psi_1, t)$ is the stimulation signal. $X(t) = 1$ or 0 if the stimulus is on or off. I is a constant stimulus intensity, and θ is a constant phase shift parameter. The stimulation function is the first term of the Fourier expansion of a periodic function, and represents the phase-dependence of the oscillator's response to a

stimulus, which is a typical occurrence in numerous systems and quasi generic in biology [Winfree 1980, Tass 1999].

We study a transmission of a stimulus effect from the first, directly stimulated oscillator to the second not stimulated oscillator. This type of the transmission is fundamental for communication of networks of oscillators, e.g., in networks of oscillatory neuronal populations. In that case a single oscillator serves as a macroscopic model for a neuronal population. The estimation of transmission times is of great importance in neuroscience and neurology: Transmission times provide the functional roles of different brain areas and constitute the so-called mental chronometry (see [51], chapter four), according to which sensory information is subsequently processed in different brain areas and is transmitted from an active area to the next.

4.1 Dynamics of the model. Effect of the stimulation.

In this section we briefly overview the dynamics of the system. In addition the effect of the stimulation is briefly discussed. A more detailed study of the dynamics of this system without stimulation is reported elsewhere [52].

We introduce first two new variables: a phase difference φ_1 and a mean phase φ_2

$$
\begin{cases}
\varphi_1(t) = \psi_2(t) - \psi_1(t), \\
\varphi_2(t) = \dfrac{1}{2}(\psi_2(t) + \psi_1(t)),
\end{cases}
\tag{4.3}
$$

which will be used in the synchronization analysis. We also norm all phases ψ_1, ψ_2, φ_1 and φ_2 to the interval $[0; 2\pi]$. The dynamics in the system is asynchronous if the phase difference φ_1 exhibits unbounded rotations. In the case of phase-locked synchronization (see below) φ_1 is a constant. We also use the following notations: $\Delta_1 = \omega_2 - \omega_1$ is a natural frequency mismatch, and $\Delta_2 = (\omega_2 + \omega_1)/2$ is a mean frequency.

In the uncoupled regime ($K = 0$) each phase in the system grows with its own frequency ω_i such that the phase difference $\varphi_1(t)$ has the frequency Δ_1. A desynchronized dynamics is preserved in the system for small values of K. One can see this in Fig. 4.1(a). With increasing values of K the first pair of phase-locked states appears (see Fig. 4.1).

According to authors of [52] a phase-locked state is:

Definition 4.1 *A solution $(\psi_1(t), \psi_2(t))$ of system (4.1) is called a* phase-locked *state if both phases $\psi_1(t)$ and $\psi_2(t)$ linearly grow with the frequency Ω (Ω is constant) and the phase difference $\psi_2(t) - \psi_1(t)$ is preserved equal to α and is*

constant:

$$\begin{cases} \psi_1(t) = \Omega t - \dfrac{\alpha}{2}, \\ \psi_2(t) = \Omega t + \dfrac{\alpha}{2}. \end{cases} \tag{4.4}$$

We also call phase-locked states *fixed points.* An equivalent form of a phase-locked state (see chapter 2) reads:

$$\begin{cases} \varphi_1(t) = \alpha, \\ \varphi_2(t) = \Omega t + \mathrm{C} \end{cases} \tag{4.5}$$

To characterize any such fixed-point it is sufficient to indicate its frequency Ω and a constant phase difference α. The constant C is determined by initial conditions.
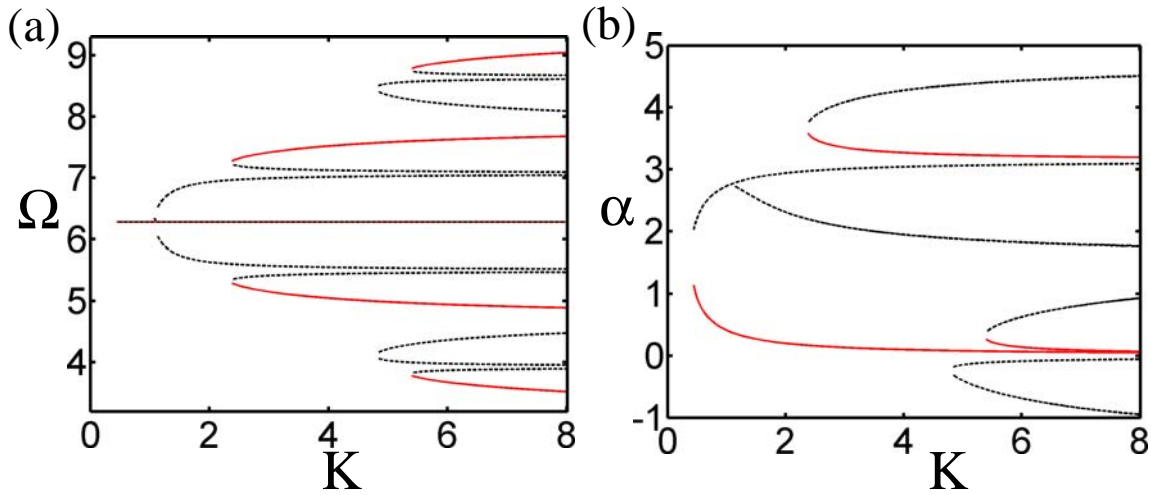
Figure 4.1: Appearance of phase-locked states in the dynamics of the system versus coupling parameter K. (a) Pairs of oscillation frequencies Ω are depicted. (b) Corresponding constant phase shifts α are depicted. Frequencies (phase shifts) appear in pairs. Red curves denote stable phase-locked states, black dashed curves - unstable ones. The first pair of phase-locked states has the same frequency $\Omega = 2\pi$. Parameters: $\tau = 2$, $\Delta_1 = 0.4$, $\Delta_2 = 2\pi$.

As K increases pairs of frequencies Ω appear (see Fig. 4.1) which indicates that the number of phase-locked states is increasing. Some of these fixed-points are stable. In general at larger K there are multiple stable phase-locked states.

Now we investigate how the stimulation affects system (4.1). We suppose that the stimulus is strong, i.e., $I \gg \omega_1$, $I \gg \omega_2$ and $I \gg K$. Then for such a stimulus during stimulation system (4.1) reads

$$\begin{cases} \dot{\psi}_1(t) \approx I \cos(\psi_1(t) - \theta) \\ \dot{\psi}_2(t) = \omega_2 + \dfrac{K}{2} \sin\left[\psi_1(t - \tau) - \psi_2(t)\right]. \end{cases} \tag{4.6}$$

To find fixed points, induced by the stimulation, one should put $\psi_1(t) = C_1$ and $\psi_2(t) = C_2$, where C_1, C_2 are constants, and solve system (4.6) using this conditions. Doing this we have:

$$
\begin{cases}
0 = I\cos(\mathrm{C}_1 - \theta) \\
0 = \omega_2 + \dfrac{K}{2}\sin\left[\mathrm{C}_1 - \mathrm{C}_2\right].
\end{cases}
\tag{4.7}
$$

We see that the phase ψ_1 is always reset by the strong stimulus to constant values $\psi_1^* = \mathrm{C}_1 = \theta + \pi/2 + \pi n$, where $n \in \mathrm{Z}$. But the stimulation resets the second phase ψ_2 only if stimulus is also long enough ($T_{st} \gg \tau$) and the coupling K is large enough ($K \geq 2|\omega_2|$ [the second of Eqs.(4.7) has a solution]). In this case we have that ψ_2 is also reset by the stimulation to a constant value C_2. The next equation give us values C_1 and C_2 in the case of full reset:

$$
\psi_1^* = \theta + \pi/2 + \pi n, \qquad \psi_2^* =
\begin{bmatrix}
\psi_1^* + \arcsin\left[\dfrac{2\omega_2}{K}\right] + 2\pi m \\
\psi_1^* - \pi - \arcsin\left[\dfrac{2\omega_2}{K}\right] + 2\pi m
\end{bmatrix}
\tag{4.8}
$$

where $n, m \in \mathrm{Z}$.

To summarize at this point we remark that a complete reset of both phases is possible only for sufficiently strong coupling $K \geq 2|\omega_2|$ for a long and strong stimulus. If at least one of the mentioned conditions is violated then only the phase of the first oscillator is reset by the stimulus, the second oscillator exhibits just some changes in its phase dynamics which start after τ time from the beginning of the stimulus.

4.2   Transmission time indices

Here we discuss two approaches to determine the transmission time of a stimulus from the first oscillator to the second one, based on both cross-trial analysis and standard averaging techniques.

The cross-trial analysis is performed as follows: The system is stimulated repetitively N times, with the interval between stimuli being stochastically varied, and always taken long enough to let the system return to its unperturbed behavior. For each stimulus we look at a time window which begins and ends at a fixed time before and after the stimulus. Cross-trial diagrams can then be compose by plotting the distribution of the phases of the oscillators, taken over all trials, as a function of time, relative to the beginning of the stimulus. Various indices can then be calculated from these distributions, which are used to investigate phase-resetting and clustering of trials.

One of these indices which reveals a clustering of trials is the order parameter of ν-order:

$$\lambda_\nu(\psi(t)) = \left| \frac{1}{N} \sum_{k=1}^{N} \exp(i\nu\psi^k(t)) \right|, \tag{4.9}$$

where k indicates the stimulus number, N is the number of stimuli, and ψ is a phase variable which could be any of $\{\psi_1, \psi_2, \varphi_1, \varphi_2\}$.

The resetting index is defined as:

$$\rho_j(t) = \lambda_1(\psi_j(t)) \tag{4.10}$$

The resetting index indicates how stereotypical the behavior of the system is across trials. Prior to a stimulus each trial will exhibit a different phase as a function of time, which will be uniformly distributed on the circle due to the stochastic timing of the stimuli. The stimulus will cause the oscillators to move towards a specific phase, which depends on a specific nature of the stimulus. This means that the cross-trial distribution of the phases, as a function of time, will no longer be uniformly distributed on the circle post stimulus. The resetting allows us to quantify the degree to which this distribution forms a single peak. It is equal to 0 when at time t the phases over all trials are uniformly distributed over the interval $[0; 2\pi]$, and 1 when the distribution of phases across all trials forms a single δ peak. The time t_{re}^j when maximum of ρ_j occurs is thus associated with the time of maximal effect of a stimulus on the oscillator j.

A long enough and strong stimulus results in $\rho_j \approx 1$, which means that a full reset of the phase ψ_j occurs. In the case where only one of the oscillators is stimulated, that oscillator is fully reset, and coupling brings the second oscillator to a partial reset after a certain time. We define the resetting transmission time of the stimulus as:

$$t_{\text{re}} = t_{\text{re}}^2 - t_{\text{re}}^1 \tag{4.11}$$

where t_{re}^j are defined as above.

Standard averaging techniques are based on the concept that each of the N trials of the phases represents the true signal plus additive noise. In that case by a simple averaging of trials as N tends to infinity, one should be able to extract the true signal. We take each trail number k of the form

$$x_j^k(t) = \cos(\psi_j^k(t)). \tag{4.12}$$

The averaged signal of the jth oscillator is:

$$x_j(t) = \frac{1}{N} \sum_{k=1}^{N} x_j^k(t) \tag{4.13}$$

The averaged signal may take on values ranging from -1 to 1. We denote $t_{\text{av}}^{j,\text{min}}$ and $t_{\text{av}}^{j,\text{max}}$ as times when $x_j(t)$ attains its minimum and maximum over

trials. For the oscillator #1 $x_1^{\max}$ indicates the maximal effect of a stimulus. This was arranged by an appropriate choice of θ, which determines the position of the reset state so as to have $cos(\psi_{1,reset}^k) \approx 1$ and thus x_1 to be maximal at the end of the stimulus. It is supposed that one of the events $x_2^{\min}$ or $x_2^{\max}$ indicates the maximal effect of stimulus on the oscillator 2. Following that, we define two transmission time indexes based on the averaged signal:

$$
\begin{aligned}
t_{av}^{\max} &= t_{av}^{1,\max} - t_{av}^{2,\max}, \\
t_{av}^{\min} &= t_{av}^{1,\max} - t_{av}^{2,\min}.
\end{aligned}
\tag{4.14}
$$

4.3 Convergence of the phase reset transmission time index

First we want to identify how the transmission indices let us estimate the transmission time of the stimulus in the system. For that purpose we fix the delay parameter τ and fix the rest of the parameters (ω_j, I, θ). The only parameter that is varied is K. In Fig. 4.2 all three transmission times are depicted versus K.
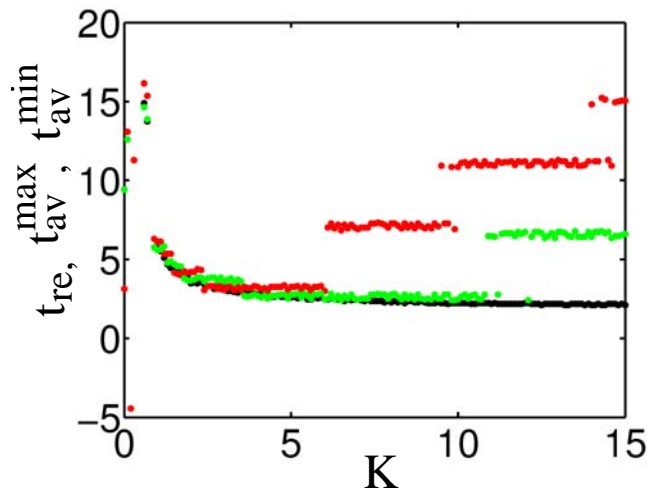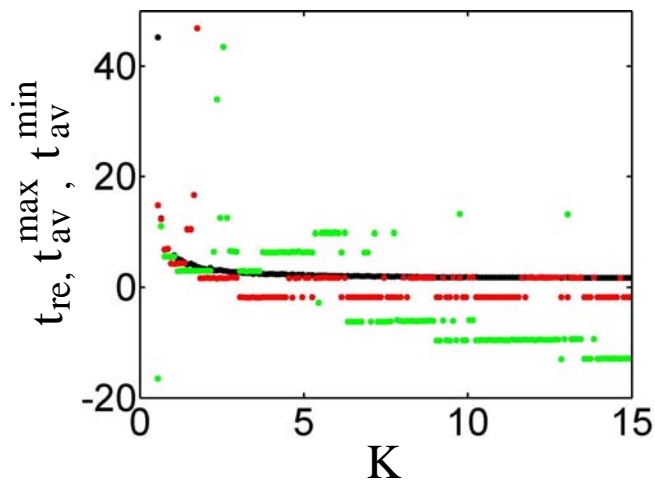

Figure 4.2: The transmission time indexes t_{re} (black), $t_{av}^{\max}$ (red) and $t_{av}^{\min}$ (green) versus K. Parameters: $\tau = 2$, $\Delta_1 = 0.4$, $\Delta_1 = 2\pi$, $I = 100$ and $\theta = 4.78$.

One can see that the transmission time t_{re} is changing gradually as K increases. When the coupling strength is large t_{re} converges to a value close to τ.

For small K ($K < 2|\omega_2|$) the $t_{av}^{\max}$ and $t_{av}^{\max}$ indices are changing gradually as well. On the other hand, as the coupling increases, $t_{av}^{\max}$ jumps from an initial value close to $\tau = 2$, to a value of approximately 7, and with growth of K to

even higher values of approximately 14, and so on. In this case one can not speak about a convergence to a finite value.

In Fig. 4.3 the results of the transmission time calculation are shown for another parameter set of system (4.1). Here we see that for K ranging from 0 to 2.5, all three transmission time indexes demonstrate gradual behavior. Afterwards t_{re} continues to converge to $\tau = 1.7$. However $t_{\text{av}}^{\min}$ exhibits discontinuities. As K grows $t_{\text{av}}^{\min}$ becomes negative and diverges from τ. The index $t_{\text{av}}^{\max}$ also exhibits discontinuities for intermediate coupling. For larger coupling strengths $t_{\text{av}}^{\max}$ comes closer to τ and convergence to τ may be possible.

Simulation with other parameter sets confirms the hypothesis that for large enough values of K, the resetting transmission index t_{re} converges to the value of the delay τ in a communication between the oscillators. We prove now this fact analytically.

Figure 4.3: The transmission time indexes t_{re} (black), $t_{\text{av}}^{\max}$ (red) and $t_{\text{av}}^{\min}$ (green) versus K. Parameters: $\tau = 1.7$, $\Delta_1 = 0.4$, $\Delta_1 = 2.4$, $I = 25$ and $\theta = 1.78$.

Consider the second of Eqs. (4.1), where $\psi_F = \psi_1(t - \tau)$ is the instantaneous value of ψ_1 (after a short transient time ψ_F becomes approximately constant during a strong stimulus):

$$\dot{\psi}_2(t) = \omega_2 + \frac{K}{2}\sin(\psi_F - \psi_2(t)) \tag{4.15}$$

For coupling strength $K > 2|\omega_2|$ solving Eq. (4.15) we obtain:

$$\psi_2(t) = 2\tan^{-1}\left(\frac{\exp(-p(t+C))(\frac{K}{2}+p) - \frac{K}{2} + p}{\omega_2(\exp(-p(t+C)) - 1)}\right) + \psi_F, \tag{4.16}$$

where $p = \sqrt{\frac{K^2}{4} - \omega_2^2}$, and C is a constant value determined by initial conditions.

At the end of a strong stimulus the first oscillator is reset in such a way that all trials ψ_1 attain the same value ψ_F. Exactly at this moment we observe a maximum of ρ_1. After time τ all trials of phase ψ_2 obtain this value of ψ_1. The phase ψ_2 then exponentially quick converges across trials to a single value according to Eq. (4.16). For large K the convergence time tends towards 0. This means that the maximum of ρ_2 occurs after the stimulus occurrence with offset equal the delay τ.

We proved analytically that resetting transmission time index converges to the communication delay time τ in the system as coupling grows. Hence if one is able to change a coupling in a system our method allows to determine the delay in the system.

4.4 Behavior of the averaged transmission time indices

Now we consider how the averaged transmission time indices behave as K grows. First let us denote that in case of multistability the averaged transmission time indices are not a simple superposition of analogous indices calculated for each stable phase-locked state separately. For example, if at some fixed K value we have M groups of trials belonging to M different stable phase-locked states, then to find maxima of an averaged signal x_j one should solve following equation:

$$\dot{x}_j(t) = \sum_{i=1}^{M} \frac{N_i}{N} \dot{x}_j^i(t) \tag{4.17}$$

where N_i is the number of trials in i^{th} phase-locked state, and x_j^i is the averaged signal over trials from i^{th} group. To find $t_{\text{av}}^{\max}$ and $t_{\text{av}}^{\min}$, one should find extremal points of the averaged signal (such a method is common among neurologists).

One can see that the averaged transmission time for each group of trials calculated separately does not necessarily constitute a solution of Eq. (4.17). Thus we can not speak about superposition of them and study transition $M \to \infty$. But nevertheless relying on Eq. (4.17) we can illustrate the mechanism of an averaged transmission time index formation. To do this consider results of the simulation of the system in the multistable regime at $K = 8$:

At this coupling strength we have the situation that all trials are distributed among two stable phase-locked states (Ω_1, α_1) and (Ω_2, α_2). Here $\Omega_1 = 2\pi$, $\alpha_1 = 0.0$, $\Omega_2 \approx 4.9$ and $\alpha_2 \approx 3.2$.

The maximum of the averaged signal of $x_1(t)$ is determined in this case by the stimulation. Therefore we provide an analysis of the extrema of the signal $x_2(t)$ only. Let us separate trials of ψ_2 into two groups, 1 and 2, each belonging to a different stable state, and calculate the averaged signal x_2 for each of them. Figure 4.4(a) demonstrates all four signals $x_1(t)$, $x_2(t)$, $x_2^1(t)$ and $x_2^2(t)$.
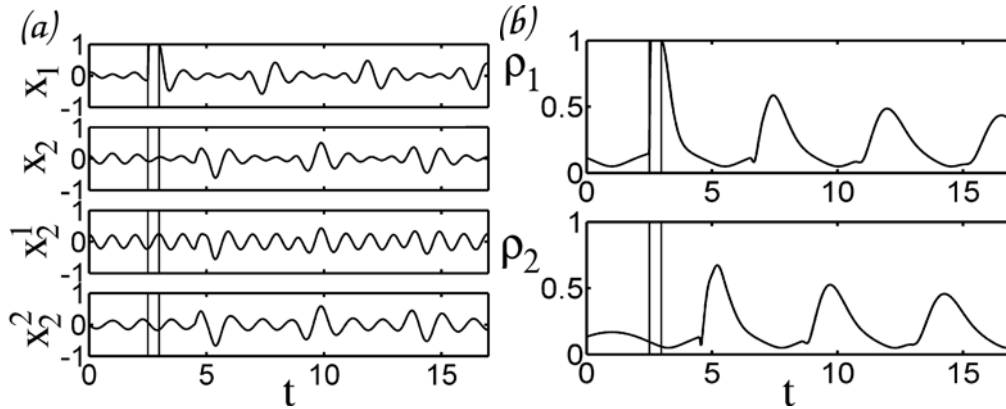

Figure 4.4: Averaged signals and resetting indexes for a fixed coupling K value. Vertical black lines show the onset and offset of stimuli. (a) Two upper plots: averaged signals $x_1(t)$ and $x_2(t)$. Two lower plots: all trials of the second oscillator are split into two groups 1 and 2. For every group the averaged signals $x_1^1(t)$ and $x_2^2(t)$ are shown. (b) Resetting indexes $\rho_1(t)$ and $\rho_2(t)$. Parameters: $\tau = 2$, $\Delta_1 = 0.4$, $\Delta_1 = 2\pi$, $K = 8$, $I = 100$ and $\theta = 4.78$.

The maximum of $x_1(t)$ occurs at the end of stimuli at $t \approx 2.42$. For $x_2(t)$ the maximum occurs at $t \approx 9.37$ and the minimum occurs at $t \approx 4.95$. That gives $t_{av}^{max} \approx 6.95$ and $t_{av}^{min} \approx 2.53$. The first stable phase-locked state has period of oscillations $T_1 = 1$ and the second one - $T_2 \approx 1.28$, correspondingly. The minimum of $x_2(t)$ coincides in time with the minima of both $x_2^1(t)$ and x_2^2. Likewise for the maximum of $x_2(t)$. In this case Eq. (4.17) has a simple solution. We just find absolute minimum and maximum of x_2^1 and x_2^2, and they give us desirable t_2^{min} and t_2^{max}. This occurs because the stimuli reset ψ_2 in such a way that at the end of the stimuli x_2^1 has a local maximum and x_2^2 has a local minimum. After 2.53 time units x_2^1 makes 2.5 cycles and attains a minimum, and during the same time x_2^2 performs 2 cycles and also attains a minimum. This resonance of minima gives the absolute minimum of x_2. The analogous mechanisms explains the formation of the maximum of x_2.

How to explain "jumps" in the staircases in Figs.4.2, 4.3? We see that every "jump" increments or decrements t_{av}^{min} and t_{av}^{max} on $\approx$ 4-5 time units, which does not coincide with any of periods of stable phase-locked states. To answer this question we need consider not only timing of peaks in the averaged signals, but try to explain dynamically their formation for example through presence of an

amplitude dynamics of the averaged signals. The amplitude dynamics of oscillations of all four averaged signals x_1, x_2, x_2^1, and x_2^2 is more interesting and is stimulus induced.

For example at $K = 9.7$ all trials in experiment distribute among two stable phase-locked states (Ω_1, α_1) and (Ω_2, α_2). Here $\Omega_1 \approx 3.45$, $\alpha_1 = 0.05$, $\Omega_2 \approx 4.85$ and $\alpha_2 \approx 3.18$. Figure 4.5(a) shows frequencies of three exemplary trials of the
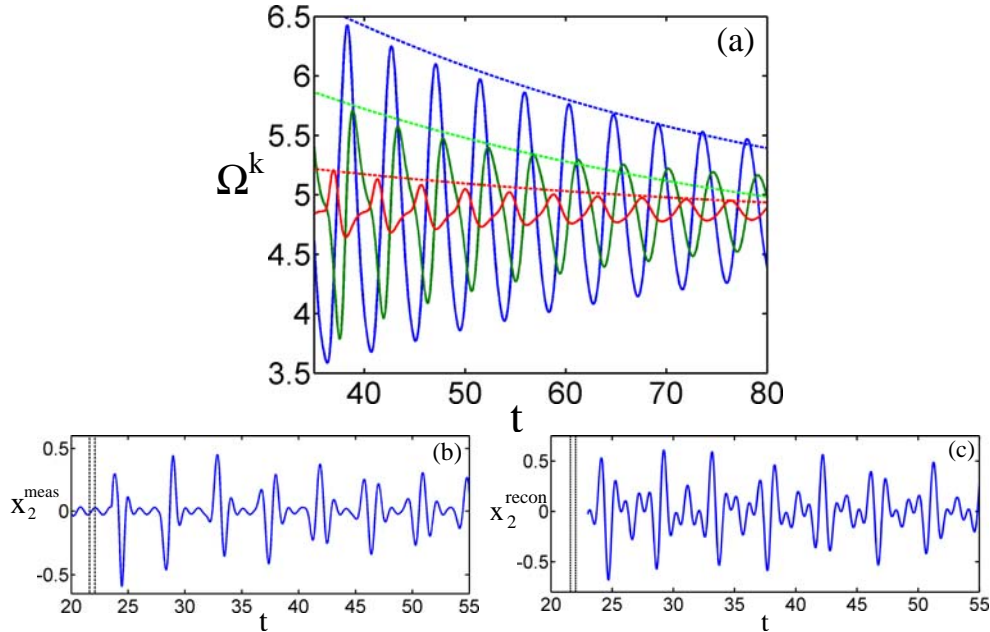

Figure 4.5: (a) Oscillations in frequencies of three exemplary trials in (Ω_2, α_2) phase-locked state after stimulus. Dashed curves provide envelope for amplitude decay. (b) x_2^2 averaged signal as it results from the stimulation ("meas" stands for "measured"). (c) x_2^2 averaged signal reconstructed using suggestions about frequencies of every trial. Parameters: $\tau = 2$, $\Delta_1 = 0.4$, $\Delta_1 = 2\pi$, $K = 9.7$, $I = 100$ and $\theta = 4.78$.

second oscillator in (Ω_2, α_2) phase-locked state after stimulus. Instantaneous frequencies oscillate around $\Omega_2 = 4.84$ with period $T \approx 4.4$. Such an oscillation of frequencies is induced by the stimulation and has period which coincides neither with T_1 (1.82) nor T_2 (1.29). As the stable phase-locked state (Ω, α_2) attracts the oscillators a phase itinerary is spiraling to it. Taking this into consideration, a period of oscillations of frequencies is determined by an eigenvalue of the stable phase-locked state with the maximal positive real part $\lambda^{max} = \mu + i\nu$ ($\mu = \max_i \mathrm{Re}(\lambda_i)$). Therefore ν gives us an estimate of the period above, namely $T \approx \frac{2\pi}{\nu}$. For the case depicted in Figure 4.5 $\lambda^{max} = -0.02 + i1.41$ and $T \approx 4.41$ (see value above). The real part μ of λ^{max} gives us an amplitude decay of oscillations of frequencies for each trial: $A(t) \approx e^{\mu t}$. In figure 4.5(a) the amplitude

decay is shown by dashed lines. Below an equation of a hypothetical dependency of frequency of each trial is shown:

$$\Omega^k(t) = A^k(t_0)e^{\mu(t-t_0)}\cos(\nu t + \omega^k(t_0)) \tag{4.18}$$

where t_0 is time, from which on frequency is supposed to be approximated by equation (4.18), $\Omega^k(t)$ is a frequency of the trial number k, $A^k(t_o)$ is amplitude of oscillations of frequencies of the trial k measured at time t_0 and $\omega^k(t_0)$ is a measured phase of frequency's oscillation at time t_0.

Having information about the behavior of the frequencies of every trial we made surrogate averaged signal according to the formula

$$x_2^{recon}(t) = \frac{1}{N}\sum_{k=1}^{N}\cos(\Omega^k(t) + \Omega_2 t + \psi_2^k(t_0)) \tag{4.19}$$

where the summation is taken over all N trials, Ω_2 is the frequency of the stable phase-locked state, $\psi_2^k(t_0)$ is an initial phase of the kth trial of the second oscillator measured at time t_0.

We show signal x_2^{recon} reconstructed according to the equations 4.18, 4.19 in comparison to the real averaged signal (see Fig.4.5(b),(c)). They are in an agreement to each other. We observe that peaks in the averaged signals x_2 and x_2^{recon} follow one another with period sometimes 4 sometimes 5 time units, which are the nearest periods multiples of T_1 and T_2 close to $T \approx 4.4$. When the coupling K increases distribution of trials between the different stable phase-locked states changes and one of the peaks in averaged signals becomes more prominent. In such a way staircases attain "jumps" near 4-5 time units as K grows.

We described how the stimulation disturbs own dynamics of the system and modulates oscillations of each trial of the signals of the oscillators. The resulting averaged signals have period of oscillations determined by a stability of the phase-locked state. Averaged transmission time indices reflect these oscillatory processes of the signals, but not directly a transmission time of the stimulus.

Chapter 5

Prospects

Beyond the scope of present work for this dissertation there are some aspects, which deserve the interest of researchers and could be studied in the future.

Coming back to the dynamics of system (2.1), we see that all phase-locked states are classified and belong to one of the swallow regions in the $\tau - K$ parameter space. We derived the equation which defines swallow birth curves (see 2.2.2), but did not solve it. It is possible to solve this equation and, in that way, to find coordinates of some phase-locked states analytically. Moreover, we estimate the stability range for the parameter K of the stable phase-locked states belonging to the swallow birth curves for some pairs of (τ, K) parameters. Knowing the coordinates of all stable phase-locked states on these curves it might be possible to determine their stability ranges in K or τ parameters.

Besides the fixed points of the system (2.1) on the swallow birth curves there are those fixed points, which originate in pitchfork bifurcations. It is an open question whether their coordinates and stability ranges could be derived analytically. Answers to the questions above could probably give us a scaling law accoding to which one "swallow" is mapped onto the other.

We omitted in our work the stimulation of system (2.1) in regimes of the coexistence of two stable limit cycles, the chaotic phase synchronization, etc. These regimes might reveal some new and unknown aspects of the stimulation.

In the last chapter (chapter 4) we saw that the reset stimulus transmission time index T_{re} converges gradually to the delay time τ in the system as coupling strength K increases. In practice we often cannot change the coupling K in a system. If we knew the law according to which convergence occurs then for a given K and a measured T_{re} we would be able to estimate the delay time in the system. Furthermore, it seems to be useful to test the proposed stimulus transmission time index T_{re} on other different systems and discover whether a convergence $T_{re} \to \tau$ also takes place in them as soon $K \to \infty$. This index may

need to be modified or somehow generalized.

It would be of great interest to test our results in practice to try to verify our model by choosing physiological values of parameters and comparing the outcome of the models with raw data, obtained from experiments conducted on humans, rats, etc.

Chapter 6

Conclusions

The thesis contains results of consideration of the two systems of two coupled phase oscillators each. By means of these systems we modeled different aspects of an oscillatory dynamics in nature. One of the most interesting field for application of the theory discussed here is neurology. We supposed that each oscillator in this case models the dynamics of a single neuronal population. These populations interact via the coupling which includes a delayed self-feedback in the first system and a delayed signal in the second system. We studied the dynamics of both models to be able answer the question what kind of dynamical regime is present in the systems for given to parameter values.

The question how the brain reacts on an external stimulation is for a neuro-physiologist of a particular interest. Knowing this a researcher investigates brain functioning. In our models we stimulated oscillators (both in the first system and one in the second system) with a strong and sufficiently long stimulation. As results (similar to real world systems) different transient responses to stimuli were observed. A presence of a delay involved multistability phenomena in the dynamics of the oscillators, which demonstrated a rich variety of responses. In the following we discuss the main results for each system separately.

For the first system we presented a detailed study of stimulus-locked responses of two coupled phase oscillators with delayed feedback. If compared to the stimulation of coupled oscillators without delay [58], one finds that stimulated system (2.1) in its turn demonstrates two-cluster response on the stimulation. We observed two types of clustering of trials: in-stimulus clustering (during a stimulus) and post-stimulus clustering (after the stimulus). By applying the stochastic phase resetting approach [57, 58] and the bifurcation theory we explain the formation of in- and post-stimulus clustering of phase variables in stable phase-locked states.

Thus for sufficiently strong stimulation, the in-stimulus clustering is completely determined by the form of the stimulation. In application to the brain sciences it means that some stimulations may result in a clustering of registered

evoked potentials, but in fact this clustering does not correspond to different responses of the brain itself, but rather is an induced artifact.

However, the post-stimulus dynamics of the system is strongly related to the global structure of the phase space of the initial system. We uncover the role of the stable manifolds of saddles (which are very common in systems with delayed variables) in the maximal post-stimulus transients and maximal post-stimulus clustering.

Considering the stimulation phase shift θ as the main parameter, we determined the optimal value θ_{max} which is responsible for the longest post-stimulus transient and for the maximally pronounced post-stimulus clustering of the stimulus-locked system responses.

Post-stimulus clustering of trials can give a key for a neurophysiologist, who as a rule is occupied by a pattern recognition of evoked brain potentials. Our explanation of the post-stimulus clustering mechanism can help to distinguish two different stereotypical brain responses. Since θ_{max} does not coincide with a coordinate of an unstable state in the system (but is determined by it!) an unexperienced researcher, which expects this equality to be true, would be disappointed by his observation. The other meaning of θ_{max} is very important in practice and is that the stimulation with the optimal value of the parameter θ provokes the longest transient response in time, which should be exploited in DBS (deep brain stimulation) and similar techniques, which are supposed to keep an effect of the stimulation during the possibly longest time between successive stimuli.

We also studied the impact of the stimulation on the periodically modulated synchronized regime supported by a stable limit cycle. We showed that the stereotypical stimulus-locked system responses exhibit periodic oscillations established and preserved after stimulus offset. In addition, the system responses to the stimulation demonstrate an persistent spreading of trajectories within the clusters, which is connected to the properties of the limit cycle.

We illustrated the stimulus-induced switching between coexisting stable synchronized states and also between coexisting stable synchronized and desynchronized states. The multistability is a generic phenomenon in complex systems and systems with delayed variables and, thus, is expected to be a common in the nature. We showed that the stimulation can induce frequency change in a phase-locked synchronized regime. The stimulation can also completely change the long-term system dynamics from synchronized to desynchronized due to the stimulation at the coexistence of corresponding stable regimes.

Surprisingly, we found that stimulation can induce a frequency change in the multistability regime of stable phase-locked states. Stimulation can also completely change the long-term system dynamics from synchronized to desynchronized when

the corresponding stable states coexist in the system.

This property of the stimulation could be of great importance in medical application, where stimulation, for instance, can bring system from a pathologically synchronous state to a normal, desynchronized state. This study contributes to a better understanding and correct interpretations of the observed stimulus-locked responses widely used in experimental studies of complex neuronal systems.

In the second system, we examined the transmission of a stimulus from one stimulated oscillator to the other non-stimulated oscillator. Three different transmission time indices were used in the investigations: two averaged transmission time indices and the resetting transmission time index. This investigations are in a tight connection to practice, namely to the brain chronometry, the signal propagation and the signal processing investigations. Let a neurologist stimulate some brain areas and register afterwards an increased activity in other areas. How to verify if these splashes of activity are occasional or related? For this one needs a tool which surely detects transmission of a stimulus over neurons.

We studied how transmission time indices were changing in a transition of the coupling K from 0 to $+\infty$. The first two of them, averaged transmission time indexes, behaved irregularly as the coupling parameter K increases, their values formed the staircases which either led up or down with an increase of K. In contrast, the resetting transmission time index gradually changed with a smooth change of K and finally converged to the delay time τ in the system. We proved that averaged transmission time indices did not reflect the delay in communication in the system, but rather wer determined by the oscillatory dynamics of the averaged signals.

Unlike the averaged transmission time indices, the resetting transmission time index t_{re} reflects changes in the distribution of trials, and when a reset of the first oscillator is transmitted to the second oscillator it is detected by t_{re}.

Such a powerful tool as the resetting transmission time index should be tested and verified on the other oscillatory systems. Also an algorithm how to estimate the delay time τ using t_{re} could be developed. These can help to estimate latency times in the brain and, thus, to gain a new information about true parameter values in the dynamics of the neurons.

The two systems considered are complementary with respect to the role of the delay in the dynamics: each oscillator can obtain either a delayed signal from a neighbouring oscillator or a delayed self-feedback signal. We can therefore utilize them as basic elements and construct more realistic and viable models, using the benefits of delayed loops of both types.

Appendix A

Stimulus locking indexes

To quantify the extent of stimulus locking of the variables $\psi_{1,2}$ and $\varphi_{1,2}$ of system (2.1), (2.2), following Ref. [58] we consider time-dependent stimulus locking indices

$$\lambda_\nu(x(t)) = \left| \frac{1}{N} \sum_{k=1}^{N} e^{i\nu x^{(k)}(t)} \right|. \tag{A.1}$$

The time t here is the relative time within the stimulation windows considered around each stimulus. The averaging is performed over N stimulation trials, i.e., k is the stimulus number. The variable $x(t)$ in Eq. (A.1) is one of ψ_1, ψ_2, φ_1, or φ_2 and $x^{(k)}(t)$ indicates the corresponding variable in the stimulation window around the kth stimulus. Integer ν is the order of indices corresponding to the νth Fourier mode of the phase distributions over trials, which reflects an emergence of a ν-cluster state of the stimulus-induced system responses.

Further, we define resetting indices:

$$\begin{aligned} \rho_j(t) &= \lambda_1(\psi_j(t)), \\ \sigma_j(t) &= \lambda_1(\varphi_j(t)), \quad j = 1, 2, \end{aligned} \tag{A.2}$$

and clustering indices

$$\begin{aligned} \alpha_j(t) &= \lambda_2(\psi_j(t)) - \lambda_1(\psi_j(t)), \\ \delta_j(t) &= \lambda_2(\varphi_j(t)) - \lambda_1(\varphi_j(t)), \quad j = 1, 2. \end{aligned} \tag{A.3}$$

One can see that the resetting indices attain large values close to 1 if the distribution of the corresponding variable of system (2.1), (2.2) over stimulation trials exhibits a single sharp peak. On the other hand, for two peaks in the distribution with distance between them close to π, the reseting indices will be small, whereas the second order indices λ_2 will be large. The clustering indices will thus be also large indicating a two-cluster state of the distribution of the corresponding variable. For the higher-order clustering states up to a uniform distribution of the phases, both indices λ_1 and λ_2 are small and so are the resetting and clustering indices.

Bibliography

[1] E. Ahissar, and D. Kleinfeld Closed-loop Neuronal Computations: Focus on Vibrissa Somatosensation in Rat. Oxford University Press 2003.

[2] R. Bellman and K.L. Cooke, *Differential-Difference Equations*, Academic Press,1963.

[3] A. L. Benabid, P. Pollak, C. Gervason, D. Hoffmann, D. M. Gao, M. Hommel, J. E. Perret, & J. De Rougemont, Long-term suppression of tremor by chronic stimulation of the ventral intermediate thalamic nucleus, *The Lancet* **337**, 403–406 (1991).

[4] E. N. Best, Null space in the Hodgkin–Huxley equations: a critical test, *Biophys. J.* **27**, 87–104 (1979).

[5] A. Beuter, J. Bélair, and C. Labrie Feedback, Delays, and Dynamics of Oscillatory Behaviors in Patients with Neurological Diseases. –541 *Bull. Math. Biol.* **55**, 525 (1993).

[6] S. Blond, D. Caparros-Lefebvre, F. Parker, R. Assaker, H. Petit, J.-D. Guieu, & J.-L. Christiaens, Control of tremor and involuntary movement disorders by chronic stereotactic stimulation of the ventral intermediate thalamic nucleus, *J. Neurosurg.* **77**, 62–68 (1992).

[7] K.H. Chiappa, Evoked Potentials in Clinical Medicine. Raven, New York, 1983.

[8] M.Y. Choi, H.J.Kim, and D. Kim, Phys. Rev. E **61**, pp. 371-381 (2000).

[9] G.D. Dawson, A summation technique for the detection of small evoked potentials, *Electroencephalogr. Clin. Neurophysiol* **44**, 153 (1954).

[10] Elble, R. J. & Koller, W. C., *Tremor*. John Hopkins University Press, Baltimore, 1990.

[11] U. Ernst, K. Pawelzik, and T. Geisel, Delay-Induced Multistable Synchronization of Biological Oscillators. –2162 *Phys. Rev. E* **57**, 2150 (1998).

[12] J. Faro and S. Velasco, An approximation for prey-predator models with time delay. *Physica D* **110**, 313 (1997).

[13] I. Fischer, Y. Liu, and P. Davis, Synchronization of chaotic semiconductor laser dynamics on subnanosecond time scales and its potential for chaos communication. *Phys. Rev. A* **62**, 011801 (2000).

[14] J.A.C. Gallas, Structure of the Parameter Space of the Henon Map. *Phys. Rev. Lett.* **70**, 2714-2717 (1993).

[15] C. Ghez, in *Principles of Neural Science*, 3rd edition, edited by E.R. Kandel, J.H. Schwartz, and T.M. Jessell (Norwalk, Appleton and Lange, 1991), p. 626.

[16] L. Glass & M. C. Mackey, *From Clocks to Chaos. The Rhythms of Life* Princeton University Press, Princeton, 1988.

[17] R. Guttman, S. Lewis, & J. Rinzel, Control of repetitive firing in squid axon membrane as a model for a neurone oscillator, *J. Physiol. (London)* **305** 377–395 (1980).

[18] M. Hämäläinen, R. Hari, R.J. Ilmoniemi, J. Knuutila, and O.V. Lounasmaa, Magnetoencephalography: Theory, instrumentation, and applications to noninvasive studies of the working human brain. *Rev. Mod. Phys.* **65**, 413 (1993).

[19] H. Haken, A. Wunderlin, Slaving principle for stochastic differential equations with additive and multiplicative noise and for discrete noisy maps. *Z. Phys.* **47**.

[20] J.K. Hale, L.S. Verduyn, S.M. Verduyn, *Introduction to Functional Differential Equations*. Springer, 1993.

[21] C. Hauptmann, O. Popovych, P.A Tass, Delayed feedback control of synchronization in locally coupled neuronal networks. *Neurocomputing* **65-66** (2005), pp. 759-767.

[22] J.J. Hopfield Neural Networks and Physical systems with emergent collective computational abilities *Proc. Natl. Acad. Sci. U.S.A.*, 79 (1982), pp. 2554-2558.

[23] A. Hodgkin and A. Huxley. A quantitative description of membrane current and application to conduction and excitation. *J. Physiol.*, 117:500-544,1952.

[24] A. Hutt, A. Daffertshofer, U. Steinmetz Phys. Rev. E **68**, 036219 (2003)

[25] N.B. Janson, A.G. Balanov, and E. Schöll, Delayed Feedback as a Means of Control of Noise-Induced Motion. *Phys. Rev. Lett.* **93**, 010601 (2004).

[26] G. Kozyreff, A.G. Vladimirov, and Paul Mandel, Global Coupling with Time Delay in an Array of Semiconductor Lasers. *Phys. Rev. Lett.* **85**, 3809 (2000).

[27] S. Kim, S.H. Park, and C.S. Ryu, Multistability in Coupled Oscillator Systems with Time Delay. *Phys. Rev. Lett.* **79**, 2911 (1997);

[28] Y. Kuramoto, Chemical Oscillations, Waves and Turbulence. Springer, Berlin, 1984.

[29] Y.A. Kuznetsov, *Elements of applied bifurcation theory*, volume 112 of *Applied Mathematical Sciences*. Springer-Verlag, New York, second edition, 1998.

[30] F. A.Lenz, H. C. Kwan, R. L. Martin, R. R. Tasker, J. O. Dostrovsk, & Y. E. Lenz, Single unit analysis of the human ventral thalamic nuclear group. Tremor-related activity in functionally identfied cells, *Brain* **117**, 531–543 (1994).

[31] P. Limousin, J. D. Speelman, F. Gielen, & M. Janssens, Multicentre European study of thalamic stimulation in parkinsonian and essential tremor," *J. Neurol. Neurosurg. Psychiatry* **66**, 289–296 (1999).

[32] R. Llinas & H. Jahnsen, Electrophysiology of mammalian thalamic neurons in vitro, *Nature* **297**, 406–408 (1982).

[33] F. Lopes da Silva, Event-related Potentials: Methodology and Quantification. *Electroencephalography.* 4th edition,Lippincott Williams & Wilkins,1999, p.947

[34] C. C. McInryre, M. Savasta, K. Goff, & J. L. Vitek, Uncovering the mechanism(s) of action of deep brain stimulation: activation, inhibition, or both, *Clin. Neurophysiol.* **115**, 1239–1248 (2004).

[35] C.M. Marcus and R.M. Westervelt, Stability of Analog Neural Networks with Delay. *Phys. Rev. A* **39**, 347 (1989).

[36] J. Milnor, "Remarks on Iterated Cubic Maps" *Exp. Math.* **1**, 5 (1992);

[37] A. Neiman, X. Pei, D. Russel, F. Moss *at al* Synchronization oof the Noisy Electrosensitive Cells in the Paddlefish. *Phys. Rev. Lett.* **82**, 660 (1999)

[38] E. Niebur, H.G. Schuster, and D.M. Kammen, *Phys. Rev. Lett.* **67**, 2753-2756 (1991).

[39] A. Nini, A. Feingold, H. Slovin, & H. Bergman, Neurons in the globus pallidus do not show correlated activity in the normal monkey, but phase-locked oscillations appear in the MPTP model of parkinsonism," *J. Neurophysiol.* **74**, 1800–1805 (1995).

[40] D. Pare, R. Curro'Dossi, & M. Steriade, Neuronal basis of the parkinsonian resting tremor: a hypothesis and its implications for treatment, *Neuroscience* **35**, 217–226 (1990).

[41] A. Pikovsky, M. Rosenblum, J. Kurths, *Synchronization: a universal concept in nonlinear sciences.* Cambr. Univ. Press., Cambridge, 2001.

[42] L.S. Pontrjagin, *Gewönliche Differentialgleichungen.* Deutsch. Verl. der Wissen., Berlin, 1965.

[43] O. Popovych, V. Krachkovskyi, and P.A. Tass, Desynchronization Transitions in Coupled Phase Oscillator Systems with Delay. *Proceedings of the 2003 Workshop on Nonlinear Dynamics of Electronic Systems (NDES'2003).* Scoul, Switzerland, 2003, edited by R. Stoop (University of Zürich, Zürich, 2003) p. 197.

[44] O. Popovych, V. Krachkovskyi, and P.A. Tass, (in preparation).

[45] O. Popovych, Y. Maistrenko, and P.A. Tass, Phase chaos in coupled oscillators. *Phys. Rev. E* **71**, 065201(R) (2005).

[46] O. Popovych, C. Hauptmann, and P.A. Tass, Effective Desynchronization by Nonlinear Delayed Feedback. *Phys. Rev. Lett.* **2005**, 164102 (2005).

[47] D.V. Ramana Reddy, A. Sen, G.L. Johnston, Dynamics of a limit cycle oscillator under time delayed linear and nonlinear feedbacks. *Phys. Rev. Lett.* **80**, 5109 (1998); *Physica D* **144**, 335 (2000).

[48] D.V. Ramana Reddy, Abhijit Sen, George L. Johnston, Driven response of time delay coupled limit cycle oscillators. *Comunication in Nonlinear Science and Numerical Simulation* **8**, pp. 493-518.

[49] M.G. Rosenblum, A.S. Pikovsky, and J. Kurths, *Phys. Rev. Lett.* **76**, 1804 (1996).

[50] M.G. Rosenblum and A.S. Pikovsky, *Phys. Rev. Lett.* **92**, 114102 (2004); *Phys. Rev. E* **70**, 041904 (2004).

[51] *Electrophysiology of Mind Event-related Brain Potentials and Cognition*, Edited by Michael D. Rugg and Michael G. H. Coles. Oxford Univ. Press, 1996.

[52] H.G. Schuster and P. Wagner, Mutual Entrainment of Two Limit Cycle Oscillators with Time Delayed Coupling. *Prog. Theor. Phys.* **81**, 939 (1989).

[53] P. R. Schuurman, D. A. Bosch, P. M. Bossuyt, G. J. Bonsel, E. J. van Someren, R. M. de Bie, M. P. Merkus, & J. D. Speelman, A comparison of continuous thalamic stimulation and thalamotomy for suppression of severe tremor, *N. Engl. J. Med.* **342**, 461–468 (2000).

[54] L.P. Shayer and S.A. Campbell, Stability, bifurcation, and multistability in a system of two coupled neurons with multiple time delays. *SIAM J. Appl. Math.* **61**, pp.673-700 (2000)

[55] P. Tass, J. Kurths, M.G. Rosenblum, G. Guasti, and H. Hefter, Delay-Induced Transitions in Visually Guided Movements. –R2227 *Phys. Rev. E* **54**, R2224 (1996).

[56] P. A. Tass, M. G. Rosenblum, J. Weule, J. Kurths, A. Pikovsky, J. Volkmann, A. Schnitzler, H.-J. Freund, Detection of $n : m$ phase locking from noisy data: Application to magnetoencephalography, *Phys. Rev. Lett.* **81**, 3291–3294 (1998).

[57] P. Tass, Phase Resetting in Medicine and Biology- Stochastic Modelling and Data Analysis. Springer, Berlin, 1999.

[58] P.A. Tass, *Europhys. Lett.* **53**, 15 (2001); **55**, 171 (2001); **59**, 199 (2002); *Biol. Cybern.* **87**, 102 (2002); **89**, 81 (2003); *Phys. Rev. E* **66**, 36226 (2002); *Chaos* **13**, 364 (2003).

[59] P.A. Tass, Stochastic phase resetting of two coupled phase oscillators stimulated at different times. *Phys. Rev. E* **67**, 051902 (2003).

[60] P.A. Tass, A model of desynchronizing deep brain stimulation with a demand-controlled coordinated reset of neural subpopulations. *Biol. Cybern.* **89**, 2 (2003).

[61] P.A. Tass, Transmission of stimulus-locked responses in two coupled phase oscillators. *Phys. Rev. E* **69**, 051909 (2004)

[62] The fixed points of system (2.4) always have a zero eigenvalue corresponding to the invariance of the trajectories with respect to a constat shift of the variable φ_2, see Eq. (2.5).

[63] *Dynamical systems in Cosmology*, edited by J. Wainwright, G.F.R. Ellis. Cambr. Univ. Press, 1997.

[64] S. Waxman, *Multiple Sclerosis As A Neuronal Disease*. Academic Press, 2005.

[65] N. Wiener, *Cybernetics or control and communication in the animal and the machine.* The thechnology press, New York, 1948.

[66] A. T. Winfree, An integrated view of the resetting of a circadian clock, *J. Theor. Biol.* **28**, 327–374 (1970).

[67] A. T. Winfree, *The Geometry of Biological Time* Springer, Berlin, 1980.

[68] C. Woody, Characterisation of an adaptive filter for the analysis of variable latecy neuroelectric signals. *Med. & Biol. Engng.* **5**, pp. 539-553. Pergamon Press, 1967.

[69] W. Wischert *et al.*, A. Wunderlin, A. Pelster, M. Olivier, and J. Groslambert, Delay-Induced Instabilities in Nonlinear Feedback Systems. *Phys. Rev. E* **49**, 203 (1994).

[70] G.D. VanWiggeren and R. Roy, *Science* **279**, 1198 (1998).

[71] J. Volkmann, M. Joliot, A. Mogilner, A. A. Ioannides, F. Lado, E. Fazzini, U. Ribary, & R. Llinas, Central motor loop oscillations in parkinsonian resting tremor revealed by magnetoencephalography, *Neurology* **46**, 1359–1370 (1996).

[72] J. Volkmann, Depp brain stimulation for the treatment of parkinson's disease, *J. Clin. Neurophysiol.* **21**, 6–17 (2004).

[73] M.K.S. Yeung and S.H. Strogatz, *Phys. Rev. Lett.* **82**, 648 (1999).

[74] M. Yoshioka and M. Shiino, Associative Memory Based on Synchronized Firing of Spiking Neurons with Time-Delayed Interactions. –3639 *Phys. Rev. E* **58**, 3628 (1998).

[75] Y. Zhai, I. Kiss, P. Tass, and J. Hudson, Desynchronization of coupled electrochemical oscillators with pulse stimulations. *Phys. Rev. E* **71**, 065202(R) (2005)

List of Figures

Acknowledgements

I would like to thank Prof. Dr. Tassilo Küpper who enabled this Ph.D. thesis and supported my work.

I express my gratitude to Prof. Dr. Dr. Peter Tass from the Research Center Jülich who inspired me with his ideas which played the main role during the work on the thesis.

I am grateful Dr. Oleksandr Popovych for his help, his permanent interest with regard to the scientific content and the progress of this thesis, his time and patience.

Many thanks I address to my friends and collegues as at the Reaserch Centre Jülich as well at the Mathematical Institute. The collaboration with them and the friendly athmosphere positively influenced my work.

Ich versichere, daß ich die von mir vorgelegte Dissertation selbständig angefertigt, die benutzten Quellen und Hilfsmittel vollständig angegeben und die Stellen der Arbeit - einschließlich Tabellen, Karten und Abbildungen -, die anderen Werken im Wortlaut oder dem Sinn nach entnommen sind, in jedem Einzelfall als Entlehnung kenntlich gemacht habe; daß diese Dissertation noch keiner anderen Fakultät oder Universität zur Prüfung vorgelegen hat; daß sie - abgesehen von unten angegebenen Teilpublikationen - noch nicht veröffentlicht worden ist sowie, daß ich eine solche Veröffentlichung vor Abschluß des Promotionsverfahrens nicht vornehmen werde. Die Bestimmungen dieser Promotionsordnung sind mir bekannt. Die von mir vorgelegte Dissertation ist von Prof. Dr. Tassilo Küpper betreut worden.

Teilpublikation: O. Popovych, V. Krachkovskyi, and P.A. Tass
Desynchronization Transitions in Coupled Phase
Oscillator Systems with Delay
 in Proceedings of the 2003 Workshop on Nonlinear
Dynamics of Electronic Systems (NDES'2003), Scoul,
Switzerland, 2003, edited by R. Stoop
(University of Zürich, Zürich, 2003) p. 197.

Stimulus Induced Desynchronization of Oscillators Coupled with Delay: Theory and Application to neurological Patients

Valerii Krachkovskyi (v.krachkovskyi@fz-juelich.de)

In a proposed dissertation work author studies several systems of phase oscillators coupled with delay. Systems were written in a form of differential equations. These systems serve as models of certain aspects of neuronal dynamics in brain. They were subjects to an external stimulation. The stimulation is represented through additional term in equations. Possible dynamical regimes of the systems were investigated, using analytical methods, bifurcation theory and computer simulations; synchronization in the systems was one of main targets of research.

In the first system was considered two phase oscillators modeling the phase dynamics of two instantaneously interacting functional units, accompanied by a delayed feedback of each oscillator onto itself. This system is subject to external short-pulse stimulation and noise. The strong stimulus induces a phase reset of the oscillations followed by the transient dynamics leading towards multiple synchronized states. It is studied the stimulus-induced transient response of the oscillators in different synchronous regimes emerging in the considered system. It is shown that depending on the stimulation parameters used the response of the system to the stimulus may result in qualitatively different types of behavior ranging from cross-trial phase clustering to complete desynchronization. The mechanisms of in- and post-stimulus clustering of the system responses are explained. Author also emphasizes the role of the stable manifold of a saddle-focus fixed point on the cluster formation process.

The second model considered is a system of two phase oscillators modeling phase dynamics of two neuronal populations interacting with delay. The one of two oscillators is a subject to external short-pulse stimulation and both oscillators are subjects to noise. It is studied the response of the stimulated oscillator to the administered stimulation as well as a transmission of the stimulus to the second oscillator. Author proposes a novel technique for evaluation of the stimulus-induced responses and transmission time and compares it with established standard methods based on averaging procedures. It is shown that the standard techniques refer not to the transmission phenomenon itself but rather to oscillatory dynamics of the oscillators. In contrast, the suggested method based on the phase-resetting analysis is able to give a good estimate not only to stimulus transmission time but can estimate the delay time in the system.

Stimulus-induzierte Desynchronisation von gekoppelten Oszillatoren mit Zeitverzögerung: Theorie und Anwendung bei neurologischen Patienten

Valerii Krachkovskyi (v.krachkovskyi@fz-juelich.de)

Der Verfasser untersucht in dieser Dissertation Systeme von Phasenoszillatoren, welche miteinander mit einer Zeitverzögerung gekoppelt sind. Die Systeme werden in Form von Differentialgleichungen beschrieben. Diese Systeme dienen als Modelle gewisser Aspekte der neuronalen Prozesse bei neurologischen Patienten (z.B. bei Parkinson Erkrankung). Sie werden mittels einer externen Stimulation kontrolliert, wobei die Stimulation durch einen zusätzlichen Glied in den Gleichungen repräsentiert wird. Mögliche dynamische Regime werden mit der Hilfe analytischer Methoden, z.B. der Bifurkationstheorie, und Computersimulationen untersucht; die Erforschung der Synchronisation ist eines der Hauptziele.

Im ersten Teil der Arbeit werden zwei Phasenoszillatoren betrachtet, die die Phasendynamik von zwei instantan interagierenden Funktionseinheiten mit zeitverzögerter Selbstkopplung modellieren. Dieses System wird mittels einer externen Kurzpuls-Stimulation beeinflusst. Der starke Reiz ruft einen Reset der Phasen hervor, gefolgt von weiteren Übergangsprozessen zu mehreren synchronen Zuständen. Die reizinduzierte, transiente Antwort der Dynamik der Oszillatoren in den verschiedenen synchronen Regimen wird untersucht. Es wird gezeigt, dass in Abhängigkeit von den Stimulationsparametern, die Reizantwort des Systems verschiedene Formen annehmen kann: von einer Klusterbildung der Reizantwort bis zur einer kompletten Desynchronisation. Die Mechanismen der Klusterbildung der Reizantwort während und nach der Stimulation werden erklärt. Die Rolle der stabilen Mannigfaltigkeit des Sattelpunkts in der Klusterbildung wird erläutert. Die stimulus-induzierte Umschaltung zwischen koexistierenden, stabilen, synchronen Zuständen und auch desynchronen Zuständen wird illustriert.

Das zweite Modell, das betrachtet wird, ist ein System von zwei gekoppelten Oszillatoren, die die Phasendynamik von zwei interagierenden neuronalen Populationen mit einer Zeitverzögerung modellieren. Nur einer der Oszillatoren wird mittels einer externen Kurzpulse-Stimulation stimuliert und beide Oszillatoren werden von Rauschen beeinflusst. Untersucht werden die Reizantwort des stimulierten Oszillators und die Reiztransmission an den zweiten Oszillator (zwischen zwei beispielhaften Gehirnarealen). Der Autor schlägt die neue Technik für die Auswertung von stimulus-induzierten Antworten und der Transmissionszeit vor. Diese Technik wird mit den Standardmethoden, welche auf Mittelungsprozeduren basieren, verglichen. Es wird gezeigt, dass sich die Standardtechniken eher auf die oszillatorische Dynamik beziehen als auf Transmissionsphänomen. Im Gegensatz zur Standardtechnik ist die vorgeschlagene Methode nicht nur für die Ermittlung der Transmissionszeit sondern auch für die Ermittlung der Zeitverzögerung im System geeignet.